Frequency-Domain Modelling of Reset Control Systems using an Impulsive Description

R. N. Buitenhuis

Master of Science Thesis

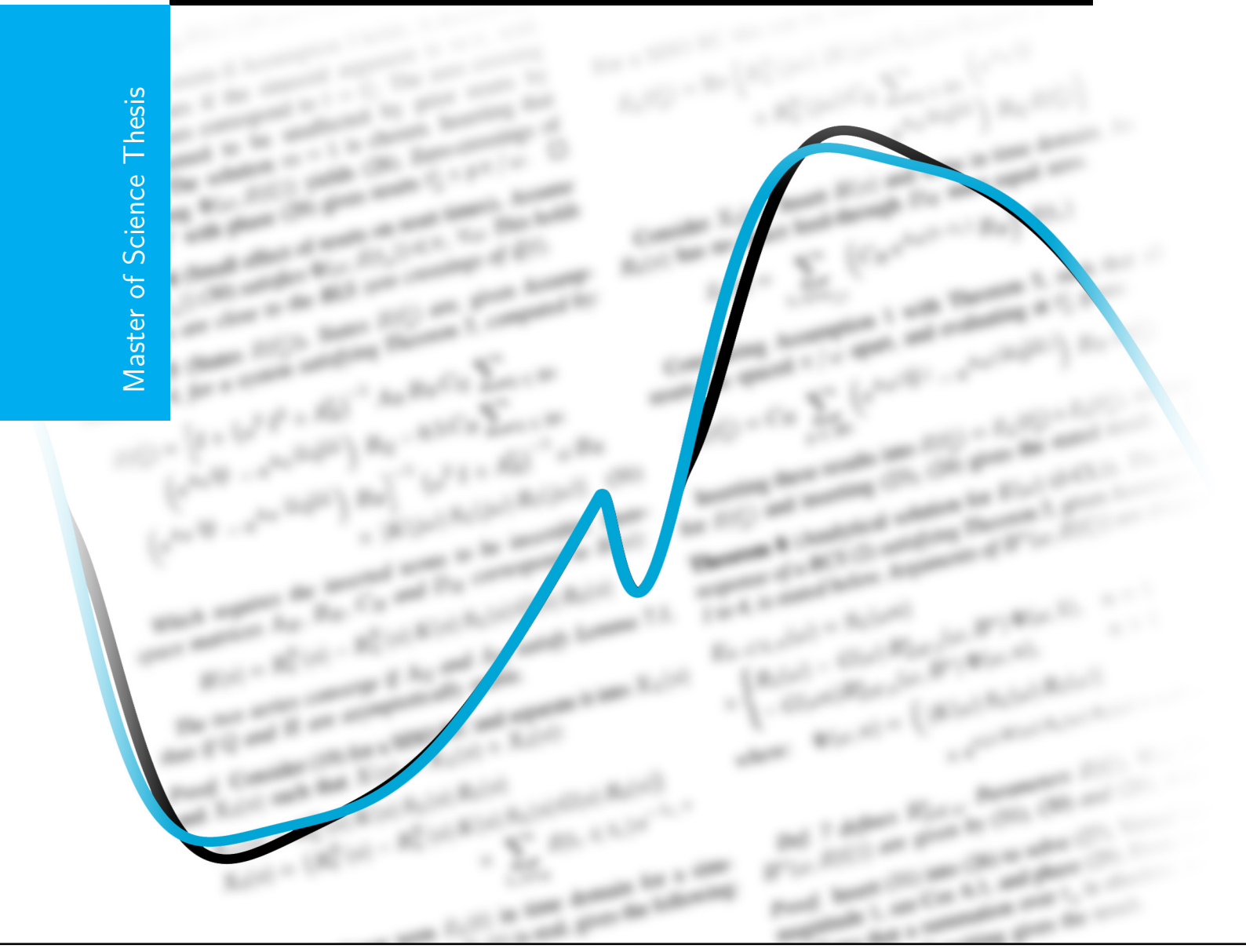

TU Delft Delft University of Technology

Delft Center for Systems and Control

Frequency-Domain Modelling of Reset Control Systems using an Impulsive Description

Master of Science Thesis

For the degree of Master of Science in Systems and Control & Mechanical Engineering at Delft University of Technology

R. N. Buitenhuis

July 28, 2020

Faculty of Mechanical, Maritime and Materials Engineering (3mE) · Delft University of Technology

Abstract

The ever-increasing industry desire for improved performance makes linear controller design run into its fundamental limitations. A nonlinear controller, such as Reset Control (RC), is needed to overcome these. RC is promising since, unlike other nonlinear methods, it easily integrates into the PID design framework preferred by industry. Thus far, closed-loop behaviour of RC has been analysed in the frequency domain either through Describing Function analysis or by direct closed-loop numerical computation. The former method computes a simplified closed-loop RC response by ignoring all harmonics, an approach which literature has found to inflict significant modelling errors. The latter method gives an accurate solution but does not provide understanding of how open-loop RC design affects closed-loop performance. No methods link these aspects, which impairs RC design and tuning. The main contribution of this work is aimed at providing this link, while achieving an accurate closed-loop RC model. A novel approach for modelling RC is considered, which uses state-dependent impulse inputs. This approach is shown to permit an accurate computation of closed-loop RC behaviour starting from an open-loop model, thus linking both aspects, enhancing system understanding. A frequency-domain description for closed-loop RC is obtained, as needed for the PID design framework, which is solved for analytically by inserting several well-defined assumptions. This solution is verified using a simulated high-precision stage, critically examining sources of modelling errors. The accuracy of the proposed method is further substantiated using controllers designed for various specifications.

Table of Contents

List of Figures

Preface

This report provides the results of my master thesis at the departments of Delft Center for Systems and Control (DCSC) and High Tech Engineering (HTE) within the faculty of Mechanical, Maritime and Materials Engineering (3mE), part of Delft University of Technology (TU Delft). I was looking for a challenging graduation project that would combine the theoretical approach of my first master, Systems & Control, along with the more industry-focussed approach of my second master, High Tech Engineering.

Hassan HosseinNia and Niranjan Saikumar suggested several projects to me, which would allow me to combine these masters. These projects involved Reset Control (RC), which drew my attention because of its applicability in industry whilst being theoretically challenging. RC has the potential to significantly improve performance of many systems, since it is able to overcome fundamental limitations of linear control. It was noticed that the body of literature for RC is limited. This made me enthusiastic to work on something new and challenging.

This project was initially aimed at a MIMO extension of RC. However, I found that, to this date, no methods were available that modelled RC with sufficient accuracy to permit a MIMO implementation. Therefore, I shifted the aim of this towards towards developing a new theory for modelling RC, in an effort to allow a MIMO extension of RC in the future.

Acknowledgements

I would like to thank the following people for all their help and support throughout this thesis:

Niranjan Saikumar: As daily supervisor you have consistently provided me with lots and lots feedback. You always challenged my ideas, engaged in helpful, critical discussions, and encouraged me to move on. When I no longer saw the point of Reset Control, you explained me its purpose again, helping me to stay on track. I have been astonished by your tireless effort in proof-reading my paper and report, I really appreciate that!

Hassan HosseinNia: I want to thank you for introducing me to Reset Control, a topic that has greatly frustrated, motivated, and challenged me, yet most of all gave me a very interesting thesis. Your positive approach encouraged me with every meeting we have had, motivating me to keep improving.

Michel Verhaegen: Thank you for your critical questions, motivation, and willingness to be a supervisor during this project.

Bas Kieft: I found it very helpful to work together during this thesis, helping each other figure out how Reset Control works. I appreciated our discussions, where you gave me insight into various applications of Reset Control.

Last, I would like to thank my flatmates and family, who supported me during this thesis, especially once I had to work from home. They had to hear me explain them Reset Control so many times, which ultimately led me to understand Reset Control myself. Thank you for hanging on and not getting too bored with me! I greatly appreciated all our lunch breaks together, giving me a nice break from study work.

Enjoy reading this thesis!

Delft, University of Technology — R. N. Buitenhuis
July 28, 2020

Chapter 1

Introduction

Industry is continuously pushing control limitations by increasing their performance demands. For example, the high-tech industry may ask to upkeep or boost throughput and simultaneously improve on precision in order satisfy their desire for more precise machines. This leads to increasingly stringent requirements on bandwidth, disturbance rejection, noise attenuation and reference tracking.

Proportional Integral Derivative (PID) controllers are standard to industry, including high-tech applications. This status is expected to persist, because PID permits controller tuning using the industry-preferred loop shaping framework [1]. This frequency-domain framework allows for intuitive tuning. Numerous guidelines have been developed for PID design in continuous [2, 3] and discrete time [4], making use of industry-standard tools such as Bode and Nyquist plots.

Design trade-offs become apparent when linear controllers, such as a PID, are pushed to their limits. One limitation inherent to linear control is the Bode gain-phase relationship [5], which relates the phase of system G to the slope of gain over frequency, $N(\omega_0)$. For minimum-phase systems this relationship is given by:

$$\angle G(j\omega_0) \approx 90^\circ \times N(\omega_0), \quad N(\omega_0) = \left| \frac{d \ln |G(j\omega)|}{d \ln \omega} \right|_{\omega=\omega_0} \tag{1-1}$$

This relationship links a system's slope to its phase, presenting a trade-off to the designer. Increasing the gain at low frequencies improves reference tracking and disturbance rejection, while lowering the gain at high frequencies improves noise attenuation [6]. Having more phase around the cross-over frequency improves stability, which in turn can be traded for a higher bandwidth. Two linear designs in Figure 1-1 demonstrate this inferred trade-off. The double integrator system has better reference tracking, disturbance rejection and noise attenuation than the integrator with tamed lead filter, yet the latter has better stability properties. This trade-off, inherent to linear controllers, hinders the industry push for better performance.

This trade-off can only be overcome by nonlinear controllers. However, these are usually not suitable for the industry-preferred loop shaping methodology, as they generally do not

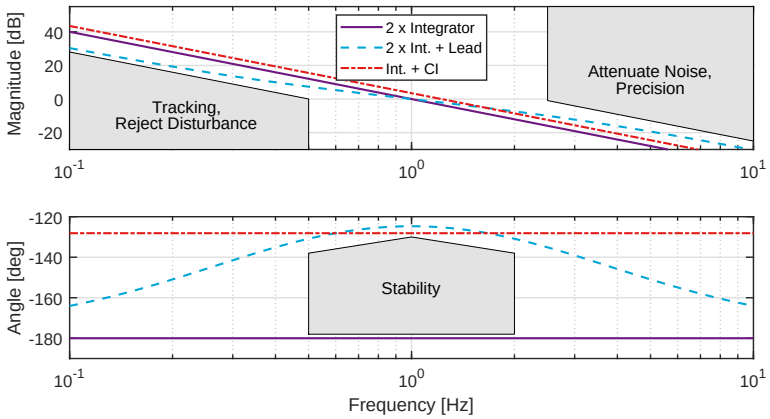

Figure 1-1: Bode plots of two linear controllers, an integrator and an integrator with added lead/lag filter, demonstrating the trade-off due to Bode's gain-phase relationship, along with the Describing Function (DF) response of a Clegg Integrator (CI).

permit a frequency-domain description. Popular nonlinear controllers are nonlinear filters [7], the Variable Gain Integrator [8, 9], Sliding Mode Control [10], Optimal Control [11] and Nonlinear Feedback Control [12].

Hybrid control is a promising nonlinear domain for overcoming the fundamental design trade-off in linear control, while also permitting loop shaping. Examples include the Filtered Split-Path Nonlinear Integrator [13], which switches the integrator sign based on a switching law, and the Hybrid Integrator-Gain System [14], which provides a zeroth order smooth output [15, 16, 17].

Reset Control (RC), a subclass of hybrid control, is found to have various implementations that allow a frequency-domain description. This permits RC to be tuned through loop shaping [18]. RC has the promising advantage of embedding nicely into the industry preferred PID framework, whilst introducing nonlinearity by which it overcomes the Bode's gain-phase relationship.

The RC concept was first introduced as the CI [19], which is an integrator with its value resetting to zero whenever its input crosses zero. Figure 1-2 illustrates this. Through Describing Function (DF) analysis [20] it is shown that the CI inflicts 52° less phase lag than the in gain similar linear integrator, as shown in Figure 1-1. It follows that CI overcomes the Bode gain-phase relationship, eliminating the corresponding trade-off. Since then, many different implementations of RC have been developed.

Several works have demonstrated that RC can push performance beyond limits attainable through linear control [21, 22], for example by improving noise attenuation [23] or reducing overshoot [24] without affecting other specifications. RCs have been implemented in various control applications, including solar collectors [25], truss elements [26], chemical processes [27], vibration isolation [28] and motion control systems [29, 30, 31, 32, 33].

A frequency-domain description of RC is imperative for design using the preferred loop shaping methodology. Most commonly, DF analysis is utilized. Despite its popularity, several works found closed-loop predictions based on DF analysis to deviate widely from measurements [34, 28, 29]. This discrepancy is caused by DF ignoring all reset-induced harmonics. An

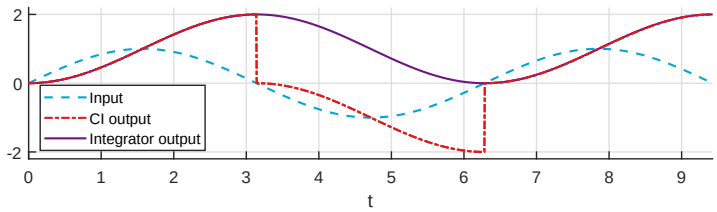

Figure 1-2: Clegg Integrator (CI) and integrator responses for a sinusoidal input.

open-loop extension to DF analysis, incorporating harmonics [18], was used to compute a novel closed-loop frequency-domain description, the Closed-loop Describing Function (CL-DF) [35], which uses assumptions to close the loop. Both CL-DF and DF assume the reset element input to be sinusoidal, which at best holds approximately in closed-loop. These methods also model two resets per input period only, which is known to not hold generally [30]. A different method was suggested that computes the closed-loop directly by solving it numerically [36]. This yields a precise solution at the cost of being computationally intensive and not providing a link between the open- and closed-loop. None of the frequency-domain methods available thus accurately link open-loop RC design to closed-loop RC performance. Without such a link, RC design is impaired, as effects of open-loop RC tuning on the closed-loop performance can only be evaluated empirically or with various assumptions. This implies that underlying principles are not well understood. This work aims to bridge that gap.

Some authors have mentioned that RC can be modelled as a linear controller with a train of state-dependent weighted impulse inputs [23, 37, 38], but this idea is only developed for certain open-loop CI implementations [23] and for closed-loop nonlinear systems [39]. The latter does not provide a link to open-loop. An advantage of this impulsive description is that it models RC with a linear controller, simplifying derivations. Yet, no works are found that generalize this description. Other authors directly analyse RC using its state-space description, see e.g. [40]. Such an approach typically leads to controller optimization through solving Linear Matrix Inequalities [41]. Neither of these methods directly permits a frequency-domain analysis.

This work takes the impulsive RC modelling approach, and generalizes that approach to obtain a closed-loop frequency domain description of RC systems, enabling accurate computation of closed-loop solutions in a way compatible to the industry preferred loop shaping methodology. In doing so, it analytically links open-loop RC design to its closed-loop performance, providing several advantages. First, having such a link enables better tuning and design of RCs, as it provides understanding on the implications of open-loop tuning and design on closed-loop performance, which is an insight that existing methods do not provide. A second advantage is that this link provides a first step into enabling a future extension of loop-shaping tunable RCs to MIMO systems.

All existing MIMO RC literature use, to the author's knowledge, time-domain, state-space optimization [42, 43, 44, 45, 46] and therefore do not permit the industry preferred loop shaping methodology. A precise, well-understood closed-loop frequency-domain RC model is needed to alleviate this gap, which can be provided by establishing the link between open- and closed-loop. Without such a link it for example remains unknown when resets cause subsequent resets on other channels, which may once again create new ones elsewhere. In

such cases, system knowledge severely degenerates, which impairs RC design and analysis.

Chapter 2 will first establish a generic RC framework along with related definitions and a stability result. Various methods for nonlinear frequency-domain analysis of RC, as imperative for the industry-preferred loop shaping methodology, are provided afterwards in Chapter 3. Third, Chapter 4 provides various implementations of RCs found in literature, tailored towards a frequency-domain implementation. Chapter 5 then states the problem definition based on the discussed literature, to which a solution is provided in Chapter 6. That chapter, written in paper format, derives and analyses a frequency-domain description for closed-loop RC systems based on the impulsive modelling approach. Chapter 7 discusses these results in more detail. Conclusions are given in Chapter 8 and subsequent recommendations for future research in Chapter 9. The appendices provide several relevant MATLAB scripts, which can be used in future research for further developments or for result reproduction.

Chapter 2

Preliminaries

This chapter provides the fundamental background to Reset Control (RC). First, a generic RC framework is established, including related definitions. Notations introduced there are used throughout this report. Various reset laws, which determine when resets occur, are given afterwards, tailored to the desired frequency-domain description. This section ends by stating RC stability results.

2-1 Reset Control framework

This section defines RC, first in open-loop and afterwards in closed-loop. The impulsive approach is also provided, based on the established framework.

2-1-1 Open-loop

A very generic RC formulation is used, which maps RC input $\vec{q}(t) \in \mathbb{R}^{m_q}$, $m_z \in \mathbb{N}$ onto RC output $\vec{z}(t) \in \mathbb{R}^{m_z}$, $m_q \in \mathbb{N}$. This setup thus permits a MIMO system. The RC is denoted by $\not{R}$, where the crossing arrow indicates the reset action. The following mathematical notions are used:

- *Reset element* $\not{R}$ is described by dimension-compatible state-space matrices A_R, B_R, C_R and D_R. $\not{R}$ has internal states $\vec{x} \in \mathbb{R}^{n_{ol}}$ with dimension $n_{ol} \in \mathbb{N}$.
- *Reset matrices* $A_{\rho,k}$ describe the effects of a reset, $\forall\, k \in \{1, \ldots, \bar{k}\}$, where $\bar{k} \in \mathbb{N}$ denotes the number of reset matrices used. Most literature does not include parameter k, thus implicitly using $\bar{k} = 1$. However, generality is enhanced by including k, as doing so permits using multiple reset matrices.
- *Reset instants* are the times when resets take place. Reset instants corresponding to reset matrix $A_{\rho,k}$ occur at time $t = t_{r,k}$. The set of all reset times $t_{r,k}$ is denoted as $t_{R,k}$. Rthe union of $t_{R,k}$ over all k yields the set of all reset times, $\cup_k\, t_{R,k} = t_R$.

- *Reset law k* computes the corresponding reset times $t_{R,k}$, based on other parameters, for example on $\vec{q}(t)$, $\vec{z}(t)$ or $\vec{x}_r(t)$. The exact parameters used depend on which reset law is used.

These definitions are used in the general RC description:

$$\not{R}: \begin{cases} \dot{\vec{x}}(t) = A_R\,\vec{x}(t) + B_R\,\vec{q}(t), & t \notin t_R \\ \vec{x}^+(t) = A_{\rho,k}\,\vec{x}(t), & t \in t_{R,k},\ \forall\, k \\ \vec{z}(t) = C_R\,\vec{x}(t) + D_R\,\vec{q}(t) \end{cases} \tag{2-1}$$

After-reset states are denoted by $\vec{x}^+$.

Implementation Eq. (2-1) accepts a MIMO setting. Eq. (2-1) also permits having multiple reset matrices and laws through parameter k. This is often required for MIMO implementations [46], for example when one reset law/matrix pair for each of the input channels in used. Such cases can be described by Eq. (2-1) because of parameter k.

RC Literature often restricts itself to using diagonal reset matrices. These can be parametrized as $A_{\rho,k} = \text{diag}\,(\gamma_{1,k}, \ldots, \gamma_{n_{ol},k})$, $\gamma_{i,k} \in [-1,\ 1]$, $i \in \{1, \ldots,\ n_{ol}\}$, $\forall k$. The following terminology is used for this diagonal case:

- *Fully resetting RC*: any RC which has diagonal matrices $A_{\rho,k}$ with all parameters $\gamma_{i,k} \in \{0,\ 1\}$, $\forall\ i,\ \forall\ k$, whilst, for all k, there is at least one $\gamma_{i,k}$ equal to 0, such that one or more states are reset. The resetting states are set to zero at all resets.
- *Partially resetting RC*: a RC with diagonal $A_{\rho,k}$, which must have at least one value $\gamma_{i,k} \in [-1,\ 1] \setminus \{0, 1\}$. A reset element permitting a partial reset is also referred to as a *generalized* reset element [47]
- *No reset:* any RC with, for all k, $A_{\rho,k} = I$. Such an RC has no reset effects and thus acts linear. This linear open-loop RC, denoted as $R_L(s)$, is described by:

$$R_L \triangleq C_R\,(s\,I - A_R)^{-1}\,B_R + D_R \tag{2-2}$$

Example 2-1.1 (Open-loop RC)**.** *Consider an open-loop Clegg Integrator (CI) [19], having dimensions $m_z = 1$, $m_q = 1$ and $\bar{k} = 1$. The following design parameters are used:*

- *Matrices $A_R = 0$, $B_R = 1$, $C_R = 1$ and $D_R = 0$.*
- *Reset instants $t_{r,1} \in t_{R,1}$ occur whenever the RC input $\vec{q}(t)$ crosses zero. This corresponds to the reset law $t_{R,1} = \{t \in \mathbb{R} \mid \vec{q}(t) = 0\}$. Only one reset law is used, which implies that $t_R = t_{R,1}$.*
- *Three different reset matrices $A_{\rho,1}$ are used:*
  1. *Full reset, using $A_{\rho,1} = 0$.*
  2. *Partial reset (generalized), using $A_{\rho,1} = 0.5$.*
  3. *No reset (linear), using $A_{\rho,1} = 1$.*

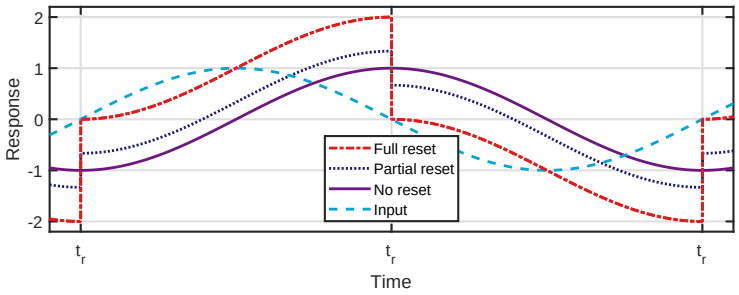

Figure 2-1: Time-domain outputs $\vec{z}(t)$ of a CI with full, partial and no reset, using a sinusoidal input with magnitude 1 and frequency 1 rad/s. Reset instants $t_r = t_{r,1} \in t_{R,1} = t_R$ are indicated.

Figure 2-1 provides the open-loop outputs $\vec{z}(t)$ for each of the three different reset matrices governing the CI. A sinusoidal input $\vec{q}(t)$ with frequency 1 rad/s is used. The no-reset case, $A_{\rho,1} = 1$ (R_L) responds as a classic linear integrator, thus integrating $\vec{q}(t)$.

Either resetting output behaves similar to an integrator between resets, though having some offset. The state of the fully resetting CI is reset to zero at all zero crossings of $\vec{q}(t)$ ($t_r = t_{r,1}$), consistent with the definition of full reset. The state of the partially resetting CI are multiplied by $A_{\rho,1} = 0.5$ at all $t_{r,1}$, implying that the output, which equals the state in this case, is also multiplied by 0.5 at those instants. Figure 2-1 illustrates this.

2-1-2 Closed-loop

A generic closed-loop RC system as depicted in Figure 2-2 is used, also referred to as a Reset Control System (RCS). As conventional in MIMO literature, reference $\vec{r}_I(t)$ is drawn at the right-hand side, output $\vec{y}(t)$ on the left. This setup consists of RC $\mathcal{R}$, surrounded by linear systems K and G, which may represent any combination of linear systems, for example controllers or plants. The reference, error and output signal are defined as $\vec{r}_I(t), \vec{e}(t), \vec{y}(t) \in \mathbb{R}^{m_y}$, $m_y \in \mathbb{N}$, respectively.

Let the dimension-compatible state-space matrices A_K, B_K, C_K and D_K describe K, and synonymously let A_G, B_G, C_G and D_G describe G. If $D_G = 0$, which holds for most physical plants, the closed-loop state-space matrices A_{cl}, B_{cl}, C_{cl}, D_{cl} and $A_{\rho cl,k}$ of the RCS depicted in Figure 2-2 are defined as:

$$\left[\begin{array}{c|c} A_{cl} & B_{cl} \\ \hline C_{cl} & D_{cl} \end{array}\right] = \left[\begin{array}{ccc|c} A_G - B_G D_R D_K C_G & B_G C_R & B_G D_R C_K & B_G D_G D_R \\ -B_R D_K C_G & A_R & B_R C_K & B_R D_K \\ -B_K C_G & 0 & A_K & B_K \\ \hline C_G & 0 & 0 & 0 \end{array}\right] \tag{2-3}$$

$$A_{\rho cl,k} = \text{diag}\{I,\, A_{\rho,k},\, I\}$$

These matrices are used to define the RCS. The RCS is denoted by $\mathcal{T}$, which maps reference

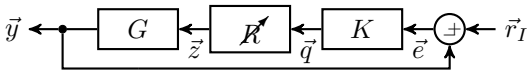

Figure 2-2: Block diagram of a closed-loop RC system with input $\vec{r}_I$ and output $\vec{y}$, consisting of reset element $\vec{R}$ surrounded by linear systems K and G.

$\vec{r}_I(t)$ to output $\vec{y}(t)$. The internal states $\vec{x}_{cl}$ have dimension $n_{cl} \in \mathbb{N}$. $\vec{\mathcal{I}}$ is given as:

$$\vec{\mathcal{I}}: \begin{cases} \dot{\vec{x}}_{cl}(t) = A_{cl}\,\vec{x}_{cl}(t) + B_{cl}\,\vec{r}_I(t), & t \notin t_R \\ \vec{x}_{cl}^{+}(t) = A_{\rho cl,k}\,\vec{x}_{cl}(t), & t \in t_{R,k},\ \forall\, k \\ \vec{y}(t) = C_{cl}\,\vec{x}_{cl}(t) + D_{cl}\,\vec{r}_I(t) \end{cases} \tag{2-4}$$

RCs Eq. (2-1) and RCSs Eq. (2-4) are SISO if $m_y = 1$, $m_q = 1$, $m_z = 1$ and $\bar{k} = 1 \Leftrightarrow \{k\} = 1$. This thesis focusses on the SISO case. Subscripts k are dropped from this point onwards, because sets $t_{R,k}$ and t_R are identical and only one reset law with corresponding A_ρ is used. All RCs and RCSs in the proceeding are taken to be SISO, except if stated otherwise. Several additional definitions are provided:

- The *Base Linear System (BLS)* is defined as Eq. (2-4) with $A_{\rho cl} = I$. This implies that there are no reset effects [30], thus that the closed-loop behaves fully linear. The BLS loop gain L_{BLS}, sensitivity S_{BLS} and complementary sensitivity T_{BLS} are given by:

$$L_{BLS}(s) \triangleq G(s)\,R_L(s)\,K(s) \tag{2-5}$$
$$S_{BLS}(s) \triangleq (I + L_{BLS}(s))^{-1} \tag{2-6}$$
$$T_{BLS}(s) \triangleq L_{BLS}(s)\,(I + L_{BLS}(s))^{-1} \tag{2-7}$$

  These are used to link the reference, error, and output in the Laplace domain:

$$Y_{BLS}(s) = L_{BLS}(s)\,E(s) \tag{2-8}$$
$$E_{BLS}(s) = S_{BLS}(s)\,R(s) \tag{2-9}$$
$$Y_{BLS}(s) = T_{BLS}(s)\,R(s) \tag{2-10}$$

- *Time regularization* suppresses any new reset if a reset has already occurred in the last τ seconds. In mathematical terms, resets are suppressed if $t < t_p + \tau$, where τ is a tunable parameter and t_p denotes the time of the last occurred reset [40].

RC can induce problems affecting the uniqueness or existence of solutions. This includes *beating*, *deadlock* and *Zenoness* [30]. A common technique to avoid these problems in continuous-time is time regularization [41], with $\tau > 0$. This is inherently included in discrete-time control with τ equal to the sampling interval [48, 49]. Because most practical implementations are implemented in a digital manner, rendering these problems irrelevant, it is chosen to disregard these issues during this thesis. Uniqueness and existence of solutions to Eq. (2-4) is thus assumed.

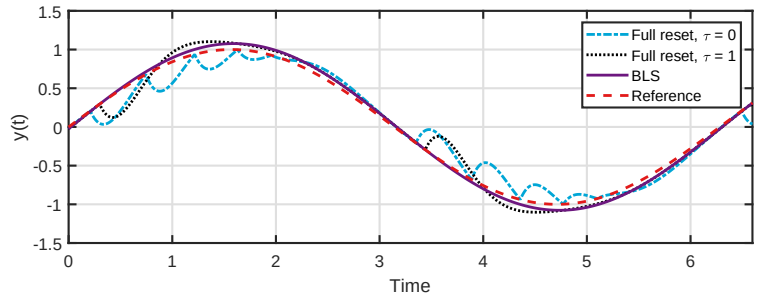

Figure 2-3: RCS outputs $y(t)$ when using time regularization parameters $\tau = 0$ and $\tau = 1$. The BLS is also provided.

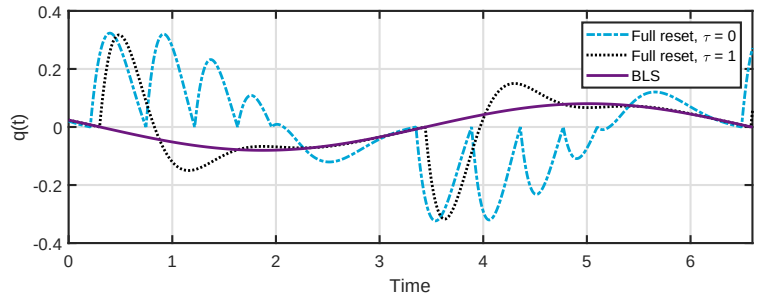

Figure 2-4: RCS responses $q(t)$ when using time regularization parameters $\tau = 0$ and $\tau = 1$. The BLS is also provided.

Example 2-1.2 (Closed-loop RC)**.** *Consider the fully resetting RC provided by Example 2-1.1. This RC is inserted in a RCS as in Figure 2-2 with linear systems $K(s)$ and $G(s)$ as given below. The BLS of this setup has a bandwidth of 5 rad/s.*

$$K(s) = 1, \quad G(s) = 50\,\frac{1}{s}\,\frac{2.5+s}{10+s} \tag{2-11}$$

Cases with and without time regularization are considered, $\tau = 1$ and $\tau = 0$, respectively. RCS outputs $\vec{y}(t)$ are shown in Figure 2-3, signals $\vec{q}(t)$ in Figure 2-4. Multiple resets are seen to occur per half period when no time regularization is applied.

The setting $\tau = 1$ suppresses all resets occurring within 1 second after a prior reset. The zero crossings around 0.85 and 3.95 seconds would cause resets in case no time regularization was to be used. These, however, are suppressed, as both have a prior reset less than 1 seconds before.

By definition the BLS gives a linear response, equal to that of the RCS without reset action.

2-1-3 Impulsive description

Several authors have mentioned that open-loop RCs can be *"alternatively viewed as the injection of judiciously-timed, state-dependent impulses into an otherwise LTI feedback system"* [38]. This idea is used for time-domain stability analysis of a fully resetting, open-loop CI

[23]. The output of such a CI is written as a linear response with added impulses:

$$\vec{z}(t) = \int_0^t \left[\vec{q}(p) - \sum\nolimits_{t_r \in t_R} \vec{z}(t_r)\,\delta(p - t_r)\right] \mathrm{d}p \tag{2-12}$$

No work is found that generalizes such a description to other open-loop RCs. Another work utilizing an impulsive description does that on a general nonlinear system [39], not using conventional RC notation as in Eq. (2-1). This is applied to a combustion controller, using pre-defined reset instants $t_{R,k}$. Time-domain analysis is used. This description starts from closed-loop, and thus does not link open-loop RC design to closed-loop behaviour.

A major advantage of the impulsive description is that the RC element itself becomes linear. The state-dependent impulse inputs capture all nonlinear effects. Linear systems can be considerably easier to analyse. This may, for instance, simplify obtaining a closed-loop expression when starting from an open-loop. Despite these potential advantages, no literature is found that applies this impulsive description to close the loop starting from an open-loop description, nor to find a frequency-domain expression as needed for loop shaping.

2-2 Reset laws

Several reset laws are presented in literature, using different combinations of parameters to determine reset times t_R. A frequency domain analysis has been developed for some of these. As industry prefers loop shaping, which requires a frequency-domain description, it is chosen to focus on the reset laws permitting that. Those reset laws are discussed in greater detail, whilst others are only touched upon briefly.

2-2-1 Reset laws with developed frequency-domain description

The zero-crossing reset law, and extensions thereof, are the reset laws for which a frequency-domain description has been developed. Figure 2-5 represents these laws graphically. The zero-crossing reset law is provided first, followed by two extensions.

Zero-crossing reset

Historically, many SISO RCs have been designed to reset whenever their input, $\vec{q}(t)$, crosses zero, see e.g. [19, 50]. Frequency-domain descriptions have been developed for this reset law. Zero-crossing reset times are computed by:

$$t_R = \{t \in \mathbb{R} \mid \vec{q}(t) = 0 \wedge (I - A_{\rho cl})\,\vec{x}_{cl}(t) \neq 0\} \tag{2-13}$$

The latter condition is added to ensure that, in closed-loop, post-reset states $\vec{x}_{cl}^{+} = (I - A_{\rho,cl})\,\vec{x}_{cl}$ do not cause a new reset within the same time instance of the reset that lead to $\vec{x}_{cl}^{+}$ [51]. Preliminary work on extending the zero-crossing reset law to MIMO has been provided by [46], which also provides a discrete-time implementation.

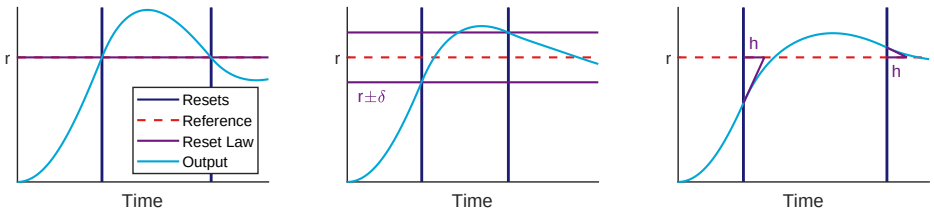

Figure 2-5: Sample reference step responses for a second-order system using a CI. Left: zero-crossing reset. Middle: reset band. Right: Variable reset band.

Reset band

Reset bands are proposed for systems with dominant time delays [52]. This band, parametrized by $\delta \in \mathbb{R} \geq 0$, is used to compensate for delays, ensuring that resets occur around the actual $\vec{q}(t) = 0$ crossings. A reset happens whenever the input $\vec{q}(t)$ enters this band, but not when $\vec{q}(t)$ leaves it:

$$t_R = \{t \in \mathbb{R} \mid (\vec{q}(t) = -\delta \wedge \dot{\vec{q}}(t) > 0) \vee (\vec{q}(t) = \delta \wedge \dot{\vec{q}}(t) < 0)\} \tag{2-14}$$

Setting $\delta = 0$ makes this reset law collapse to the basic zero-crossing reset law. When $\vec{q}(t) \in \pm\, \delta,\ \forall\, t$ no resets occur, rendering the system behaviour equal to that of the BLS. Both theory and experiments show that the reset band has the potential to improve performance over zero-crossing resets, as a well-designed band provides additional phase lead at all frequencies [25, 52].

A downside of a reset band is that it adds a different kind of nonlinearity. A RC with a reset band law responds in a nonlinear manner to the input gain, while a RC with zero-crossing resets responds in a linear way. This complicates design.

Variable reset band

A variable reset band is suggested as an alternative to band reset [25], utilizing the input derivative in predicting the next crossing. A reset occurs if, based on the first-order derivative of the error signal, a zero crossing is predicted in $h \geq 0$ seconds.

$$t_R = \{t \in \mathbb{R} \mid h\, \dot{\vec{q}}(t) + \vec{q}(t) = 0\} \tag{2-15}$$

This reset law reduces to the basic zero-crossing reset law when $h = 0$. It is shown that, for systems with time delays, variable reset bands can provide phase advantages [25]. A variable band responds linearly to input gain changes. A drawback of this reset law is that the input time derivative in the reset law may amplify noise influences.

2-2-2 Reset laws without developed frequency-domain description

Various other reset laws are presented in literature. No frequency-domain analysis was developed for these.

- *Cone reset*, also known as sector reset, enforces resets when the combination $(\vec{q}(t), \vec{z}(t))$ enters some area in the $(\vec{q}, \vec{z})$ plane. In the simplest form this area encompasses the second and fourth quadrant in this plane, but rotated or skewed versions also exist. Cone reset is mostly used because it simplifies Lyapunov-based stability results, such as $\mathcal{L}_2$ [40], $\mathcal{H}_2$ [53] or exponential $\mathcal{L}_p$ [54] stability. Robust [55] and MIMO implementations [42] have been developed.

  A frequency-domain analysis for this type of reset is developed for one specific reset element, being the Hybrid-Integrator-Gain-System [56], but not for a generic description as in Eq. (2-1).

- *Time scheduled reset.* Scheduling resets a-priori or online is an alternative to relating reset times to some signal property. Resets can for example be scheduled using adaptive iterative learning control [57], online optimization akin to finite-horizon Model Predictive Control [27, 31], or a priori using a solution much like an infinite horizon Linear Quadratic Regulator [31]. This approach has been demonstrated in practice [39, 58, 59].

- *Lyapunov-based resets* trigger a reset whenever some designed Lyapunov function is increasing. The reset is computed to cause a non-increase of the Lyapunov function and yields after-reset states from which the system can flow without increasing the Lyapunov function. This is used to prove global exponential stability for linear [55] and nonlinear [43] MIMO systems. A major advantage of this technique is that, no matter the system dimension, resets are based on a scalar condition.

- *Optimization-based* reset laws have been developed that consider MIMO RC with no pre-defined reset matrix structure [44]. An optimal reset law, reset equation and reset matrix is computed, based on some cost function. Often, matrices A_R, B_R, C_R and D_R are also designed by this optimization.

2-2-3 Stability

Stability of the CI was first shown using an approach based on a discrete-time indirect Lyapunov argument [60], which was valid solely for second-order plants with a CI. An important result of this stability proof was that it demonstrated that apparent stability indicated by standard phase- and gain margin criteria based on frequency-domain RC descriptions does not guarantee RCS stability. Such a description predicted some unstable systems to be stable, and vice versa. It follows that phase- and gain margin criteria are not sufficient for RC and that more formal stability conditions are needed.

A stability criterion tailored to SISO RC is the $\mathcal{H}_\beta$ condition, which is based on a Lyapunov argument. Before stating the $\mathcal{H}_\beta$ condition Eq. (2-3) needs to be restructured. Consider a SISO RC where the matrices A_{cl}, C_{cl}, $A_{\rho cl}$ and A_ρ can be structured as below. This factorization is always possible if $G(s)$ has no direct feed-through ($D_G = 0$).

$$A_{cl} = \begin{bmatrix} \bullet & \bullet \\ \bullet & A_R \end{bmatrix},\ C_{cl} = \begin{bmatrix} C_P & 0 \end{bmatrix},\ A_{\rho cl} = \begin{bmatrix} I_{n_{cl}-n_{ol}} & 0 \\ 0 & A_\rho \end{bmatrix},\ A_\rho = \begin{bmatrix} I_{\bar{\rho}} & 0 \\ 0 & A_\rho^* \end{bmatrix} \quad (2\text{-}16)$$

where $\bullet$ denotes any matrix. $A_\rho^* \in \mathbb{R}^{n_\rho \times n_\rho}$, $n_\rho \in \mathbb{N}_0$ is a matrix corresponding to the n_ρ resetting states. It follows that the number of non-reset states is $n_{\bar{\rho}} = n_{ol} - n_\rho$.

Theorem 2-2.1 ($\mathcal{H}_\beta$ - condition)**.** *An autonomous SISO RC system Eq. (2-4) with zero-crossing reset law is said to satisfy the $\mathcal{H}_\beta$ condition if $\exists\, \beta \in \mathbb{R}^{n_\rho}$, $P_\rho \in \mathbb{R}^{n_\rho \times n_\rho} > 0$ such that*

$$\mathcal{H}_\beta \triangleq \begin{bmatrix} \beta\, C_P & 0_{n_\rho \times n_{\bar{\rho}}} & P_\rho \end{bmatrix} (sI - A_{cl})^{-1} \begin{bmatrix} 0 \\ 0_{n_{\bar{\rho}} \times n_\rho} \\ I_{n_\rho \times n_\rho} \end{bmatrix}$$

is strictly positive real, $A_{\rho cl}$ is non-zero and [47]:

$$A_\rho^{\star T} P_\rho\, A_\rho^\star - P_\rho \leq 0$$

Strictly positive real requires there to $\exists\, \epsilon > 0$ for which (i) the elements of $H_\beta(s-\epsilon)$ are analytic in $\mathrm{Re}\,[s] > 0$ and (ii) $H_\beta^\dagger(s-\epsilon) + H_\beta(s-\epsilon) \geq 0$ for $\mathrm{Re}\,[s] > 0$ [11].

A SISO RC system Eq. (2-4) with zero-crossing reset law is quadratically stable if and only if it satisfies $\mathcal{H}_\beta$ condition [51]. Uniform exponential convergence and input-to-state convergence also hold if Eq. (2-4) satisfies $\mathcal{H}_\beta$ [36].

Chapter 3

Nonlinear frequency-domain analysis

An advantage of Reset Control (RC) is that, unlike most nonlinear controllers, it permits a frequency-domain description. However, as RC is nonlinear, it is not straightforward to obtain its frequency-domain description. Nonlinearity creates four different nonlinear effects complicating acquisition of a frequency description [61]:

1. *Intermodulation*: multiple input frequencies combining to new output frequencies.
2. *Desensitization*: output depends on input at a different frequency.
3. *Harmonics*: outputs at integer multiples of the input frequency.
4. *Input dependent gain*: gain depends on the input magnitude.

These four effects cause exact generic frequency-domain descriptions to be impossible for nonlinear systems. Take, for instance, the frequently used Bode plot, which links one input frequency to the same sole output frequency and does not consider input magnitudes. As such, these can model none of the four nonlinear effects. Approximations thus need to be made. Moreover, superposition is invalidated by these effects. This further complicates analysis.

Simply neglecting nonlinear effects is not satisfactory, as the nonlinear part of RC is intentional, designed for overcoming Bode's gain-phase relationship. Moreover, cases are known where RC destabilizes a stable Base Linear System (BLS) [62]. This cannot be detected if nonlinear effects are neglected. As such, it is imperative to have an accurate description of RC, including its nonlinear effects. Some well-established methods for modelling nonlinear systems as in Figure 3-1 are presented below [63]. Their advantages, shortcomings and applications are described, tailored to the RC case.

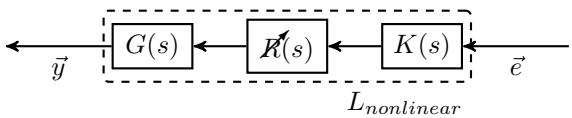

Figure 3-1: Open-Loop nonlinear system with RC $\vec{K}$ surrounded by linear systems K and G.

3-1 Nonlinear Bode plot

The nonlinear Bode plot is an extension to the conventional Bode plot. It captures input-dependent gain effects by adding a third axis, the input magnitude $\vec{q}_0$ [64]. This way, a 3D-surface Bode plot is obtained, depicting the response to an input $\vec{q}(t) = \vec{q}_0 \sin(\omega t)$. This method can only model input-dependent gain, not the other three nonlinear effects. RCs with a zero-crossing or variable reset band law do not have input-dependent gain [65]. It then follows that nonlinear Bode plots are not applicable, as they do not help in describing RC nonlinearity.

3-2 Base-Linear Approximator (BLA)

Through linearization the BLA is obtained, which is a classic LTI system. The BLA is computed such that the power spectrum of the time-domain output is, in least-squares sense, fitted to that of the real system. Typically, Gaussian Riemann equivalent noise with a set power spectrum is used as excitation signal [66]. Conditions for invariance and existence of the BLA are given by [64] and the references therein, as well as requirements for the excitation system design. An extension to MIMO has been developed [67].

This method is able to capture desensitization, intermodulation and harmonics to a limited extent, as their effects will be present in the time-domain signal the BLA is fitted to. Input-dependent gain can be approximated by running several experiments with different input magnitudes, and observing the differences using a nonlinear Bode plot. Because the BLA is an LTI approximation, it is unable to accurately represent strong non-linearities, restricting its application to systems with mostly linear behaviour [68]. The reset jump in RC is a strong nonlinearity, which thus cannot be captured in sufficient detail by the Best Linear Approximator (BLA) to be useful in further analysis.

3-3 Nonlinear Frequency Response Function (NFRF)

The NFRF provides a conservative upper bound on the magnitude frequency response for a sinusoidal input with parametric gain. Due to the upper bound a clear notion of phase no longer exists [64]. As this phase is crucial for loop-shaping, other methods are needed.

3-4 Volterra series

The Volterra series takes an approach to approximating a dynamic system similar to how a Taylor series approximates a function. Each of the series' terms, called Volterra kernels, represents an impulse response function. The Volterra series equals the standard impulse response if only one kernel is considered. It is capable of generating accurate descriptions of nonlinear systems, being the only method described in this chapter capable of accurately capturing all four nonlinear effects [64]. Taking the Fourier transform of the Volterra series yields the Generalized Frequency Response Function (GFRF) [69], which describes nonlinear systems in frequency-domain terms.

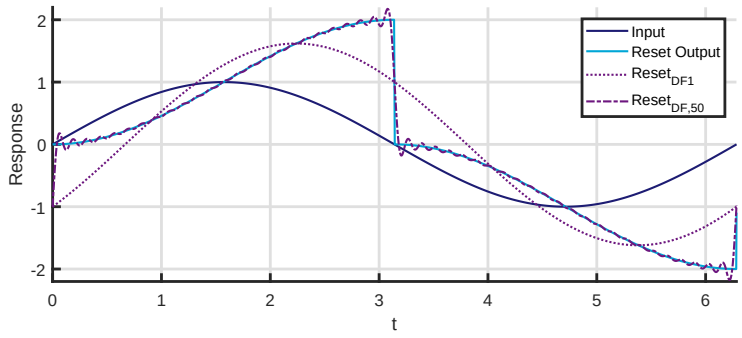

Figure 3-2: CI response u for sinusoidal e, along with the SIDF and HOSIDF approximations.

Identification of the GFRF is difficult, but has been performed successfully for several system classes. Examples are given by [64] and references therein, including impulsive systems with regular reset intervals [70]. It has, to the author's knowledge, not been computed for generic reset systems as treated in this report. Even if the GFRF would exist for the system classes considered here interpretation remains difficult. This problem is rooted in the fact that a n-th order Volterra kernel uses a n-th order input, whereas common frequency-domain methods only accept one input frequency. This gives Volterra Series the ability to be valid for almost any input, but makes it is often impractical to use.

3-5 Describing Function (DF) analysis

A method tailored to approximating nonlinear systems in a frequency-domain compatible way is DF analysis. This method assumes a predefined class of input signals, based on which the nonlinear system output is computed. A linear system is computed that minimizes its time-domain Mean-Square-Error relative to the actual system output [71]. The DF exists for various input forms, for example with Gaussian, sinusoidal or multi-sine inputs [20]. Extensions linking DF to Volterra Series are also available [72], then called the Generalized DF. This method still requires the difficult identification of Volterra kernels, but provides a more practical representation than Volterra series does, using a nonlinear Bode plot [72].

Most of the frequency-domain RC literature utilizes a Sinusoidal Input Describing Function (SIDF) analysis or related extensions, see e.g. [20, 60, 23], as this yields a description compatible to loop shaping. Other DFs, such as a Gaussian input DF [23], have been used occasionally. The SIDF methods will be presented next.

3-5-1 Sinusoidal Input Describing Function (SIDF) analysis

The input signal to SIDF, parametrized by frequency ω, is taken as $\vec{q}(t) = \vec{q}_0 \sin(\omega t)$. Input-dependent gain effects play no role for RC, which allows to ignore parameter $\vec{q}_0$ [65]. The SIDF approximation of the nonlinear system, $R_{DF,1}(\omega) = Z(\omega) \,/\, Q(\omega)$, coincides with that of a standard transfer function, $R(j\omega) = Z(j\omega) \,/\, Q(j\omega)$, making SIDF very convenient in practice. This enables SIDF solutions to easily integrate into conventional methods based on transfer

functions, such as loop shaping. Terms $Q(\omega)$ and $Z(\omega)$ correspond to the first terms in the Fourier series expansion of the RC in- and output, respectively.

A frequency-domain description requires the open-loop RC Eq. (2-1) to have a globally asymptotically stable $2\,\pi\,/\,\omega$ - periodic output $\vec{z}(t)$ when using a sinusoidal input $\vec{q}(t)$ with frequency $\omega > 0$. This is satisfied for all ω if and only if [65]:

$$\left|\lambda\left(A_\rho\, e^{A_R\,\delta}\right)\right| < 1, \quad \forall\,\delta \in \mathbb{R}^+ \tag{3-1}$$

where $\lambda(\bullet)$ denotes the eigenvalues of $\bullet$. The SIDFof SISO RC as in Eq. (2-1) satisfying Eq. (3-1) is given by [65]:

$$R_{DF}(\omega) \triangleq C_R\,(j\omega\,I - A_R)^{-1}(I + j\,\theta_D(\omega))\,B_R + D_R \tag{3-2}$$

Which uses the following definitions:

$$\begin{aligned}
\theta_D(\omega) &\triangleq -\frac{2\omega^2}{\pi}\,\Delta(\omega)\left[\Gamma_R(\omega) - \Lambda^{-1}(\omega)\right]\\
\Gamma_R(\omega) &\triangleq \Delta_R^{-1}(\omega)\,A_\rho\,\Delta(\omega)\,\Lambda^{-1}(\omega)\\
\Lambda(\omega) &\triangleq \omega^2\,I + A_R^2\\
\Delta(\omega) &\triangleq I + \mathrm{e}^{\frac{\pi}{\omega}\,A_R}\\
\Delta_R(\omega) &\triangleq I + A_\rho\,\mathrm{e}^{\frac{\pi}{\omega}\,A_R}
\end{aligned}$$

The DF approximation of an open-loop CI is given in Figure 3-2, illustrating how the SIDF approximates the nonlinear response using one sinusoid. This SIDF of corresponding CI is given below [19], showing that Clegg Integrator (CI) has a phase lag of $-\,38°$, thus having $-38 - (-\,90) = 52°$ less phase lag than a linear integrator, as mentioned in Section 1.

$$CI:\ R_{DF,1}(\omega) \;=\; \frac{1.62}{\omega}\,e^{-j38°} \tag{3-3}$$

The SIDF approximation is valid for a pure sinusoidal input only. This requirement, though restricting potential applications, enables the frequency-domain compatible solution acquired through SIDF. It is not possible to combine sinusoids to model a different input shape, as superposition does not hold. SIDF can capture input-dependent gain effects, but not other nonlinear effects [64]. In some cases, unstable systems are predicted to be stable through SIDF analysis [60]. This model is thus not perfect. Despite these drawbacks, DF analysis is the main method used by literature for analysing and describing RCs in a frequency-domain compatible manner.

An approximation of closed-loop behaviour for a system as in Figure 2-2 is given below. As it is based on DF analysis, it considers the first harmonic only, thus assuming that all higher harmonics are negligible. This assumption is alternatively phrased as assuming that the plant appending the RC has a sufficient low-pass filter characteristic. Moreover, a sinusoidal $\vec{q}(t)$ is still required, as per SIDF analysis. This cannot hold in a Reset Control System (RCS) as reset-induced harmonics are added to $\vec{q}(t)$ through feedback. This requirement $\vec{q}(t)$ also implies that the method assumes having two resets per period only, located at the zero crossings of $\vec{q}(t)$, an assumption known to not hold generally [30].

$$S_{DF} \;=\; (I + G(\omega)\,R_{DF}(\omega)\,K(\omega)) \tag{3-4}$$

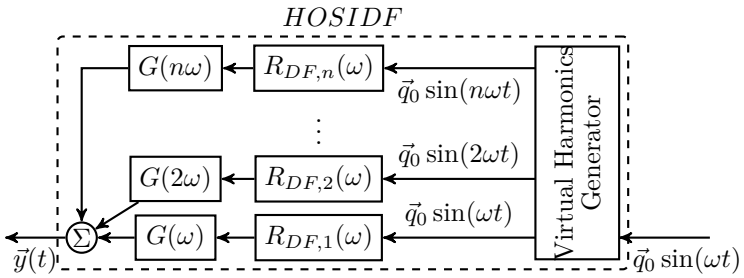

Figure 3-3: HOSIDF representation of $\vec{\mathcal{K}}$ for a sinusoidal input $\vec{q}(t)$, using a virtual harmonics generator. Adapted from [73].

Even though the SIDF signal in Figure 3-2 is seen to be a reasonable approximation of the actual response given the level of simplicity, a significant discrepancy between the actual output and the SIDF output is found. Literature mentions this modelling error [34, 28, 29], stating that, for precision applications, SIDF analysis is not satisfactory.

3-5-2 Higher Order Sinusoidal Input Describing Function (HOSIDF) analysis

HOSIDF enhances SIDF analysis by including the higher terms of the Fourier series analysis, thus modelling harmonics [74, 75]. HOSIDF can either be calculated or measured directly [76]. Figure 3-2 gives the HOSIDF approximation of a CI when the first 50 harmonics are evaluated. This illustrates the improved accuracy of HOSIDF over DF. HOSIDF becomes exact when an infinite number of harmonics is used, except for errors at discontinuities, caused by the Gibbs phenomenon.

Figure 3-3 visually represents HOSIDF analysis. The input, $\vec{q}(t) = \vec{q}_0 \sin(\omega t)$, is frequency-multiplied by the virtual harmonic generator. These harmonics are fed through the corresponding harmonics of the HOSIDF framework, $R_{DF,n}$, and inserted into the linear plant G at the corresponding harmonic frequencies. The output is acquired by summing the harmonic components.

As with SIDF, HOSIDF only holds for a pure sinusoidal input whilst Eq. (3-1) is satisfied. Superposition of two HOSIDF responses does not yield the response of RC to a multi-sine input, as shown by Figure 3-4. Large modelling errors may occur in those cases, as RC does not permit superposition.

The HOSIDF is computed for any general open-loop RC as in Eq. (2-1) [18]. The HOSIDF output $R_{DF,n}(\omega)$ of order n for any SISO RC as in Eq. (2-4) is given below:

$$R_{DF_n}(\omega) \triangleq \begin{cases} C_R \left(j\omega\, I - A_R\right)^{-1} \left(I + j\Theta_D(\omega)\right) B_R + D_R, & \text{for } n = 1 \\ C_R \left(j\omega\, I - A_R\right)^{-1} j\Theta_D\, B_R, & \text{for odd } n > 1 \\ 0, & \text{for even } n > 1 \end{cases} \tag{3-5}$$

The output $\vec{z}(t)$ as approximated by HOSIDF analysis is computed by:

$$\vec{z}(t) \approx \sum_{n=1}^{\infty} |R_{DF_n}(\omega)| \sin\left(n\omega t + \angle R_{DF_n}(\omega)\right) \tag{3-6}$$

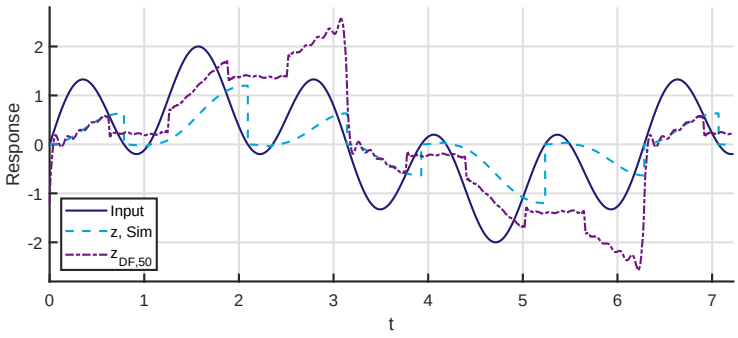

Figure 3-4: CI response $\vec{z}(t)$ for multi-sinusoidal $\vec{q}(t)$, along with a HOSIDF approximations using 50 harmonics, illustrating that HOSIDF is not valid for a multi-sine input.

In [18], no methodology was found to combine the harmonics computed by Higher Order Sinusoidal Input Describing Function (HOSIDF) in a way that enables loop shaping. Some preliminary tuning rules incorporating HOSIDF are given in [77, 78, 79], but no unified design approach is found so far.

3-5-3 Closed-Loop Describing Function (CL-DF) analysis

Recently a method was presented that extends HOSIDF to closed-loop [35], here referred to as the Closed-loop Describing Function (CL-DF). Starting from the HOSIDF definition, this method assumes (i) that there are exactly two reset instances per period, spaced π / ω_r apart, and (ii) that solely the first input harmonic of $Q(\omega)$ causes and affects resets. These assumptions are used to close the loop. This means that the closed-loop description is not exact, as the assumptions may introduce errors. The n-th order CL-DF ($S_{CLDF,n}$) is then, for an input-to-state convergent SISO RC with zero-crossing resets and a sinusoidal input $r_I(t)$ with frequency $\omega > 0$ defined by [35]:

$$S_{CLDF,n}(\omega) \triangleq \begin{cases} Sl_1(\omega), & n = 1 \\ -\, Sl_{bls}(n\omega)\, L_n(\omega)\, Sl_{1,n}(\omega), & n > 1 \end{cases} \tag{3-7}$$

Where the following definitions are used:

$$\begin{aligned} L_n(\omega) &\triangleq G(n\omega)\, R_{DF,n}(\omega)\, K(\omega) \\ Sl_n(\omega) &\triangleq (I + L_n(\omega))^{-1} \\ L_{bls}(\omega) &\triangleq G(\omega)\, R_L(\omega)\, K(\omega) \\ Sl_{bls}(\omega) &\triangleq (I + L_{bls}(\omega))^{-1} \\ Sl_{1,n}(\omega) &\triangleq (|Sl_1(\omega)| \exp(jn\angle Sl_1(\omega))) \end{aligned}$$

In practice there is often a dominant frequency component in the reference signal. This dominant mode has the largest amplitude and mostly determines when resets happen [56]. Other error signal components typically have far smaller amplitudes and therefore do not cause resets. It follows that, based on the dominant input frequency, it is often possible to

predict the reset times, and thus to know the nonlinearity. As such, the sinusoidal assumption on $\vec{q}(t)$ regularly works in closed-loop. Approximation Eq. (3-7) is shown to vastly outperform the DF approximation Eq. (3-4) in terms of precision [35].

3-5-4 Closed-loop Frequency Response (CL-FR)

The CL-FR is different from the other approaches mentioned, in that it computes the closed-loop response between a sinusoidal $\vec{r}_I(t)$ and plant output $y(t)$ for a stable Single Input Single Output (SISO) RC with zero crossing resets directly through numerical evaluation [36]. A MIMO expansion is not available. The requirement on a sinusoidal $\vec{r}_I(t)$ is less stringent than the requirement of DF and CL-DF on $\vec{q}(t)$, as $\vec{r}_I(t)$ can be designed. This method yields accurate results at the cost of not providing insight in how open-loop RC behaviour translates to RCS performance. This relation can only be induced empirically using Closed-loop Frequency Response (CL-FR), fundamental underlying principles are not obtained. As a result, it is not clear how RCs can be designed and tuned to obtain some desired behaviour.

3-6 Conclusion

Several methods for representing nonlinear systems in a frequency domain plot are discussed. Few of these are found capable of describing RC: BLA is too restrictive, NFRF provides no phase notion and GFRF requires the difficult identification of Volterra Kernels. This leaves DF based methods. RC literature has mostly used SIDF modelling, which ignores all harmonics. When harmonic effects must be modelled, e.g. to improve precision, the HOSIDF, CL-DF or CL-FR methods prevail. Only the latter two of these permit a closed-loop description.

The most accurate method, CL-FR, is numerical in nature, which enables acquisition of precise results at the cost of not showing which principles link open-loop RC design to closed-loop performance. The next best method, CL-DF, introduces assumptions to close the loop, which is thus not known exactly. This means that no method is found that provides fundamental understanding on how open-loop RC affects RCS behaviour.

Chapter 4

Reset implementations

Various reset elements have been developed in literature. Some base implementations are introduced first. Afterwards Reset Control (RC)s are presented that utilize a base RC element as part of their definition. Sample Base Linear System (BLS) and Describing Function (DF) responses of various controllers presented here are given in Figure 4-2.

4-1 Base reset elements

The first reset element, being the Clegg Integrator (CI), was developed by [19]. The CI is an integrator, which in its original formulation has full reset with a zero-crossing reset law. A generalized version, the Generalized CI (GCI), is obtained by permitting partial resets through reset parameter γ [65]. The GCI can be expressed as follows:

$$\text{GCI: } A_R = -0,\ B_R = 1,\ C_R = 1,\ D_R = 0, \quad A_\rho = \gamma \tag{4-1}$$

Several authors made contributions towards generalizing the GCI. A first suggestion was to replace the resetting integrator pole at $\omega = 0$ by a pole at a different frequency, ω_r. This creates a reset element with low-pass filter magnitude behaviour, known as the First Order Reset Element (FORE) [50]. Analogous to GCI, a generalized version is developed, the Generalized FORE (GFORE) [65]:

$$\text{GFORE: } A_R = -\omega_r,\ B_R = 1,\ C_R = 1,\ D_R = 0, \quad A_\rho = \gamma \tag{4-2}$$

For frequencies below ω_r, GFORE acts as a unity gain element and has a phase near zero, while beyond ω_r, it acts akin to a GCI.

A different reset element is obtained by resetting both poles of a second order low-pass filter, which gives the Second Order Reset Element (SORE) [80]. This is generalized to a Generalized SORE (GSORE) [34].

$$\text{GSORE: } \left[\begin{array}{c|c} A_R & B_R \\ \hline C_R & D_R \end{array}\right] = \left[\begin{array}{cc|c} 0 & 1 & 0 \\ -\omega_r^2 & -2\beta\omega_r & \omega_r^2 \\ \hline 1 & 0 & 0 \end{array}\right], \quad A_\rho = \gamma I \tag{4-3}$$

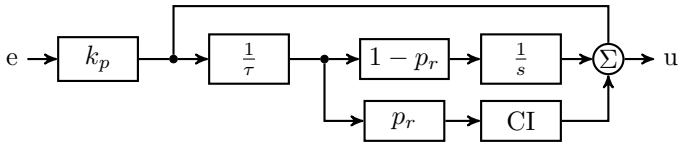

Figure 4-1: PI+CI controller diagram

Parameter β represents damping, which controls the rate at which the phase behaviour shifts from a gain element to a resetting low-pass filter around ω_r [78].

4-2 CI+PI

The PI+CI implementation is a generalization of the CI. A common problem with the CI is that it resets its value at each input zero crossing. However, if a non-zero integrator value is needed to achieve a zero error, limit cycles will occur [81].

The PI+CI overcomes the limit cycle problem by adding a linear Proportional Integral (PI) controller with gain k_p and integrator time constant τ_I in parallel to a CI [23, 82]. The linear integrator can provide the needed non-zero integrator value needed for steady-state, thus avoiding limit cycles. Reset percentage p_r determines how much reset control is used. This solution is visualized in Figure 4-1. A DF description is provided for PI+CI [83]:

$$PI + CI: \; R_{DF,1}(\omega) = k_p \left(1 + \frac{1-p_r}{\tau_I}\frac{1}{j\omega} + \frac{p_r}{\tau_I}\frac{1.62}{\omega}e^{-j38.1^\circ}\right) \tag{4-4}$$

In the limit case, where reset parameter $p_r = 1$, Eq. (4-4) equals the CI DF description given by Eq. (3-3), whereas for $p_r = 0$ it equals a PI. Tuning rules are developed by [30, 84]. The performance improvement of PI+CI over PI is shown in practice [82, 85], including process control by using robust design methods [52] and heat exchangers [62, 25].

This method is refined by tuning p_r online based on the error signal time derivative [83]. This way, the reset percentage can be increased for transitory responses and decreased during steady state operation. This approach is found to further reduce overshoot when compared to PI+CI control with fixed p_r.

4-3 Constant-in-gain Lead-in-phase (CgLp)

Recently, a novel RC structure has been developed, which unlike other RC implementations is aimed at providing phase lead instead of at reducing phase loss [32, 34]. Phase lead is achieved by taking a partially resetting GFORE or GSORE and adding a linear lead-lag filter of corresponding order, with its zero(s) coincident to the RC poles(s). This creates a RC with near-unity gain behaviour up to some tunable frequency ω_f, beyond which it acts as a low-pass filter. A tunable broadband phase lead around some design point is achieved. As such, this configuration is called the Constant in gain, Lead in phase (CgLp).

This phase lead combined with unity gain makes that CgLp can be conveniently used in combination with any linear controller. The linear gain is not affected, whilst the phase

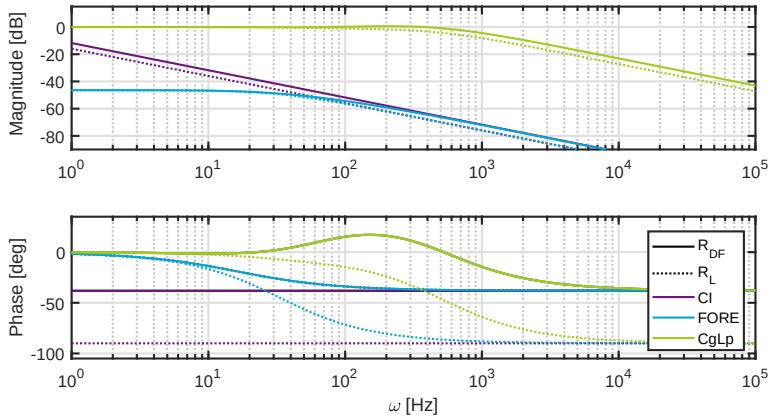

Figure 4-2: Bode Plot showing the RC response without resets, R_L, as well as the first harmonic response computed using DF analysis Eq. (3-5), R_{DF}, for the CI, FORE and FORE CgLp reset elements. Full reset is used for DF analysis.

behaviour is enhanced. Examples of CgLp improving performance over linear control are given by [86, 34].

The pole(s) of the lead-lag filter are placed at ω_f, which is therefore the corner frequency of the low-pass filter associated with CgLp. The lead-lag zero(s) are placed at ω_r. These zero(s) cancel the RC pole(s), placed at $\omega_{r\alpha} = \omega_r \,/\, \alpha$. Parameter α is used to account for pole shifts induced by the RC nonlinearity [34], ensuring that the resetting pole(s) and lead-lag zero(s) remain coincident.

4-3-1 First Order Reset Element CgLp

The FORE CgLp is given by the state-space matrices below [34]. the first and third harmonic responses as computed by Higher Order Sinusoidal Input Describing Function (HOSIDF) analysis are given by Figure 4-3.

$$\left[\begin{array}{c|c} A_R & B_R \\ \hline C_R & D_R \end{array}\right] = \left[\begin{array}{cc|c} -\omega_{r\alpha} & 0 & \omega_{r\alpha} \\ \omega_f & -\omega_f & 0 \\ \hline \omega_f \,/\, \omega_r & 1-\omega_f \,/\, \omega_r & 0 \end{array}\right], \quad A_\rho = \begin{bmatrix} \gamma & 0 \\ 0 & 1 \end{bmatrix} \tag{4-5}$$

4-3-2 Second Order Reset Element CgLp

The SORE CgLp uses damping parameter β. Figure 4-3 shows that this implementation has a considerably higher third harmonic than the FORE CgLp, while both provide the same

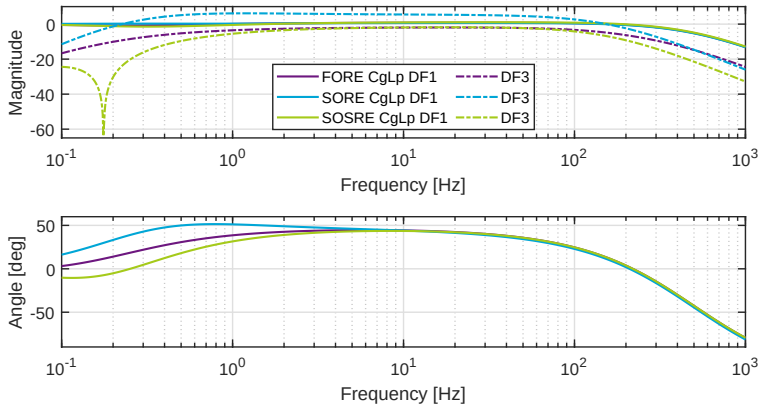

Figure 4-3: HOSIDF approximation of FORE (with additional low-pass filter to ensure all elements have similar gain responses), SORE and SOSRE based CgLp, with parameters tuned such that all give similar magnitude responses and the same phase lead at 10^1 Hz. The first and third harmonic signals, as predicted by HOSIDF analysis, are given.

amount of phase and have a very similar gain response. SORE CgLp is defined as:

$$\left[\begin{array}{c|c} A_R & B_R \\ \hline C_R & D_R \end{array}\right] = \left[\begin{array}{cccc|c} 0 & 1 & 0 & 0 & 0 \\ -\omega_{r\alpha}^2 & -2\beta\omega_{r\alpha} & 0 & 0 & \omega_{r\alpha}^2 \\ 0 & 0 & 0 & 1 & 0 \\ 1 & 0 & -\omega_f^2 & -2\omega_f & 0 \\ \hline \left(\frac{\omega_f}{\omega_r}\right)^2 & 0 & \omega_f^2\left(1-\left(\frac{\omega_f}{\omega_r}\right)^2\right) & \omega_f^2\left(\frac{2\beta}{\omega_r}-\frac{2\omega_f}{\omega_r^2}\right) & 0 \end{array}\right] \tag{4-6}$$

$$A_\rho = \mathrm{diag}\left(\gamma,\, \gamma,\, 1,\, 1\right)$$

4-3-3 Second Order Single Reset Element CgLp

The SOSRE is a novel CgLp implementation, based on a SORE CgLp, but resets one state, instead of two. Figure 4-3 shows that SOSRE has, at all frequencies, a lower third harmonic than the FORE and SORE CgLp implementations, whilst the gain and phase responses are similar. Moreover, SOSRE has one particular frequency, $\omega_{r\alpha}$, at which all harmonics except for the first equal zero. This ensures that, at $\omega_{r\alpha}$, SOSRE essentially behaves as a linear element, yet provides phase lead. This could, for example, be used to eliminate the harmonic responses to a resonance peak. SOSRE is described by the state-space matrices below [87].

$$\left[\begin{array}{c|c} A_R & B_R \\ \hline C_R & D_R \end{array}\right] = \left[\begin{array}{cccc|c} 0 & 1 & 0 & 0 & 0 \\ -\omega_{r\alpha}^2 & -2\beta\omega_{r\alpha} & 0 & 0 & 1 \\ 0 & 0 & 0 & 1 & 0 \\ \omega_{r\alpha}^2 & 0 & -\omega_f^2 & -2\omega_f & 0 \\ \hline \left(\frac{\omega_{r\alpha}\omega_f}{\omega_r}\right)^2 & 0 & \omega_f^2\left(1-\left(\frac{\omega_f}{\omega_r}\right)^2\right) & \omega_f^2\left(\frac{2\beta}{\omega_r}-\frac{2\omega_f}{\omega_r^2}\right) & 0 \end{array}\right] \tag{4-7}$$

$$A_\rho = \mathrm{diag}\left(1,\, \gamma,\, 1,\, 1\right)$$

4-4 Unstructured Reset Element

A different approach to RC is to leave the matrices A_R, B_R, C_R, D_R and A_ρ unstructured and let the entries in these matrices be defined through some optimization process. Often, controller design, reset law design and stability proofs combined in this optimization. MIMO RC literature often utilizes this unstructured approach, see e.g. [42, 44, 46, 43, 45]. Various reset laws are commonly combined with unstructured reset elements, such as cone reset [53], time scheduled reset [58, 27, 31], Lyapunov based reset [55] and unstructured reset [41].

This type of design typically relies on time-domain performance criteria and does not give insight to the designer. There are too many parameters to make manual tuning feasible. It follows that unstructured reset elements are not suitable for loop-shaping based design.

4-5 Conclusion

Various reset implementations have been discussed in this chapter. Chapter 1 mentioned that the precision motion industry prefers controller design using loop shaping. CgLp embeds quite naturally into that loop shaping framework, as it does not affect the gain whilst providing phase lead. As such, CgLp can be added to any linear controller designed through loop shaping, using its nonlinearity to boost performance. Because this work pursues a RC description suitable for loop shaping, which thus works well with CgLp reset element, it is chosen to evaluate results predominantly using CgLp controllers.

Chapter 5

Problem statement

Literature has shown that Reset Control (RC) can overcome fundamental limitations of linear controllers, whilst permitting design using the industry-preferred loop shaping methodology. This requires a frequency-domain description of RC. Several closed-loop frequency-domain descriptions are found in literature, yet none of these show the fundamental principles of how open-loop RC behaviour affects Reset Control System (RCS) performance. This limits the understanding of closed-loop RC behaviour. Having such a link would enable a better design and tuning of RC elements, as the impact of open-loop tuning on closed-loop performance would be better understood.

All frequency-domain RCS descriptions thus far were either based on a Describing Function (DF) analysis or from a direct closed-loop formulation. This thesis will investigate a different approach, taking the suggestion found in literature of modelling RC as a linear system with state-dependent impulse inputs. An advantage of this approach is that the model is linear, which potentially simplifies closed-loop computations. Whilst this does not inherently permit a frequency domain analysis, it is suggested to exploit the advantages of impulsive modelling for linking the open- to the closed-loop, and then attempt to obtain a frequency-domain description from there.

Chapter 6

Frequency-Domain Modelling of Reset Control Systems using an Impulsive Description

The main results obtained during this thesis are provided by the self-contained paper embedded in this chapter. A mathematical proof of the suggested modelling technique is provided, along with an elaborate discussion on the imposed prediction errors. Several validating examples are given, illustrating the use of this new methodology.

Frequency-Domain Modelling of Reset Control Systems using an Impulsive Description

R. N. Buitenhuis, N. Saikumar, S. H. HosseinNia
Precision and Microsystems Engineering & Delft Center for Systems and Control
Faculty of Mechanical Engineering, Delft University of Technology, The Netherlands

***Abstract*—The ever-increasing industry desire for improved performance makes linear controller design run into fundamental limitations. Nonlinear controllers such as Reset Control (RC) are needed to overcome these. RC is a promising candidate since, unlike other nonlinear methods, it easily integrates into the industry-preferred PID design framework. Thus far, RC has been analysed in the frequency domain either through Describing Function analysis or by direct closed-loop numerical computation. The former computes a simplified closed-loop RC response by assuming a sufficient low-pass behaviour. In doing so it ignores all harmonics, which literature has found to cause significant modelling errors. The latter gives a precise solution, but by its direct closed-loop computation does not clearly show how open-loop RC design translates to closed-loop performance. The main contribution of this work is aimed at overcoming these limitations by considering an alternative approach for modelling RC using state-dependent impulse inputs. This permits accurately computing closed-loop RC behaviour starting from an open-loop model, improving system understanding. A frequency-domain description for closed-loop RC is obtained, which is solved analytically by using several well-defined assumptions. This analytical solution is verified using a simulated high-precision stage, critically examining sources of modelling errors. The accuracy of the proposed method is further substantiated using controllers designed for various specifications.**

***Index Terms*—Reset control, Closed-loop, Nonlinear control, Impulsive modelling, Describing Function, Frequency domain, Precision control, Mechatronics, Motion control**

I. Introduction

Industry is continuously pushing control limitations by increasing performance demands. This causes requirements on bandwidth, disturbance rejection, noise attenuation and reference tracking to become increasingly stringent.

PID and other linear controllers are standard to industry, also to high-tech applications. This status is expected to prevail [1], because these controllers permit the industry preferred loop shaping design framework. Linear control is inherently subject to fundamental limitations, including the Bode gain-phase relationship [2]. This links bandwidth, disturbance rejection, noise attenuation and reference tracking. One cannot improve on some aspect without compromising on another. This design trade-off hinders the industry push for better performance.

This trade-off can only be overcome through nonlinear control, such as Reset Control (RC). RC is a promising candidate as various implementations embed nicely into the preferred loop-shaping framework. The first reset element was the Clegg Integrator (CI) [3], which is an integrator with its value resetting to zero whenever its input crosses zero. Through Describing Function (DF) analysis [4] it is shown that the CI inflicts 52° less phase lag than the in gain similar linear integrator, thus overcoming the Bode gain-phase relationship.

Several authors made contributions towards generalizing the CI. The first extension was by resetting a first-order low-pass filter known as the First Order Reset Element (FORE) [5] as opposed to an integrator. Additional tuning freedom was obtained by allowing states to be reset to non-zero values [6], [7]. Further developments enhancing design flexibility include second-order [8] and fractional-order [9] reset elements, as well as a second-order single-reset element [10]. Recently, the Constant-in-Gain Lead-in-phase (CgLp) RC implementation was proposed [11], designed to provide a broadband phase lead without affecting the gain. This property makes CgLp very suitable to be used in combination with any linear controller.

The reset law accompanying a reset element determines when a reset occurs. Traditionally, that is when the input of the reset element crosses zero [3]. Extensions [12], [13] and alternatives [14]–[19] are mentioned in literature, providing a variety of RC behaviours, tuning possibilities and stability results. These options are not considered here, as loop shaping based RC tuning is developed for zero-crossing reset laws only.

Several works have demonstrated that RC can push performance beyond limits attainable through linear control [20]–[23], for example by reducing overshoot [24] without affecting other specifications. RCs have been implemented in various control applications, including chemical processes [16], vibration isolation [25] and motion control systems [17], [26]–[28].

A frequency-domain description of RC is imperative for design using the loop shaping methodology preferred by industry. Most commonly, Describing Function (DF) analysis is utilized [7], which ignores all output harmonics. Despite this popularity, several works found DF to yield predictions in closed-loop that deviated widely from measurements [25], [29], [30]. An open-loop extension of DF analysis, incorporating harmonics [31], was used together with various assumptions to compute a novel closed-loop frequency-domain description, CL-DF [32]. Both DF and CL-DF assume the reset element to have a sinusoidal input, which at best holds approximately in closed-loop, whilst modelling two resets per input period only, known to not hold generally [26]. Another frequency-domain method was suggested by [33], which computes the closed-loop directly by solving numerically. This yields a precise solution at the cost of being computationally intensive and not providing a link between open- and closed-loop. None of the

available methods thus links open-loop RC design to closed-loop behaviour. Without such a link RC design is impaired, as it is not clear how open-loop RC tuning affects the closed-loop performance. This work aims to bridge this gap.

Some authors have mentioned that RC can be modelled as a linear controller with a train of state-dependent weighted impulse inputs [20], [34], [35], but this idea is only developed for a CI [20] and for certain nonlinear systems [36], not to find a frequency-domain solution. This work takes the impulsive RC modelling and generalizes that to obtain a closed-loop frequency domain description of RC systems, exploiting the resulting linear controller model, enabling accurate computation of closed-loop solutions in a way compatible to the industry preferred loop shaping methodology. This accurately connects open-loop RC design to its closed-loop performance.

The remainder of this paper is structured as follows. First, preliminaries of RC, including reset elements, definitions and stability results are given in Section II. Existing frequency domain analysis methods are presented and evaluated in Section III. Section IV introduces the impulse formulation for a general RC in open-loop, irrespective of reset law, followed by a closed-loop formulation. This impulsive modelling is then formulated in the frequency domain by Section V, which is essential for industry. Only systems with zero-crossing reset laws are considered from there on. This modelling is simplified in Section VI using clearly stated assumption to allow for an analytical solution. Section VII states the setup used to examine the effects of these assumptions in Section VIII. Afterwards, the accuracy is evaluated in Section IX by using controllers tuned for various specifications. Last, Section X concludes this paper.

II. Preliminaries on Reset Control

This section presents a generic reset control framework, along with related definitions and a stability theorem.

A. Reset control

Consider the generic setup given in Fig. 1, consisting of linear systems K and G surrounding reset element $\mathcal{R}$, with input $\vec{r}_I(t)$ and output $\vec{y}(t)$. Let $\vec{y}(t)$, $\vec{e}(t)$, $\vec{r}_I(t) \in \mathbb{R}^{m_y}$, $\vec{z}(t) \in \mathbb{R}^{m_z}$ and $\vec{q}(t) \in \mathbb{R}^{m_q}$, with m_y, m_z, $m_q \in \mathbb{N}$.

Definition 1 (Reset Controller (RC))**.** *Let a reset controller $\mathcal{R}$: $\vec{q}(t) \mapsto \vec{z}(t)$ be defined by dimension-compatible matrices A_R, B_R, C_R, D_R, states $\vec{x}(t) \in \mathbb{R}^{n_{ol}}$, $n_{ol} \in \mathbb{N}$ and reset matrix A_ρ. A reset occurs when $t = t_r \in t_R$, where t_R is the set of all reset instants. The following equations describe $\mathcal{R}$:*

$$\mathcal{R}: \begin{cases} \dot{\vec{x}}(t) = A_R\,\vec{x}(t) + B_R\,\vec{q}(t), & t \notin t_R \\ \vec{x}^+(t) = A_\rho\,\vec{x}(t), & t \in t_R \\ \vec{z}(t) = C_R\,\vec{x}(t) + D_R\,\vec{q}(t) \end{cases} \tag{1}$$

After-reset states are denoted by $\vec{x}^+$. Description (1) *permits a MIMO RC and an arbitrary reset law.*

Definition 2 (Reset types)**.** *In literature, reset matrix $A_{\rho,k}$ is generally diagonal: $A_\rho = \operatorname{diag}(\gamma_1, \ldots, \gamma_{n_{ol}})$, with values $\gamma_i \in [-1, 1]$, $i \in \{1, \ldots, n_{ol}\}$. Define the following:*

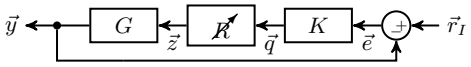

Fig. 1. Block diagram of a reset control system with input $\vec{r}_I$ and output $\vec{y}$, consisting of reset element $\mathcal{R}$ surrounded by linear systems K and G.

- *Fully resetting RC: $\gamma_i \in \{0, 1\}$, $\forall\, i$ and $\exists\, i \mid \gamma_i = 0$.*
- *Partially resetting RC: A_ρ where $\exists\, i \mid \gamma_i \notin \{0, 1\}$.*

Definition 3 (Reset control system (RCS))**.** *Let the closed-loop reset control system $\mathcal{T}$: $\vec{r}_I(t) \mapsto \vec{y}(t)$ as in Fig. 1 be defined by dimension-compatible matrices A_{cl}, B_{cl}, C_{cl}, D_{cl} and $A_{\rho cl}$, with states $\vec{x}_{cl} \in \mathbb{R}^{n_{cl}}$, $n_{cl} \in \mathbb{N}$. $\mathcal{T}$ is described by:*

$$\mathcal{T}: \begin{cases} \dot{\vec{x}}_{cl}(t) = A_{cl}\,\vec{x}_{cl}(t) + B_{cl}\,\vec{r}_I(t), & t \notin t_R \\ \vec{x}^+_{cl}(t) = A_{\rho cl}\,\vec{x}_{cl}(t), & t \in t_R \\ \vec{y}(t) = C_{cl}\,\vec{x}_{cl}(t) + D_{cl}\,\vec{r}_I(t) \end{cases} \tag{2}$$

RCs as in (1), (2) are SISO if $m_y = 1$, $m_z = 1$ and $m_y = 1$.

Definition 4 (Base-Linear System (BLS))**.** *The base-linear system of Fig. 1 is obtained by removing all resets from the RCS, rendering it linear. The BLS sensitivity function $S_L(s)$ and complementary sensitivity function $T_L(s)$ are given by:*

$$S_L(s) \triangleq (I + G(s)\,R_L(s)\,K(s))^{-1} \tag{3}$$

$$T_L(s) \triangleq G(s)\,R_L(s)\,K(s)\,(I + G(s)\,R_L(s)\,K(s))^{-1} \tag{4}$$

where R_L denotes $\mathcal{R}$ without reset action:

$$R_L(s) \triangleq C_R\,(sI - A_R)^{-1}\,B_R + D_R \tag{5}$$

Definition 5 (Zero-crossing law)**.** *A SISO RC with zero crossing law resets when $t_R = \{t \in \mathbb{R} \mid \vec{q}(t) = 0\}$.*

Definition 6 (Time regularization)**.** *Time regularization suppresses any reset if $t < t_p + \tau$, with $\tau > 0$ a tunable parameter and t_p the last occurred reset time instant [14].*

RC systems can be prone to deadlock, beating and Zeno behaviour [26], causing solutions to be ill-defined. This behaviour can be avoided by using time regularization [14], [37]. Any discrete-time implementation inherently features time regularization, having τ equal to the sampling time [38]. As most practical implementations are discretized it is chosen to disregard deadlock, beating and Zenoness in this paper. It is assumed that solutions to (2) are well-defined.

B. Reset elements

Various reset elements are presented in literature. Several relevant ones are given below, all of them most commonly using zero-crossing reset laws. Fig. 2 gives the Bode plots for these, depicting their base-linear and first harmonic responses.

1) Generalized Clegg Integrator (GCI): The Clegg Integrator [3] is a resetting integrator, which can be generalized by allowing partial resets through γ. The GCI is defined with:

$$A_R = 0,\ B_R = 1\ C_R = 1,\ D_R = 0,\ A_\rho = \gamma \tag{6}$$

2) Generalized First Order Reset Element (GFORE): FORE is a RC based on a first order low-pass filter. It was first given by [5] and later generalized by permitting partial resets [17]. A GFORE with corner frequency ω_r is given as:

$$A_R = -\omega_r,\ B_R = \omega_r,\ C_R = 1,\ D_R = 0,\ A_\rho = \gamma \quad (7)$$

3) Constant in gain, Lead in phase (CgLp): CgLp is a novel RC element providing broadband phase lead while maintaining unit gain [27]. This characteristic enables CgLp to be combined with any linear controller, increasing phase without inflicting gain alterations. This is achieved by merging a GFORE, having pole $\omega_{r\alpha}$, with a lead-lag filter, having pole ω_f and zero $\omega_r = \omega_{r\alpha}\,\alpha$. Parameter α corrects for the GFORE pole shift induced by reset nonlinearity [29], ensuring that the GFORE pole remains coincident with the lead-lag zero.

$$\left[\begin{array}{c|c} A_R & B_R \\ \hline C_R & D_R \end{array}\right] = \left[\begin{array}{cc|c} -\omega_{r\alpha} & 0 & \omega_{r\alpha} \\ \omega_f & -\omega_f & 0 \\ \hline \omega_f \,/\, \omega_r & 1-\omega_f \,/\, \omega_r & 0 \end{array}\right] \quad (8)$$
$$A_\rho = \operatorname{diag}[\gamma,\, 0]$$

C. Stability

Consider a SISO RCS where the matrices A_{cl}, C_{cl}, $A_{\rho cl}$ and A_ρ can be structured as below. This factorization is always possible if $G(s)$ has no direct feed-through.

$$A_{cl} = \begin{bmatrix} \bullet & \bullet \\ \bullet & A_R \end{bmatrix} \qquad A_{\rho cl} = \begin{bmatrix} I_{n_{cl}-n_{ol}} & 0 \\ 0 & A_\rho \end{bmatrix}$$
$$C_{cl} = \begin{bmatrix} C_P & 0 \end{bmatrix} \qquad A_\rho = \begin{bmatrix} I_{\bar{\rho}} & 0 \\ 0 & A_\rho^* \end{bmatrix}$$

where $\bullet$ denotes any matrix. $A_\rho^* \in \mathbb{R}^{n_\rho \times n_\rho}$, $n_\rho \in \mathbb{N}_0$ is a matrix corresponding to the n_ρ resetting states. It follows that the number of non-reset states is $n_{\bar{\rho}} = n_{ol} - n_\rho$.

Theorem 1 ($\mathcal{H}_\beta$ - condition)**.** *An autonomous SISO RCS* (2) *with zero-crossing reset law is said to satisfy the $\mathcal{H}_\beta$ condition if $\exists\, \beta \in \mathbb{R}^{n_\rho}$, $P_\rho \in \mathbb{R}^{n_\rho \times n_\rho} > 0$ such that*

$$\mathcal{H}_\beta \triangleq \begin{bmatrix} \beta\, C_P & 0_{n_\rho \times n_{\bar{\rho}}} & P_\rho \end{bmatrix} (sI - A_{cl})^{-1} \begin{bmatrix} 0 \\ 0_{n_{\bar{\rho}} \times n_\rho} \\ I_{n_\rho \times n_\rho} \end{bmatrix}$$

is strictly positive real, $A_{\rho cl}$ is non-zero and [39]:

$$A_\rho^{\star T} P_\rho\, A_\rho^\star - P_\rho \leq 0$$

The SISO RCS (2) *with a zero-crossing reset law is quadratically stable if and only if it satisfies $\mathcal{H}_\beta$ condition [6]. Uniformly exponential convergence and input-to-state convergence also hold if* (2) *satisfies $\mathcal{H}_\beta$ [33].*

III. Frequency-Domain Describing Methods

The available frequency-domain methods for describing RCs are given next. These methods are applicable to zero-crossing resets only. Table I provides an overview of the various assumptions used by methods describing RCSs.

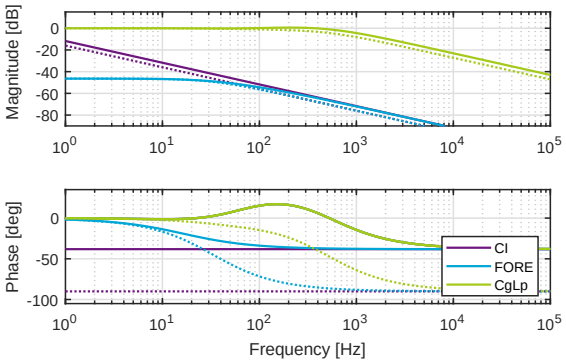

Fig. 2. Bode Plot with the linear, R_L (dashed line), and first harmonic, R_{DF} (solid line), responses for a CI, FORE and CgLp reset element. The harmonic responses, computed through DF analysis (10), use full reset ($\gamma = 0$).

A. DF and HOSIDF analysis

Analysing SISO RCs in the frequency domain is typically performed using Sinusoidal Input Describing Function (DF) analysis, which computes the first harmonic in the Fourier series expansion of $\vec{z}(t)$. This requires (1) to have a globally asymptotically stable $2\,\pi\,/\,\omega$ - periodic output $\vec{z}(t)$, for a sinusoidal input $\vec{q}(t)$ with frequency $\omega > 0$. This happens if and only if [7]:

$$\left|\lambda\left(A_\rho\, e^{A_R\,\delta}\right)\right| < 1, \quad \forall\, \delta \in \mathbb{R}^+ \quad (9)$$

DF analysis is extended to Higher Order Sinusoidal Input Describing Function (HOSIDF) analysis by also considering the harmonics in the Fourier series expansion of $\vec{z}(t)$. [31].

Theorem 2 (DF [7], HOSIDF [31])**.** *The n-th order HOSIDF for an open-loop SISO RC* (1) *satisfying* (9) *with zero-crossing resets and a sinusoidal input with frequency $\omega > 0$ is computed by:*

$$R_{DF,n}(\omega) \triangleq C_R(j\omega n\, I - A_R)^{-1} \times \begin{cases} (I + j\theta_D(\omega))\ B_R + D_R, & n = 1 \\ j\theta_D(\omega)\, B_R, & \textit{odd } n > 1 \\ 0, & \textit{even } n > 1 \end{cases} \quad (10)$$

Where:
$$\theta_D(\omega) \triangleq -\frac{2\omega^2}{\pi}\,\Delta(\omega)\left[\Gamma_R(\omega) - \Lambda^{-1}(\omega)\right]$$
$$\Gamma_R(\omega) \triangleq \Delta_R^{-1}(\omega)\, A_\rho\, \Delta(\omega)\, \Lambda^{-1}(\omega)$$
$$\Lambda(\omega) \triangleq \omega^2\, I + A_R^2$$
$$\Delta(\omega) \triangleq I + e^{\frac{\pi}{\omega} A_R}$$
$$\Delta_R(\omega) \triangleq I + A_\rho\, e^{\frac{\pi}{\omega} A_R}$$

DF analysis equals (10) *for $n = 1$. The corresponding DF-approximated sensitivity function for* (2) *is:*

$$S_{DF}(\omega) = \left(I + G(\omega)\, R_{DF,1}(\omega)\, K(\omega)\right)^{-1} \quad (11)$$

This approximation assumes (i) that all harmonics are negligible in closed-loop, (ii) $\vec{q}(t)$ to be sinusoidal, which (iii) implicitly assumes the RCS to have two resets per input period.

TABLE I
OVERVIEW OF ASSUMPTIONS EXISTING METHODS FOR COMPUTING FREQUENCY-DOMAIN CLOSED-LOOP RC BEHAVIOUR USE. EMPTY FIELDS INDICATE THAT THERE ARE NO ASSUMPTIONS.

	DF	CL-DF	CL-FR
Modelled resets per period:	2	2	
Signals assumed sinusoidal:	$\vec{q}(t)$	$\vec{r}_I(t)$, $\vec{q}(t)$	$\vec{r}_I(t)$
Resets assumed at:		$\vec{q}_{DF,1} = 0$	
Neglects harmonics:	Yes		

HOSIDF analysis models the RC response in open-loop for input $\vec{q}(t) = \vec{q}_0 \sin(\omega t)$, as shown in Fig. 3.

$$Z(\omega) = \sum_{n=1}^{\infty} R_{DF,n}(\omega)\, Q(n\omega) \Leftrightarrow \not{R}(s)\, Q(s) \tag{12}$$

$$\vec{z}(t) = \sum_{n=1}^{\infty} |R_{DF,n}\, \vec{q}_0|\ \mathrm{e}^{j\angle R_{DF,n} + jn\omega t} \tag{13}$$

Assumptions for S_{DF} do not hold. Reset induces harmonics, which through feedback prevent $\vec{q}(t)$ from being fully sinusoidal. RCSs often have more than two resets per period [26].

B. Closed-loop HOSIDF analysis

Recently a method was presented that extends HOSIDF to RCS [32]. Starting from open-loop HOSIDF, this method assumes (i) that there are exactly two resets per input period, spaced π / ω_r apart, and (ii) that solely the first harmonic, $Q(\omega) = K(\omega)\, S_{DF,1}(\omega)$, causes and affects resets.

Theorem 3 (Closed-loop HOSIDF (CL-DF) [32])**.** *The n-th order CL-DF for an input-to-state convergent SISO RC* (1) *satisfying* (9)*, having zero-crossing resets and a sinusoidal input with frequency $\omega > 0$, is defined by:*

$$S_{DF_{CL},n}(\omega) \triangleq \begin{cases} Sl_1(\omega), & n = 1 \\ -\, Sl_{bls}(n\omega)\, L_n(\omega)\, Sl_{1,n}(\omega), & n > 1 \end{cases} \tag{14}$$

Where:

$$\begin{aligned} L_n(\omega) &\triangleq G(n\omega)\, R_{DF,n}(\omega)\, K(\omega) \\ Sl_n(\omega) &\triangleq (I + L_n(\omega))^{-1} \\ L_{bls}(\omega) &\triangleq G(\omega)\, R_L(\omega)\, K(\omega) \\ Sl_{bls}(\omega) &\triangleq (I + L_{bls}(\omega))^{-1} \\ Sl_{1,n}(\omega) &\triangleq (|Sl_1(\omega)|\, \mathrm{e}\,(jn\angle Sl_1(\omega))) \end{aligned}$$

CL-DF uses assumptions to close the loop, thus not providing an exact link between RC design and RCS performance, yes improves upon S_{DF} as it includes harmonics.

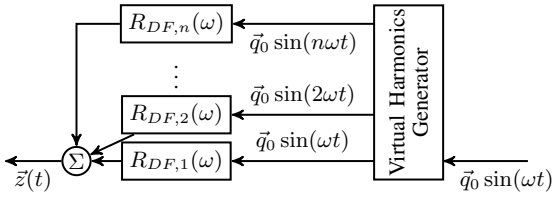

Fig. 3. HOSIDF representation of $\not{R}$ for a sinusoidal input $\vec{q}(t)$, using a virtual harmonics generator. Adapted from [40].

C. Closed-Loop Frequency Response (CL-FR)

CL-FR is different from the other approaches mentioned, as it analyses a stable SISO RCS with zero crossing resets and a sinusoidal input directly through numerical evaluation [33]. This direct closed-loop computation yields accurate results at the cost of not providing insight in how open-loop RC design translates to RCS performance.

IV. IMPULSE RESET MODELLING

RCs are modelled as linear systems with a state-dependent timed impulse train input, a description first mentioned by [20]. The following theorem will prove that any general open-loop RC as in (1) is equivalent to a linear system with impulse inputs. This result is then used to acquire the RCS description.

Theorem 4 (Impulse-based RC modelling)**.** *The states $\dot{\vec{x}}(t)$ of any open-loop RC as in* (1) *are computed as:*

$$\dot{\vec{x}}(t) = A_R\, \vec{x}(t) + B_R\, \vec{q}(t) + \sum_{t_r \in t_R} (A_\rho - I)\, \vec{x}(t)\, \delta(t_r) \tag{15}$$

Proof. Consider an open-loop RC (1). The after-reset states $\vec{x}^+(t)$ at $t = t_r \in t_R$ are given by:

$$\vec{x}^+(t_r) = A_\rho\, \vec{x}(t_r) \equiv I\, \vec{x}(t_r) + (A_\rho - I)\, \vec{x}(t_r)$$

The term $(A_\rho - I)\, \vec{x}(t_r)$ is added at a reset, $t = t_r$. This can be modelled as a Heaviside step function $H(t_r)$. Doing so, differentiating and substituting $\dot{\vec{x}}(t)$ from (1) gives:

$$\begin{aligned} \vec{x}^+(t_r) &= \vec{x}(t_r) + (A_\rho - I)\, \vec{x}(t_r)\, H(t_r) \\ \dot{\vec{x}}^+(t_r) &= \dot{\vec{x}}(t_r) + (A_\rho - I)\, \vec{x}(t_r)\, \delta(t_r) \\ &= A_R \vec{x}(t_r) + B_R\, \vec{q}(t_r) + (A_\rho - I)\, \vec{x}(t)\, \delta(t_r) \end{aligned}$$

where $\delta(t)$ is the Dirac delta function. It is noted that the reset only changes $\dot{\vec{x}}(t)$ at t_r. At $t \notin t_R$, the states thus flow according to R_L. Summing over $t_r \in t_R$ yields the result. □

Corollary 4.1 (RC Laplace formulation)**.** *The output and states of* (1) *are given in the Laplace domain by:*

$$Z(s) = R_L(s)\, Q(s) + R_\delta(s) \sum_{t_r \in t_R} \vec{x}(t_r)\, \mathrm{e}^{-\,t_r\, s} \tag{16}$$

$$X(s) = R_L^X(s)\, Q(s) + R_\delta^X(s) \sum_{t_r \in t_R} \vec{x}(t_r)\, \mathrm{e}^{-\,t_r\, s} \tag{17}$$

where $R_\delta(s)$ is given by $R_\delta(s) \triangleq C_R\, (sI - A_R)^{-1}\, (A_\rho - I)$, transfer functions to $X(s)$ by $R_L^X(s) \triangleq (sI - A_R)^{-1}\, B_R$ and $R_\delta^X(s) \triangleq (sI - A_R)^{-1}\, (A_\rho - I)$.

Proof. Start by writing (15) in the Laplace domain:

$$sX(s) = A_R\, X(s) + B_R\, Q(s) + \sum_{t_r \in t_R} (A_{\rho,k} - I)\ \vec{x}(t_r)\, \mathrm{e}^{-\,t_r\, s}$$

Vector $\vec{x}(t_r)$ is evaluated at a specific time instant and can therefore be treated as a constant. Rewriting for $X(s)$ and substitution of $R_L^X(s)$ and $R_{\delta,k}^X(s)$ gives (17). Solving for $X(s)$, using (1) to write $Z(s) = C_R\, X(s) + D_R\, Q(s)$ and afterwards inserting (17), $R_L(s)$ and $R_\delta(s)$ yields (16). □

Corollary 4.2 (Closed-loop $E(s)$)**.** *The RCS error response $E(s)$ is computed to be the BLS summed by impulse responses:*

$$E(s) = S_L(s)\,R_I(s) - S_L(s)\,G(s)R_\delta(s)\sum_{t_r\in t_R}\vec{x}(t_r)\,\mathrm{e}^{-\,t_r\,s} \quad (18)$$

The second term is denoted as $E_\delta(s,t_r)$ to simplify notation, giving $E(s) = S_L(s)\,R_I(s) + \sum_{t_r\in t_R} E_\delta(s,t_r)$.

Proof. From Fig. 1 it follows that $Q(s) = K(s)\,E(s)$. Together with (16) this gives:

$$Z(s) = R_L(s)\,K(s)\,E(s) + R_\delta(s)\sum_{t_r\in t_R}\vec{x}(t_r)\,\mathrm{e}^{-\,t_r\,s}$$

In Fig. 1 it is seen that $E(s) = R_I(s) - G(s)\,Z(s)$:

$$E(s) = R_I(s) - G(s)\,R_L(s)\,K(s)\,E(s) - G(s)R_\delta(s)\sum_{t_r\in t_R}\vec{x}(t_r)\,\mathrm{e}^{-\,t_r\,s}$$

The result follows by solving for $E(s)$ and inserting (3). □

Corollary 4.3 (Closed-Loop $X(s)$)**.** *The closed-loop states of $\mathcal{H}(s)$ are computed to be:*

$$X(s) = R_L^X(s)\,K(s)\,S_L(s)\,R_I(s) - R_L^X(s)\,K(s)\,S_L(s)\,G(s)R_\delta(s)\sum_{t_r\in t_R}\vec{x}(t_r)\,\mathrm{e}^{-\,t_r\,s} + R_\delta^X(s)\sum_{t_r\in t_R}\vec{x}(t_r)\,\mathrm{e}^{-\,t_r\,s} \quad (19)$$

Proof. Take (17) and substitute $Q(s)$ with $K(s)E(s)$, using the RCS error $E(s)$ as defined by (18). □

Remark 4.1. *All results based on Theorem 4 require uniqueness and existence of a solution to* (1) *only. No requirements on input types, system dimensions, stability or reset types are needed to compute the response. The RCS behaviour can thus be computed exactly, given that reset times t_R and corresponding $\vec{x}(t_r)$ are known.*

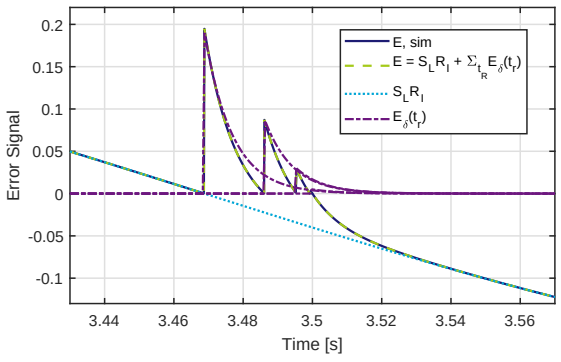

Fig. 4. Detail on a series of resets around a zero crossing for a FORE closed-loop reset system as given by Example 4.1, using $\vec{r_I} = \sin(t\,/\,2\pi)$. The components of (18), their sum and the simulated response are shown.

Remark 4.2. *These results accept MIMO systems. However, MIMO reset control implementations often use multiple reset conditions [41], [42]. The obtained results permit a straightforward extension to an arbitrary number of reset conditions, where each of these corresponds to some reset matrix and resets at some subset of reset times t_R. It follows that these results can describe closed-loop MIMO RC behaviour.*

Example 4.1. *Consider a SISO FORE in closed-loop with a zero-crossing reset law, using $K(s) = 100$, $G(s) = 1$, $\omega_r = 25$ and $\gamma = 0$. Fig. 4 illustrates in time-domain how the linear response $S_L(s)\,R_I(s)$ and impulse responses $E_\delta(s,t_r)$ are summed to create* (18)*, which equals the simulated response.*

Remark 4.3. *Result* (18) *adds insight into RCs by linking how open-loop RC design affects RCS performance. In closed-loop the RC behaves as the BLS, but having impulse responses with tunable weighting $I - A_\rho$ added to it. Thus, the closed-loop can be estimated by considering the BLS and weighted impulse response based on the open-loop design. This analysis allows to explain in a different way why RCs are found to have a lower sensitivity peak than their corresponding BLSs [11]. From* (18) *it follows that this must occur because impulse responses partially cancel out the BLS error.*

V. Periodic Results

A precise RCS solution is obtained if the values t_R and $\vec{x}(t_r)$ are computed. It might be possible to obtain these in a numerical manner to yield a precise and generic solution, without needing further assumptions or setup requirements. However, such a solution does not generally permit a frequency-domain description, while having that is imperative for loop shaping. Periodicity is used to rewrite (18) in frequency-domain terms for zero-crossing reset systems.

A. Periodicity of RC

Theorem 5 (Periodic RC [33])**.** *If a SISO RCS* (2) *with zero-crossing law (a) has A_{cl} Hurwitz, (b) satisfies $\mathcal{H}_\beta$, and (c) has a purely sinusoidal $\vec{r}_I(t)$ with frequency ω, then, in steady-state, the RCS has (i) a unique periodic solution $\vec{x}_{cl}(t)$, $\vec{y}(t)$ with period $2\,\pi\,/\,\omega$, (ii) all even harmonics equal to zero, and (iii) a periodic pattern of reset instants with period $\pi\,/\,\omega$.*

Remark 5.1. *[33] Theorem 5 also holds if, instead of* (2) *satisfying $\mathcal{H}_\beta$, it is Uniformly Bounded Steady-State.*

Example 5.1. *Fig. 5 gives the steady-state time response of the RCS given by Example 4.1 to a 1 Hz sinusoidal reference. This setup meets the requirements of Theorem 5, which therefore predicts that reset instants have a $\pi\,/\,\omega$ periodic pattern. Fig. 5 illustrates that this holds.*

Corollary 5.1 (Periodic impulse response)**.** *Define a new set of reset times, $t = t_r \in t_\rho$ with $t_\rho = \{t \in t_R \mid t \in [0,\ \pi\,/\,\omega\rangle\}$. If Theorem 5 is satisfied the following simplification holds:*

$$R_\delta(s)\sum_{t_r\in t_R}\vec{x}(t_r)\,\mathrm{e}^{-\,t_r\,s} = \sum_{t_r\in t_\rho}\xi\left(s,t_r,\vec{x}(t_r)\right) \quad (20)$$

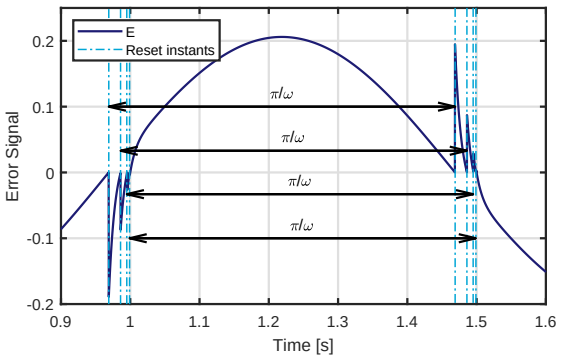

Fig. 5. Time response of a FORE RCS system satisfying Theorem 5 with indicated time intervals between resets, for $\vec{r}_I = \sin(t\,/\,2\pi)$.

The term $\xi(s, t_r, \vec{x}(t_r))$ is by definition $2\,\pi\,/\,\omega_r$ periodic:

$$\xi(s, t_r, \vec{x}(t_r)) \triangleq R_\delta(s) \sum_{p\,\in\,2\mathbb{Z}} \Big(\vec{x}(t_r)\,\mathrm{e}^{-\,(t_r + p\frac{\pi}{\omega})\,s} - \vec{x}(t_r)\,\mathrm{e}^{-\,(t_r + (p+1)\frac{\pi}{\omega})\,s} \Big)$$

Proof. If Theorem 5 is satisfied it reset instants are $\pi\,/\,\omega_r$ periodic. As such, t_ρ can be used to represent all resets, $\cup_p \{t_\rho + p\,\pi\,/\,\omega_r\} = t_R,\ p \in \mathbb{Z}$. These are thus equal:

$$\sum_{t_r \in t_R} \vec{x}(t_r)\,\mathrm{e}^{-\,t_r\,s} = \sum_{t_r \in t_\rho} \sum_{p \in \mathbb{Z}} \vec{x}(t_r + p\,\pi\,/\,\omega)\,\mathrm{e}^{-\,(t_r + p\frac{\pi}{\omega})\,s}$$

Using Theorem 5, $\vec{x}(t_r + p\,\pi\,/\,\omega)$ can be expressed in $\vec{x}(t_r)$.

$$\sum_{t_r \in t_R} \vec{x}(t_r)\,\mathrm{e}^{-\,t_r\,s} = \sum_{t_r \in t_\rho} \sum_{p\,\in\,2\mathbb{Z}} \Big(\vec{x}(t_r)\,\mathrm{e}^{-\,(t_r + p\frac{\pi}{\omega})\,s} - \vec{x}(t_r)\,\mathrm{e}^{-\,(t_r + (p+1)\frac{\pi}{\omega})\,s} \Big)$$

Pre-multiplication with $R_\delta(s)$ and inserting $\xi(s, t_r, \vec{x}(t_r))$ as defined above completes the proof. □

B. Impulse HOSIDF analysis

HOSIDF describes the open-loop response, as given by (15), thus modelling both the impulse responses and the linear response to the input. For convenience in further derivations a new HOSIDF definition is proposed which solely models the impulse responses. This new definition requires a sinusoidal input, as conventional for HOSIDF.

Definition 7 (Impulse HOSIDF)**.** *The n-th order impulse HOSIDF analysis for a SISO RC* (1) *satisfying* (9) *with zero-crossing resets, given a sinusoidal input with frequency $\omega > 0$, is defined as a function of input matrix $B^\star$:*

$$R^\star_{DF,n}(\omega, B^\star) \triangleq C_R\,(j\omega\,n\,I - A_R)^{-1} \times \begin{cases} j\theta_D(\omega)B^\star, & \textit{odd } n > 0 \\ 0, & \textit{even } n > 1 \end{cases} \tag{21}$$

If $B^\star = B_R$, the two HOSIDF formulations obey:

$$\sum_{n=1}^{\infty} R_{DF,n}(\omega) = R_L(\omega) + \sum_{n=1}^{\infty} R^\star_{DF,n}(\omega,\, B_R) \tag{22}$$

C. Closed-loop frequency-domain description

This section shows that open-loop Impulse HOSIDF can be used to exactly model RCSs. A virtual input $Q^\star$ and input matrix $B^\star$ are computed, which cause the open-loop Impulse HOSIDF response to exactly model that of the RCS (2). The open-loop states are first established for Impulse HOSIDF.

Lemma 5.1. *The following is used to simplify results:*

$$\mathrm{Re}\left\{(j\omega\,I - A_R)^{-1} j\right\} \equiv \left(\omega^2\,I + A_R^2\right)^{-1} \omega\,I \tag{23}$$

$$\mathrm{Re}\left\{(j\omega\,I - A_R)^{-1}\right\} \equiv -\left(\omega^2\,I^2 + A_R^2\right)^{-1} A_R \tag{24}$$

Theorem 6 (Open-loop states $\vec{x}(t_r)$)**.** *Consider an open-loop SISO RC* (1) *using zero-crossing resets with a sinusoidal input $\vec{q}(t)$ having amplitude $\vec{q}_0 \in \mathbb{R}$ and frequency ω. Define reset sets based on the derivative $\dot{\vec{q}}(t)$:*

$$t_r^{\downarrow} \in t_R^{\downarrow} = \{t \in t_R : \dot{\vec{q}}(t) \le 0\}, \quad t_r^{\uparrow} \in t_R^{\uparrow} = \{t \in t_R : \dot{\vec{q}}(t) > 0\}$$

so that $t_R^{\downarrow} \cup t_R^{\uparrow} = t_R$. The states $\vec{x}(t_r^{\downarrow})$ obey:

$$\vec{x}(t_r^{\downarrow}) = \left(I - \left(I + \mathrm{e}^{A_R\frac{\pi}{\omega}} A_\rho\right)^{-1} \mathrm{e}^{A_R\frac{\pi}{\omega}}\,(A_\rho - I)\right) \times \left(\omega^2\,I + A_R^2\right)^{-1} \omega\,I\,B_R\,\vec{q}_0 \tag{25}$$

where $(I + \mathrm{e}^{A\frac{\pi}{\omega}} A_\rho)$ is assumed to be invertible.

Proof. Split the open-loop states (17) in two parts, so that $X(s) = X_L(s) + X_\delta(s)$:

$$X_L(s) = R_L^X(s)\,Q(s)$$
$$X_\delta(s) = R_\delta^X(s) \sum_{t_r \in t_R} \vec{x}(t_r)\,\mathrm{e}^{-\,t_r\,s}$$

First consider the linear term, $X_L(s)$. States $\vec{x}_L(t)$ can be obtained by taking the real part of $X_L(s) = X_L(j\omega)$ evaluated at some time instance. This is possible because of linearity combined with having a sinusoidal input. Rewriting the sinusoidal input $\vec{q}(t)$ gives:

$$\vec{q}(t) = \vec{q}_0\,\sin(\omega t) = \mathrm{Im}\{\vec{q}_0\,\mathrm{e}^{j\omega t}\} = \mathrm{Re}\{\vec{q}_0\,\mathrm{e}^{j\omega(t-\frac{\pi}{2})}\}$$

This is used to write $X_L(j\omega)$ in time domain:

$$X_L(j\omega) = (j\omega I - A_R)^{-1} B_R\,Q(j\omega)$$
$$\vec{x}_L(t) = \mathrm{Re}\{(j\omega I - A_R)^{-1} B_R\}\vec{q}(t)$$
$$= \mathrm{Re}\{(j\omega I - A_R)^{-1} B_R\,\vec{q}_0\,\mathrm{e}^{j\omega(t-\frac{\pi}{2})}\}$$

The zero-crossing reset law is used to determine $\vec{x}_L(t_r^{\downarrow})$, which requires finding $\vec{q}(t_r^{\downarrow})$. A zero-crossing of $\vec{q}(t)$ implies $\mathrm{Re}\{\vec{q}(t_r)\} = 0 \Leftrightarrow \vec{q}_0\,\mathrm{e}^{j\omega(t-\frac{\pi}{2})} = \pm\,j\vec{q}_0$. As $\omega > 0$, function $\vec{q}_0\,\mathrm{e}^{j\omega(t-\frac{\pi}{2})}$ propagates counter-clockwise, implying that solution $+\,j\vec{q}_0$ occurs when sinusoid $\vec{q}(t)$ crosses 0 from above ($\dot{\vec{q}}(t) \le 0$). Applying this and using (23) to simplify gives:

$$\vec{x}_L(t_r^{\downarrow}) = \mathrm{Re}\left\{(j\omega\,I - A_R)^{-1} B_R\,j\,\vec{q}_0\right\}$$
$$\vec{x}_L(t_r^{\downarrow}) = \left(\omega^2\,I + A_R^2\right)^{-1} \omega\,I\,B_R\,\vec{q}_0$$

The impulsive part is considered next. Write in time domain:

$$\vec{x}_\delta(t) = \sum_{t_r \in t_{R_{\leq t}}} \mathrm{e}^{A_R(t-t_r)}(A_\rho - I)\,\vec{x}(t_r)$$

From $\vec{q}(t)$ it follows that resets are spaced $\pi\,/\,\omega$ apart. Thus, $\forall\, t_r^\downarrow \in t_R^\downarrow$, $\exists\, \tilde{t}_r^\uparrow \in t_R^\uparrow \mid t_r^\downarrow - \tilde{t}_r^\uparrow = \pi\,/\,\omega$. Evaluating at $t_r^\downarrow$ and expressing in terms of the states at the previous reset, $x_\delta(\tilde{t}_r^\uparrow)$:

$$\begin{aligned}\vec{x}(t_r^\downarrow) = {} & \mathrm{e}^{A_R(t_r^\downarrow - \tilde{t}_r^\uparrow)}(A_\rho - I)\,\vec{x}(\tilde{t}_r^\uparrow) \\ & + \mathrm{e}^{A_R(t_r^\downarrow - \tilde{t}_r^\uparrow)} \sum_{t_r \in t_{R_{\leq \tilde{t}_r^\uparrow}}} \mathrm{e}^{A_R(\tilde{t}_r^\uparrow - t_r)}(A_\rho - I)\,\vec{x}(t_r)\end{aligned}$$

The last term is per definition equal to $x_\delta(\tilde{t}_r^\uparrow)$. Therefore,

$$\begin{aligned}\vec{x}(t_r^\downarrow) &= \mathrm{e}^{A_R(t_r^\downarrow - \tilde{t}_r^\uparrow)}(A_\rho - I)\,\vec{x}(\tilde{t}_r^\uparrow) + \mathrm{e}^{A_R(t_r^\downarrow - \tilde{t}_r^\uparrow)}\,\vec{x}_\delta(\tilde{t}_r^\uparrow) \\ \vec{x}(t_r^\downarrow) &= \mathrm{e}^{A_R\frac{\pi}{\omega}}\left((A_\rho - I)\,\vec{x}(\tilde{t}_r^\uparrow) + \vec{x}_\delta(\tilde{t}_r^\uparrow)\right)\end{aligned}$$

If (9) is satisfied, as required for HOSIDF analysis, $\vec{x}(t) = -\vec{x}(t+\pi\,/\,\omega)$ [7]. Inserting $t_r^\downarrow$, $\tilde{t}_r^\uparrow$ gives $\vec{x}(t_r^\downarrow) = -\vec{x}(\tilde{t}_r^\uparrow)$. Expanding $\vec{x}(t)$ shows that $\vec{x}(t_r^\downarrow) = \vec{x}_L(t_r^\downarrow) + \vec{x}_\delta(t_r^\downarrow) = -\vec{x}_L(\tilde{t}_r^\uparrow) - \vec{x}_\delta(\tilde{t}_r^\uparrow)$. From $\vec{x}_L(t_r)$ having $\pm j\vec{q}_0$ solutions on alternating reset times $\vec{x}_L(\tilde{t}_r^\downarrow) = -\vec{x}_L(t_r^\uparrow)$ follows. Thus, $\vec{x}_\delta(t_r^\downarrow) = -\vec{x}_\delta(t_r^\uparrow)$. Inserting this and writing for $\vec{x}(t_r^\downarrow)$ gives:

$$\vec{x}_L(t_r^\downarrow) + \vec{x}_\delta(t_r^\downarrow) = -\mathrm{e}^{A_R\frac{\pi}{\omega}}\left((A_\rho - I)\,\vec{x}_L(t_r^\downarrow) + A_\rho\,\vec{x}_\delta(t_r^\downarrow)\right)$$

Solving for $\vec{x}_\delta(t_r^\downarrow)$ in terms of $\vec{x}_L(t_r^\downarrow)$ and inserting that in $\vec{x}(t_r^\downarrow) = \vec{x}_L(t_r^\downarrow) + \vec{x}_\delta(t_r^\downarrow)$ yields the desired solution. □

Remark 6.1. *These states $\vec{x}_\delta(t_r^\downarrow)$ (25) equal those of the Impulse HOSIDF case, given that $B_R = B^\star$ and $Q(\omega) = Q^\star(\omega)$.*

Next, the virtual input $Q^\star(\omega)$ to the Impulse HOSIDF and corresponding input matrix $B^\star$ are computed as a function of $\vec{x}(t_r^\downarrow)$. These are then used to find the closed-loop formulation.

Corollary 6.1 (HOSIDF can model any $\vec{x}(t_r^\downarrow)$)**.** *Impulse HOSIDF (21) can model any periodic impulse response with states $\vec{x}(t_r^\downarrow)$ by choosing the virtual input magnitude $\vec{q}_0^\star(\omega, \vec{x}(t_r^\downarrow)) = 1$ and the input matrix $B^\star(\omega, \vec{x}(t_r^\downarrow))$ as:*

$$B^\star(\omega, \vec{x}(t_r^\downarrow)) = \zeta(\omega)\,\vec{x}(t_r^\downarrow) \tag{26}$$

Where $\zeta(\omega)$ is defined as:

$$\begin{aligned}\zeta(\omega) = {} & \left(\left(\omega^2\,I + A_R^2\right)^{-1}\omega\,I\right)^{-1} \\ & \times \left(I - \left(I + \mathrm{e}^{A_R\frac{\pi}{\omega}}A_\rho\right)^{-1}\mathrm{e}^{A_R\frac{\pi}{\omega}}\,(A_\rho - I)\right)^{-1}\end{aligned}$$

Proof. Substitution of $B^\star(\omega, \vec{x}(t_r^\downarrow))$ for B_R in (25) while using virtual input $Q^\star(\omega, \vec{x}(t_r^\downarrow))$ with magnitude $\vec{q}_0^\star(\omega, \vec{x}(t_r^\downarrow))$ instead of $Q(\omega)$, and rewriting for $B^\star(\omega, \vec{x}(t_r^\downarrow))\,\vec{q}_0^\star(\omega, \vec{x}(t_r^\downarrow))$ afterwards, yields the result. This shows that by computing $B^\star(\omega, \vec{x}(t_r^\downarrow))$ any periodic reset state can be created, thus that Impulse HOSIDF can model any periodic impulse response.

$B^\star(\omega, \vec{x}(t_r^\downarrow))$ makes magnitude $\vec{q}_0^\star(\omega, \vec{x}(t_r^\downarrow))$ obsolete, which is why $q_0^\star(\omega, \vec{x}(t_r^\downarrow)) = 1$ is chosen. The phase of $Q^\star(\omega)$ determines reset times, which is covered in a later section. □

Remark 6.2. *Solutions to (26) require $\omega > 0$ as well as $\left(I + \mathrm{e}^{A_R\frac{\pi}{\omega}}A_\rho\right)^{-1}\mathrm{e}^{A_R\frac{\pi}{\omega}}\,(A_\rho - I) \neq I$, which hold generally.*

Theorem 7 (HOSIDF analysis in closed-loop)**.** *A summation of Impulse HOSIDF responses on top of the BLS can accurately describe $e(t)$ for any system satisfying Theorem 5, given continuity of $\vec{e}(t)$ ($\vec{e}(t) \in C^0$):*

$$\begin{aligned}E(\omega) = {} & S_L(\omega)\,R_I(\omega) - \sum_{n=1}^{\infty} S_L(n\omega)\,G(n\omega) \\ & \times \sum_{t_\rho} R^\star_{DF,n}(\omega, B^\star(\omega, \vec{x}(t_r^\downarrow)))\,Q^\star(\omega, \vec{x}(t_r^\downarrow))\end{aligned} \tag{27}$$

With $Q^\star(\omega, \vec{x}(t_r^\downarrow))$ having magnitude 1 and phases to ensure the correct reset times. Fig. 6 represents (27) graphically.

Proof. Take (12) and insert (22), with a designable input matrix $B_R = B^\star(\omega, \vec{x}(t_r^\downarrow))$ and sinusoidal input $Q^\star(\omega, \vec{x}(t_r^\downarrow))$ with amplitude 1. Arguments of $B^\star$ and $Q^\star$ are dropped.

$$Z(\omega) = R_L(\omega)\,Q^\star(\omega) + \sum_{n=1}^{\infty} R^\star_{DF,n}(\omega, B^\star)\,Q^\star$$

Inserting the open-loop $Z(\omega)$ (16), using $B^\star$ and $Q^\star$ computed according to the actual states $\vec{x}(t_r^\downarrow)$, and rewriting gives:

$$\sum_{n=1}^{\infty} R^\star_{DF,n}(\omega, B^\star)\,Q^\star = R_\delta(\omega) \sum_{t_r \in t_R} \vec{x}(t_r)\,\mathrm{e}^{-\,t_r j\omega}$$

The reset times $t = t_r \in t_R = \cup_p \{t_r + p\,\pi\,/\,\omega\},\ p = \mathbb{Z}$ follow from zero-input resets. Using these yields:

$$\begin{aligned}\sum_{n=1}^{\infty} R^\star_{DF,n}(\omega, B^\star)\,Q^\star = {} & R_\delta(\omega) \sum_{p\,\in\,\mathbb{Z}} \vec{x}(t_r + p\,\pi\,/\,\omega) \\ & \times \mathrm{e}^{-\,(t_r\,+\,p\,\pi\,/\,\omega)j\omega}\end{aligned}$$

The correct HOSIDF response for resets at t_ρ with weight $\vec{x}(t_r)$ is ensured if $B^\star$ and $Q^\star$ are computed according to Theorem 6.1. HOSIDF has odd harmonics only, thus $\vec{x}(t_r) = -\vec{x}(t_r + \pi\,/\,\omega)$. Simplifying using periodicity and inserting the definition of $\xi\,(s, t_r, \vec{x}(t_r))$ from Cor. 5.1 gives:

$$\begin{aligned}\sum_{n=1}^{\infty} R^\star_{DF,n}(\omega, B^\star)\,Q^\star = {} & R_\delta(\omega) \sum_{p\,\in\,2\mathbb{Z}} \Big(\vec{x}(t_r)\,\mathrm{e}^{-\,(t_r + p\frac{\pi}{\omega})\,j\omega} \\ & - \vec{x}(t_r)\,\mathrm{e}^{-\,(t_r + (p+1)\frac{\pi}{\omega})\,j\omega}\Big)\end{aligned}$$

$$\sum_{n=1}^{\infty} R^\star_{DF,n}(\omega, B^\star)\,Q^\star = \xi\,(\omega, t_r, \vec{x}(t_r))$$

Thus far, this holds for open-loop Impulse HOSIDF. Conveniently, $\xi\,(s, t_r, \vec{x}(t_r))$ as in (20) is obtained, which can be substituted in the closed-loop response (18), which requires inserting the closed-loop values for t_r and $\vec{x}(t_r)$. □

Remark 7.1. *Theorem 7 proves that any SISO RC (2) with (i) zero-crossing resets (ii) satisfying the $\mathcal{H}_\beta$ condition and (iii) having $\vec{e}(t) \in C^0$ can be described without error by a summation of Impulse HOSIDF responses, if the set t_ρ and states $\vec{x}(t_r)$ are known $\forall\, t_r \in t_\rho$.*

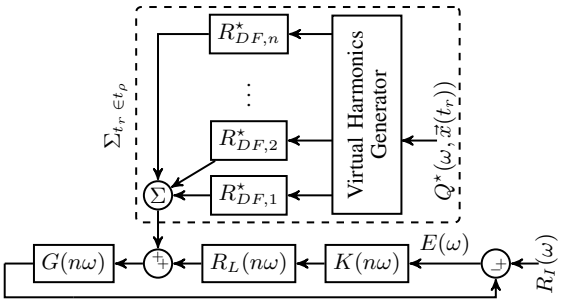

Fig. 6. Block diagram representing (27). The dashed area must be summed over all $t_r \in t_\rho$. Arguments of $R^\star_{DF,n}(\omega, B^\star(\omega, \vec{x}(t_r^\downarrow)))$ are dropped.

Remark 7.2. *Theorem 7 also holds if $\vec{e}(t) \notin C^0$, except for prediction errors caused by the Gibbs phenomenon in the vicinity of discontinuities.*

With (27) an accurate description is provided that can model the same RCSs in frequency-domain as CL-FR can, given that t_ρ and $\vec{x}(t_r)$ are known, without needing further conditions.

VI. Analytical solution

To solve (27) times t_r and states $\vec{x}(t_r)$ must be computed $\forall\, t_r \in t_\rho$. This can be done numerically or analytically. For the sake of simplifying analysis and staying close to what is familiar to the linear control/based loop shaping methodology it is chosen to pursue an analytical solution. This choice comes at the cost of requiring assumptions, impacting precision.

Assumption 1 (Two resets per period)**.** *Assume that sufficient accuracy is achieved by modelling a closed-loop RC* (2) *satisfying Theorem 7 with exactly two resets per period, taking $|t_\rho| = 1$. Accurate modelling of the two modelled resets requires that any unmodelled reset does not significantly influence their position nor states.*

Assumption 2 (Zero crossing direction)**.** *It is assumed that at any reset the direction of $\vec{q}(t)$ crossing zero is equal to that predicted by the nearby BLS zero crossing: $\operatorname{sign}(\dot{\vec{q}}(t)) = \operatorname{sign}(\dot{\vec{q}}_L(t)),\ \forall\, t \mid \vec{q}(t) = 0$. This holds for most RCSs and can be checked analytically.*

Assumption 3 (Existence of a reset instant)**.** *Assume that, at any reset instant, the absolute combined magnitude of all prior resets-induced impulse responses is less than the absolute peak value of the BLS response. This must hold in any real system satisfying Theorem 5. Otherwise, there cannot be a reset at $\pi\ /\ \omega$ distance from the previous reset, which contradicts Theorem 5. However, this assumption may be violated in cases where other assumptions affect solutions.*

Lemma 7.1 (Convergence)**.** *The series $\sum_{p\,\in\,\mathbb{N}} \mathrm{e}^{Ap}$, with A square, is convergent if all $\lambda\,(A) < 0$.*

Proof. Start by expanding e^{Ap}:

$$\mathrm{e}^{A\,p} = \mathrm{e}^{\sum_{i\,=\,1}^{p} A} = \prod\nolimits_{i\,=\,1}^{p} \mathrm{e}^{A}$$

The ratio test is evaluated based on this result:

$$\lim_{p\,\to\,\infty} \left| \frac{\mathrm{e}^{A(p+1)}}{\mathrm{e}^{Ap}} \right| < I \Leftrightarrow \left| \frac{\prod_{i\,=\,1}^{p+1} \mathrm{e}^{A}}{\prod_{i\,=\,1}^{p} \mathrm{e}^{A}} \right| = \left| \mathrm{e}^{A} \right| < I$$

The series is convergent if this condition holds. Convergence thus follows if the eigenvalues of A are strictly negative. □

Lemma 7.2 (Closed-loop reset instant)**.** *A RCS reset instant at a descending zero crossing, $t_\rho^\downarrow$, can, for any RC satisfying Theorem 7, be computed using Assumptions 1 to 3:*

$$\omega\, t_\rho^\downarrow + \angle\left(K(j\omega)\, S_L(j\omega)\, R_I(j\omega)\right) + \Phi(\omega, \vec{x}(t_r^\downarrow)) = \pi \quad (28)$$

This $t_\rho^\downarrow$ corresponds to the zero crossings of $Q^\star$ with:

$$\angle\, Q^\star(\omega) = \angle\left(K(j\omega)\, S_L(j\omega)\, R_I(j\omega)\right) + \Phi(\omega, \vec{x}(t_r^\downarrow)) \quad (29)$$

If $\Phi(\omega, \vec{x}(t_r^\downarrow)) = 0$, (28) *computes the descending zero crossings of the BLS. Phase shift $\Phi(\omega, \vec{x}(t_r^\downarrow))$ is defined as:*

$$\Phi(\omega, \vec{x}(t_r^\downarrow)) \triangleq \sin^{-1}\Big(C_Q \sum\nolimits_{p\,\in\,2\mathbb{N}} \left(\mathrm{e}^{A_Q \frac{p\pi}{\omega}} - \mathrm{e}^{A_Q \frac{(p-1)\pi}{\omega}} \right) \times B_Q\, \vec{x}(t_\rho)\ \left(\left| K(j\omega)\, S_L(j\omega)\, R_I(j\omega) \right| \right)^{-1} \Big) \quad (30)$$

where A_Q, B_Q, C_Q and D_Q denoting state-space matrices of $Q_\delta(s) = K(s)\, S_L(s)\, G(s)\, R_\delta(s)$. Lemma 7.1 states series convergence, which requires asymptotic stability of Q_δ. Throughout this work, set $\mathbb{N}$ is taken to exclude zero.

Proof. Take (18) for a SISO RC and pre-multiply by $K(s)$ to acquire the closed-loop description of $Q(s)$:

$$Q(s) = K(s)\, S_L(s)\, R_I(s) - K(s) S_L(s)\, G(s)\, R_\delta(s) \sum_{t_r \in t_R} \vec{x}(t_r)\, \mathrm{e}^{-\,t_r\, s}$$

Combining Assumption 1 with Theorem 5 shows that $t_R = t_\rho + p\,\pi\,/\,\omega,\ p \in \mathbb{Z}$, where t_ρ has one entry. Inserting this and substituting $Q_\delta(s)$ as defined above gives:

$$Q(s) = K(s)\, S_L(s)\, R_I(s) - Q_\delta(s) \sum_{p\,\in\,\mathbb{Z}} \vec{x}(t_\rho + \frac{p\,\pi}{\omega})\, \mathrm{e}^{-\,(t_\rho\, +\, \frac{p\,\pi}{\omega})\, s}$$

Reset instant periodicity causes all resets instants prior to t_r to be at times $t_r - \frac{p\,\pi}{\omega},\ p \in \mathbb{N}$. The time-domain solution for $\vec{q}(t)$ is obtained for a sinusoidal r_I with frequency ω:

$$\vec{q}(t_r) = \left| K(j\omega)\, S_L(j\omega)\, R_I(j\omega) \right| \times \sin\left(\omega t + \angle\left(K(j\omega)\, S_L(j\omega)\, R_I(j\omega)\right)\right) - \sum_{p\,\in\,\mathbb{N}} \left(C_Q\, \mathrm{e}^{A_Q \frac{p\pi}{\omega}}\, B_Q + D_Q \right) \vec{x}(t_\rho + \frac{p\,\pi}{\omega})$$

where the impulse response is expressed in state-space terms. Cor. 4.1 shows that $R_\delta(s)$ has no direct feed-through, which by definition of $Q_\delta(s)$ implies that $D_Q = 0$.

The following expression is obtained by utilizing the periodicity of $\vec{x}(t)$ proven by Theorem 5:

$$\begin{aligned}\vec{q}(t_r) = &\ |K(j\omega)\,S_L(j\omega)\,R_I(j\omega)| \\ &\times \sin\left(\omega t_r + \angle\left(K(j\omega)\,S_L(j\omega)\,R_I(j\omega)\right)\right) \\ &+ C_Q\left(\sum\nolimits_{p\,\in\,2\mathbb{N}} \mathrm{e}^{A_Q\frac{p\pi}{\omega}} - \mathrm{e}^{A_Q\frac{(p-1)\pi}{\omega}}\right) B_Q\,\vec{x}(t_r)\end{aligned}$$

Per definition of a zero-crossing reset law $\vec{q}(t_r) = 0$. Inserting this and taking the inverse sine gives, for $m \in \mathbb{Z}$:

$$\begin{aligned}m\,\pi = &\ \omega\,t_r + \angle\left(K(j\omega)\,S_L(j\omega)\,R_I(j\omega)\right) \\ &+ \sin^{-1}\Big[C_Q\sum\nolimits_{p\,\in\,2\mathbb{N}}\left(\mathrm{e}^{A_Q\frac{p\pi}{\omega}} - \mathrm{e}^{A_Q\frac{(p-1)\pi}{\omega}}\right) \\ &\times B_Q\,\vec{x}(t_r)\,\left(|K(j\omega)\,S_L(j\omega)\,R_I(j\omega)|\right)^{-1}\Big]\end{aligned}$$

The inverse sine exists if Assumption 3 holds. A descending zero-crossing occurs if the sinusoid argument is $m\,\pi$, with odd m. These cases correspond to $t = t_r^{\downarrow}$. The zero crossing direction is assumed to be unaffected by prior resets by Assumption 2. The solution $m = 1$ is chosen. Inserting that while substituting $\Phi(\omega, \vec{x}(t_r^{\downarrow}))$ yields (28). Zero-crossings of a sinusoidal $Q^{\star}$ with phase (29) gives resets $t_\rho^{\downarrow} + p\,\pi\,/\,\omega$. □

Assumption 4 (Small effect of resets on reset times)**.** *Assume that* $\Phi(\omega, \vec{x}(t_\rho))$ (30) *satisfies* $\Phi(\omega, \vec{x}(t_\rho)) \ll \pi,\ \forall\omega$. *This holds if reset times are close to the BLS zero crossings of* $\vec{q}(t)$.

Lemma 7.3 (States $\vec{x}(t_\rho^{\downarrow})$)**.** *States* $\vec{x}(t_\rho^{\downarrow})$ *are, given Assumptions 1 to 4, for a system satisfying Theorem 5, computed by:*

$$\begin{aligned}\vec{x}(t_\rho^{\downarrow}) = &\Big[I + \left(\omega^2\,I^2 + A_R^2\right)^{-1} A_R\,B_R\,C_Q\sum\nolimits_{k\,\in\,2\mathbb{N}} \\ &\left(\mathrm{e}^{A_Q\frac{k\pi}{\omega}} - \mathrm{e}^{A_Q\frac{(k-1)\pi}{\omega}}\right) B_Q - 0.5\,C_H\sum\nolimits_{k\,\in\,2\mathbb{N}} \\ &\left(\mathrm{e}^{A_H\frac{k\pi}{\omega}} - \mathrm{e}^{A_H\frac{(k-1)\pi}{\omega}}\right) B_H\Big]^{-1}\left(\omega^2\,I + A_R^2\right)^{-1}\omega\,B_R \\ &\times\ |K(j\omega)\,S_L(j\omega)\,R_I(j\omega)| \quad (31)\end{aligned}$$

Which requires the inverted terms to be invertible. State-space matrices A_H, B_H, C_H *and* D_H *correspond to* $H(s)$*:*

$$H(s) = R_\delta^X(s) - R_L^X(s)\,K(s)\,S_L(s)\,G(s)\,R_\delta(s)$$

The two series converge if A_Q *and* A_H *satisfy Lemma 7.1, thus if* Q *and* H *are asymptotically stable.*

Proof. Consider (19) for a SISO RC and separate it into $X_L(s)$ and $X_\delta(s)$ such that $X(s) = X_L(s) + X_\delta(s)$:

$$\begin{aligned}X_L(s) &= R_L^X(s)\,K(s)\,S_L(s)\,R_I(s) \\ X_\delta(s) &= \left(R_\delta^X(s) - R_L^X(s)\,K(s)\,S_L(s)\,G(s)\,R_\delta(s)\right) \\ &\qquad\times \sum_{t_r\in t_R}\vec{x}(t_r \in t_r)\,\mathrm{e}^{-\,t_r,\,s}\end{aligned}$$

Writing the linear term $\vec{x}_L(t)$ in time domain for a sinusoidal input, while using that $\vec{x}_L(t)$ is real, gives the following:

$$\begin{aligned}\vec{x}_L(t) = \mathrm{Re}\Big\{&R_L^X(j\omega)\ |K(j\omega)\,S_L(j\omega)\,R_I(j\omega)| \\ &\times \mathrm{e}^{j\omega(t-\frac{\pi}{2}) + j\angle(K(j\omega)\,S_L(j\omega)\,R_I(j\omega))}\Big\}\end{aligned}$$

Evaluating at $t_\rho^{\downarrow}$ by rewriting and inserting (28) shows:

$$\begin{aligned}\vec{x}_L(t_\rho^{\downarrow}) = \mathrm{Re}\Big\{&R_L^X(j\omega)\ |K(j\omega)\,S_L(j\omega)\,R_I(j\omega)| \\ &\times \mathrm{e}^{j\left(\frac{\pi}{2} - \Phi(\omega,\vec{x}(t_{\rho^{\downarrow}}))\right)}\Big\}\end{aligned}$$

Take $\Phi(\omega, \vec{x}(t_\rho^{\downarrow}))$ from (30) and apply Assumption 4, such that $\Phi(\omega, \vec{x}(t_\rho^{\downarrow})) = \sin^{-1}(\bullet) \approx (\bullet)$, where $\bullet$ denotes the terms within Φ. Then, the last term of $\vec{x}_L(t_\rho^{\downarrow})$ becomes $\mathrm{e}^{j\left(\frac{\pi}{2} - \bullet\right)}$. Given Assumption 4, the first Taylor expansion can be used, giving the simplification $\mathrm{e}^{j\left(\frac{\pi}{2} - \bullet\right)} \approx j + (\bullet)$. Inserting this and expanding $\Phi(\omega, \vec{x}(t_\rho^{\downarrow}))$ gives:

$$\begin{aligned}\vec{x}_L(t_\rho^{\downarrow}) = \mathrm{Re}\Big\{&R_L^X(j\omega)\ |K(j\omega)\,S_L(j\omega)\,R_I(j\omega)| \\ &\times \Big[j + C_Q\sum\nolimits_{p\,\in\,2\mathbb{N}}\left(\mathrm{e}^{A_Q\frac{p\pi}{\omega}} - \mathrm{e}^{A_Q\frac{(p-1)\pi}{\omega}}\right) \\ &\times B_Q\,\vec{x}(t_\rho^{\downarrow})\,\left(|K(j\omega)\,S_L(j\omega)\,R_I(j\omega)|\right)^{-1}\Big]\Big\}\end{aligned}$$

For a SISO RC this can be simplified to:

$$\begin{aligned}\vec{x}_L(t_\rho^{\downarrow}) = \mathrm{Re}\Big\{&R_L^X(j\omega)\ |K(j\omega)\,S_L(j\omega)\,R_I(j\omega)|\ j \\ &+ R_L^X(j\omega)\,C_Q\sum\nolimits_{p\,\in\,2\mathbb{N}}\Big(\mathrm{e}^{A_Q\frac{p\pi}{\omega}} \\ &- \mathrm{e}^{A_Q\frac{(p-1)\pi}{\omega}}\Big)\ B_Q\,\vec{x}(t_\rho^{\downarrow})\Big\}\end{aligned}$$

Consider $X_\delta(s)$. Insert $H(s)$ and write in time domain. As $R_\delta(s)$ has no direct feed-through D_H must equal zero.

$$\vec{x}_\delta(t) = \sum_{t_r\in t_{R_{\leq t}}}\left(C_H\,\mathrm{e}^{A_H(t-t_r)}\,B_H\right)\vec{x}(t_r)$$

Considering Assumption 1 with Theorem 5, such that all resets are spaced $\pi\,/\,\omega$ apart, and evaluating at $t_\rho^{\downarrow}$ gives:

$$\vec{x}_\delta(t_\rho^{\downarrow}) = C_H\sum_{p\,\in\,2\mathbb{N}}\left(\mathrm{e}^{A_H(\frac{p\pi}{\omega})} - \mathrm{e}^{A_H(\frac{(p-1)\pi}{\omega})}\right)B_H\,\vec{x}(t_\rho^{\downarrow})$$

Inserting these results into $\vec{x}(t_\rho^{\downarrow}) = \vec{x}_L(t_\rho^{\downarrow}) + \vec{x}_\delta(t_\rho^{\downarrow})$, solving for $\vec{x}(t_\rho^{\downarrow})$ and inserting (23), (24) gives the stated result. □

Theorem 8 (Analytical solution for $E(\omega)$ (δ-CL))**.** *The error response of a RCS* (2) *satisfying Theorem 5, given Assumptions 1 to 4, is stated below. Arguments of* $B^{\star}(\omega, \vec{x}(t_r^{\downarrow}))$ *are dropped.*

$$\begin{aligned}&E_{\delta-CL,n}(\omega) = S_L(\omega n) \\ &\times\begin{cases}R_I(\omega) - G(\omega)\,R_{DF,1}^{\star}(\omega, B^{\star})\,\Psi(\omega, 1), & n = 1\\ -\,G(\omega n)R_{DF,n}^{\star}(\omega, B^{\star})\,\Psi(\omega, n), & n > 1\end{cases} \quad (32)\\ &\textit{where:}\quad \Psi(\omega, n) = \Big(|K(\omega)\,S_L(\omega)\,R_I(\omega)| \\ &\qquad\times \mathrm{e}^{nj\angle K(\omega)\,S_L(\omega)\,R_I(\omega) + nj\Phi(\omega,\vec{x}(t_r^{\downarrow}))}\Big)\end{aligned}$$

Def. 7 defines $R_{DF,n}^{\star}$*. Parameters* $\vec{x}(t_r^{\downarrow})$, $\Phi(\omega, \vec{x}(t_r^{\downarrow}))$ *and* $B^{\star}(\omega, \vec{x}(t_r^{\downarrow}))$ *are given by* (31)*,* (30) *and* (26)*, respectively.*

Proof. Insert (31) into (26) to solve (27). Virtual input $Q^{\star}$ has magnitude 1, see Cor. 6.1, and phase (29). From Assumption 1 it follows that a summation over t_ρ is obsolete, as this set has one entry only. Rewriting gives the result.

These equations combine harmonic and reference frequencies. Multiplying the phase by n accounts for this. □

Corollary 8.1 (Analytical solution for $S(\omega)$)**.** *Sensitivity is defined as* $S(\omega) = E(\omega)\, R_I(\omega)^{-1}$. *Applying this to* (32) *while correcting the phase for harmonics gives:*

$$S_{\delta-CL,n}(\omega) = E_{\delta-CL,n}(\omega) \left(|R_I(\omega)|\, \mathrm{e}^{nj\angle R_I(\omega)} \right)^{-1} \quad (33)$$

Corollary 8.2 (Complementary Sensitivity)**.** *The complementary sensitivity* $T(\omega)$ *is defined as* $I - S(\omega)$*:*

$$T_{\delta-CL,n}(\omega) = I - E_{\delta-CL,n}(\omega) \left(|R_I(\omega)|\, \mathrm{e}^{nj\angle R_I(\omega)} \right) \quad (34)$$

Corollary 8.3 (Control Sensitivity)**.** *Split the linear system* $G(s)$ *in plant* $P(s)$ *and controller* $C(s)$, $G(s) = P(S)\, C(S)$. *Control input* $U(s)$ *enters* $P(s)$*:* $Y(s) = P(s)\, U(s)$. *The control input* $CS(\omega)$*:*$\vec{r}_I(t) \mapsto \vec{u}(t) \triangleq CS(\omega) = P^{-1}(\omega)\, T(\omega)$*:*

$$CS_{\delta-CL,n}(\omega) = P^{-1}(jn\omega)\, T_{\delta-CL,n}(\omega) \quad (35)$$

These results can be transformed into time-domain signals:

$$\vec{y}(t) \approx \sum_{n=1}^{\infty} |T_{DF,n}(\omega)| \sin(n\omega t + \angle T_{DF,n}(\omega)) \quad (36)$$

$$\vec{e}(t) \approx \sum_{n=1}^{\infty} |E_{DF,n}(\omega)| \sin(n\omega t + \angle E_{DF,n}(\omega)) \quad (37)$$

$$\vec{u}(t) \approx \sum_{n=1}^{\infty} |CS_{DF,n}(\omega)| \sin(n\omega t + \angle CS_{DF,n}(\omega)) \quad (38)$$

Assumption 5 (Superposition for multi-sine inputs)**.** *Consider a closed-loop RC* (2) *with multiple sinusoidal references superimposed, having magnitudes* R_{I_1} *to* $R_{I_{\bar{k}}}$, $\bar{k} \in \mathbb{N}$. *Define the corresponding BLS magnitudes for* $\vec{q}(t)$ *as* $|\vec{q}_{I_1}|$ *to* $|\vec{q}_{I_{\bar{k}}}|$*, individually computed for each reference. If* $\exists\, p : |\vec{q}_{I_k}| \gg |\vec{q}_{I_j}|$, $\forall\, j \in \{1, \ldots, \bar{k}\}$, $j \neq k$, *assume that solely reference* R_{I_k} *determines reset times and weights. If so, all other references are handled by the BLS and can be merged with the nonlinear RC response for* R_{I_k} *through superposition. This allows modelling of multi-sine references [32].*

This framework extends to permitting disturbances, as any sinusoidal disturbance $\vec{d}$ *after the nonlinear reset element gives, for a linear plant, some sinusoidal signal* $\vec{q}_d$*. This can be handled analogous to* $\vec{q}_{I_j}$ *as described above.*

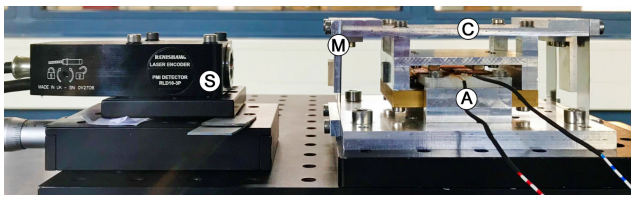

Fig. 7. 1 Degree-of-Freedom precision positioning stage that moves cart (C) using Lorentz actuator (A). This cart is attached to the frame by means of two leaf flexures, which constrain all movements but one translation. This translation is measured using laser encoder (S), which measures its distance relative to cart-fixed mirror (M).

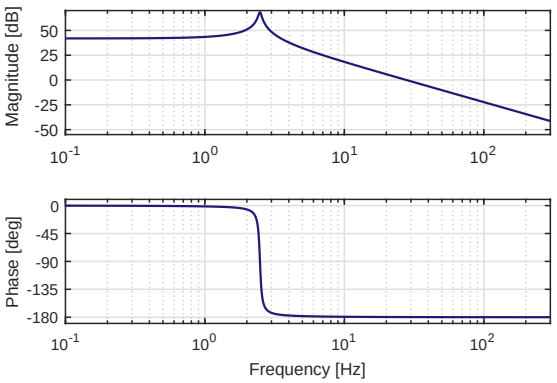

Fig. 8. Bode Plot corresponding to the system (39) shown in Fig. 7.

VII. Setup

The implications of the various assumptions are investigated in this section, evaluating where they cause δ-CL to not predict $\vec{e}(t)$ correctly. First, a precision positioning system will be introduced. Afterwards, performance metrics are defined.

For analysis $n = 1000$ harmonics are used. Series over impulse responses as in (30), (31) are evaluated with sufficient terms to ensure convergence.

A. Precision Positioning Stage

The 1 Degree-of-Freedom precision positioning stage depicted in Fig. 7 is used to validate the derived method. This SISO stage is a classic mass-spring-damper system. The transfer function of this stage is identified to be:

$$P(s) = \frac{3.038 \times 10^4}{s^2 + 0.7413\, s + 243.3} \quad (39)$$

The corresponding Bode Plot is given in Fig. 8. For the sake of analysis consider the simple case where (i) there is no noise, (ii) there are no disturbances, (iii) no quantization effects are present and (iv) a continuous-time controller is used.

B. Controllers

A linear PID controller $C(s)$ is added between the reset element and the plant, such that $G(s) = P(s)\, C(s)$. Parameter β is introduced, placing zero ω_d and pole ω_t symmetrically around bandwidth, defined as crossover frequency ω_c.

$$C(s) = k_p \frac{s + \omega_i}{s} \frac{s + \omega_c / \beta}{s + \omega_c\, \beta}, \quad \beta = \frac{\omega_c}{\omega_d} = \frac{\omega_t}{\omega_c} \quad (40)$$

Bandwidth ω_c is set to 100 Hz. Gain k_p is adjusted to achieve this bandwidth, based on DF analysis. For all implementations, $\omega_i = 10$ Hz is chosen.

Various CgLp - PID controller combinations tuned for different specifications are used for validation. Table II provides the corresponding tuning parameters. PM_{BLS} denotes the BLS phase margin. Let PM_{DF} be the phase margin as predicted by DF analysis. Then, the phase added through RC is given by $\phi_{RC} = PM_{DF} - PM_{BLS}$.

TABLE II
PARAMETERS FOR VARIOUS CGLP AND PID CONTROLLER DESIGNS. FOR ALL $\mathcal{R}^\star$ CONTROLLERS $\omega_i = 10$ HZ, $\omega_c = 100$ HZ AND $\omega_f = 500$ HZ. GAIN k_p IS ADJUSTED TO ACHIEVE BANDWIDTH ω_c.

	PM_{BLS}	ϕ_{RC}	γ	ω_r [Hz]	α	β
$\mathcal{R}_0^\star$	30°	20°	0	98.38	1.07	2.67
$\mathcal{R}_1^\star$	30°	20°	0.5	23.08	1.04	2.57
$\mathcal{R}_2^\star$	20°	20°	0.5	23.08	1.04	2.03

TABLE III
OVERVIEW OF ASSUMPTIONS ANALYTICAL METHODS FOR COMPUTING FREQUENCY-DOMAIN CLOSED-LOOP RC BEHAVIOUR USE. EMPTY FIELDS INDICATE THAT THERE ARE NO ASSUMPTIONS. NOTE THAT ASSUMPTIONS ON $\vec{r}_I$ DO NOT HAVE TO CAUSE ERRORS, AS $\vec{r}_I$ IS DESIGNABLE.

	DF	CL-DF	δ-CL
Modelled resets per period:	2	2	2
Signals assumed sinusoidal:	$\vec{q}(t)$	$\vec{r}_I(t)$, $\vec{q}(t)$	$\vec{r}_I(t)$
Resets assumed at:		$\vec{q}_{DF,1} = 0$	$\vec{q}_{BLS} \approx 0$
Neglects harmonics:	Yes		

C. Performance Metrics

The signal $\vec{e}(t)$ as predicted by (32) is compared to the corresponding simulated signal. A metric often used in literature for capturing the time-domain prediction accuracy is Integral Square Error (ISE). A normalized version is given by:

$$ISE(\omega) \triangleq \frac{\int (\vec{e}_\omega(t) - \hat{\vec{e}}_\omega(t)^2 \,\mathrm{d}t}{\int \hat{\vec{e}}_\omega^2(t) \,\mathrm{d}t} \tag{41}$$

where simulation data is denoted by $\vec{e}$ and prediction data by $\hat{\vec{e}}$. A time vector with parameter ω, such as $\vec{e}_\omega(t)$, denotes the time response for a reference with frequency ω.

In the high-tech industry peak error values indicate precision, described by the $\mathcal{L}_\infty$ norm, which is normalized:

$$L_\infty(\omega) \triangleq \frac{|\max_t |\vec{e}_\omega(t)| - \max_t |\hat{\vec{e}}_\omega(t)||}{\max_t |\hat{\vec{e}}_\omega(t)|} \tag{42}$$

VIII. VALIDATION

Table III provides an overview of the various assumptions used by the three analytical RCS describing methods. CL-DF and δ-CL use similar assumptions, except for using different reset positions and CL-DF assuming a sinusoidal $\vec{q}(t)$.

Assumptions 2 and 3 of δ-CL are not mentioned, because no results in this paper found Assumption 2 to not hold, whilst Assumption 3 is violated only for a few frequencies in one result, Fig. 16. Assumption 5 is used to alleviate the constraint on having a sinusoidal $\vec{r}_I(t)$. This case will be demonstrated, after the effects of other assumptions on sensitivity prediction errors are verified using a sinusoidal input.

A. Effects of Assumption 1

Assumption 1 simplifies analysis by modelling two resets per period only, an assumption used by all analytical methods under consideration. However, this is known to invoke errors. A time domain example is provided to illustrate the types of errors inflicted. Then, it is shown how time regularization can decouple this error source from other sources.

Fig. 9 shows the simulated and δ-CL modelled error signals for a RCS generating three resets per half period, marked as (A), (B) and (C). Reset (A) is the one modelled by δ-CL, whereas (B) and (C) are not modelled, causing errors.

1) Consecutive resets: A pair of resets is said to be consecutive if they occur close together temporally, relative to period π / ω. Reset (B) in Fig. 9 is therefore consecutive to (A). Let the corresponding reset times be t_A and t_B, $t_B > t_A$. An ODE solution is used to express $\vec{x}(t_B)$ in terms of $\vec{x}(t_A^+)$:

$$\vec{x}(t_B) = e^{A_R(t_B - t_A)} x^+(t_A) + \int_{t_A}^{t_B} e^{A_R(t-\tau)} B_R \, u(\tau) \,\mathrm{d}\tau$$

Consider the limit case for consecutive resets, $t_B \to t_A$. Insert (1) to obtain $\vec{x}(t_B^+)$ as a function of $\vec{x}(t_A)$:

$$\lim_{t_B \to t_A} \vec{x}(t_B) = \vec{x}^+(t_A) = A_\rho \, \vec{x}(t_A)$$
$$\lim_{t_B \to t_A} \vec{x}^+(t_B) = A_\rho \, \vec{x}^+(t_A) \;=\; A_\rho^2 \, \vec{x}(t_A)$$

When comparing to (1) it follows that, for $t_{r,B} \to t_{r,A}$, the response becomes equivalent to that obtained by having one reset with reset matrix A_ρ^2. As all analytical methods model only one reset with reset matrix A_ρ, errors occur if $A_\rho \neq A_\rho^2$. For diagonal A_ρ parametrized by γ, such as in (8), modelling errors thus occur if $\gamma \neq \gamma^2 \Leftrightarrow \gamma \notin \{0, 1\}$. Full reset therefore does not invoke errors here. Fig. 9 uses $\gamma = 0.5$, meaning that the actual response to resets (A), (B) is almost equivalent to having one reset with $\gamma = 0.5^2 = 0.25$. This increases the reset-induced impulse weight (19), explaining the higher than modelled reset spike after (B).

2) Additional resets: Reset (C) in Fig. 9 is relatively far away from (A) in temporal sense. As such, $t_C \to t_A$ cannot be used here, implying that full reset is not exempt from errors caused by not modelling (C). Fig. 9 shows how (C) causes the error peak prediction to be wrong, inflicting L_∞ errors.

Fig. 11 gives ISE results for all three methods, plotted for a range of reference frequencies. Controllers $\mathcal{R}_0^\star$ ($\gamma = 0$) and $\mathcal{R}_1^\star$ ($\gamma = 0.5$) are used to control (39). Controller $\mathcal{R}_0^\star$ has, unlike

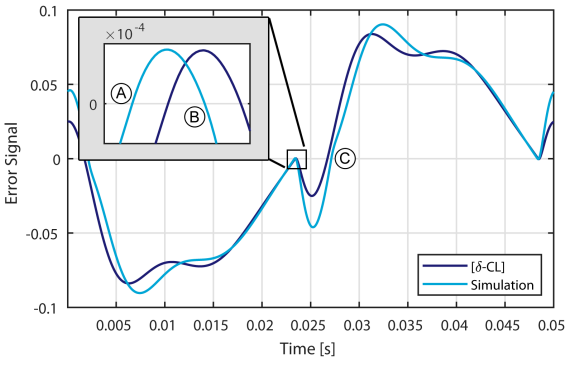

Fig. 9. Simulated and δ-CL predicted error response for a 20 Hz reference signal on controller $\mathcal{R}_1^\star$ and plant (39), thus using $\gamma = 0.5$. Points (A), (B) and (C) indicate reset instants. (B) is an undesired consecutive reset to (A), (C) is an additional reset.

$\mathcal{R}_1^\star$, negligible effects caused by consecutive resets because it is fully resetting. Both are affected by additional resets. Modelling errors of $\mathcal{R}_1^\star$ are, for all methods, at most frequencies, several factors above those of $\mathcal{R}_0^\star$, illustrating the considerable effects of consecutive resets on modelling accuracy. δ-CL is seen to invoke comparatively small prediction errors when consecutive resets do not affect the response ($\gamma = 0$).

3) Time regularization: Time regularization allows to remove consecutive or even additional resets, eliminating errors caused by Assumption 1. The following options are used:

- No time regularization: $\tau = 0$, such that all errors caused by consecutive and additional resets remain visible.
- Optimal time regularization: $\tau = 2\pi / (10\,\omega_c)$, ω_c in rad/s, suggested to be optimal when handling quantization [43]. This generally removes consecutive reset effects.
- Full time regularization: $\tau = \pi / \omega$, enforcing two resets per period, removing all errors caused by Assumption 1.

Full time regularization does not necessarily improve RC system performance. However, it decouples modelling error sources for δ-CL, as all remaining errors are caused by Assumption 4. This is employed to simplify analysis.

All three time regularization methods are applied to partially resetting controller $\mathcal{R}_1^\star$. Corresponding ISE results are given in Fig. 10. The DF and CL-DF descriptions show some improvement for more aggressive time regularization, but results are not consistent over all frequencies. δ-CL shows a significant performance improvement for more aggressive time regularization. In case of full time regularization, ISE values for δ-CL drop below $1.5\,\%$, errors that are thus solely caused by Assumption 4. ISE values for CL-DF with full time regularization are caused by the assumed reset positions and sinusoidal $\vec{q}(t)$, see Table III. These two assumptions thus inflict considerably larger errors than Assumption 4 of δ-CL.

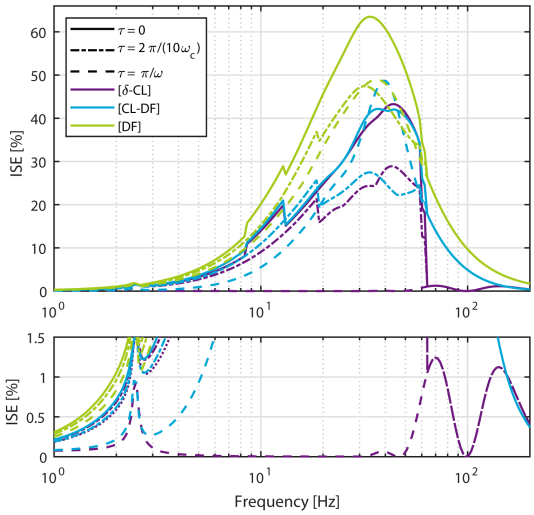

Fig. 10. Normalized ISE values for the three prediction methods, using controller $\mathcal{R}_1^\star$ on (39). Three different time regularization settings τ are used. The bottom figure provides a detail view on lower ISE values.

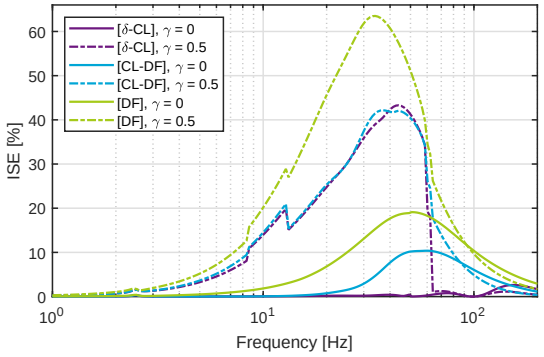

Fig. 11. Normalized ISE values for the three analytical modelling methods. No time regularization is used. Results are provided for controllers $\mathcal{R}_0^\star$ ($\gamma = 0$) and $\mathcal{R}_1^\star$ ($\gamma = 0.5$), both controlling plant (39).

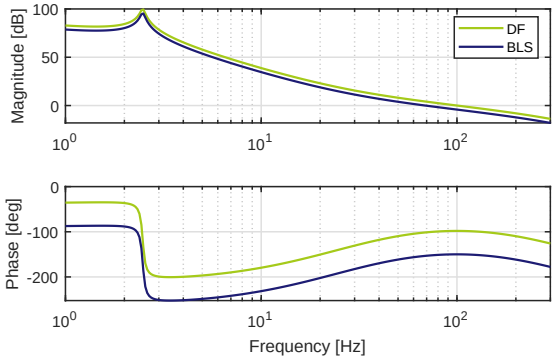

Fig. 12. Bode plot of (39) controlled by a CI and a linear controller C_{CI}. The BLS and first harmonic values as computed using DF analysis are given.

Example 8.1 (CI modelling)**.** *Potential errors caused by Assumption 1 are illustrated by means of a RCS with CI controller. Poor prediction performance is expected, as a CI often yields responses with many additional resets. Consider* (39) *with a fully resetting CI ($\gamma = 0$) in series with the following PD² controller:*

$$C_{CI}(s) = k_p \left(\frac{s + \omega_c / \beta}{s + \omega_c \beta} \right)^2, \quad \beta = 3.73$$

where k_p is adjusted to ensure $\omega_c = 100$ Hz. This system has $PM_{BLS} = 30°$, with $\phi_{RC} = 51.9°$ added through CI [3]. The Bode plot is given in Fig. 12. As full reset is used, consecutive resets have negligible effects.

The ISE and L_∞ metrics are given for all three description methods by Fig. 13. ISE values in particular are found to be excessive, exceeding $100\,\%$ for many frequencies, for all methods. This is explained by the time response for a 20 Hz reference, provided by Fig. 14. Without time regularization the simulated response is seen to have numerous resets per period, even affecting the weight of the modelled one.

For full time regularization the simulated response visually coincides with the δ-CL prediction. The marginal errors left

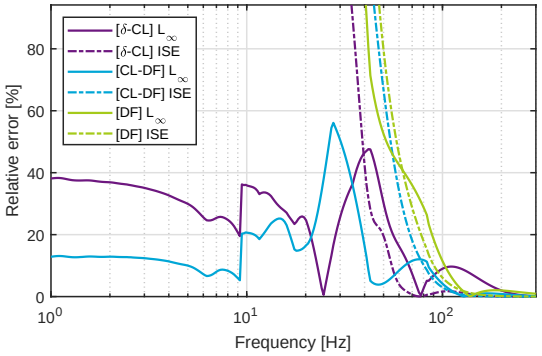

Fig. 13. ISE and L_∞ performance indicators for (39) controlled using a CI and C_{CI}. Results are shown for the three analytical describing methods.

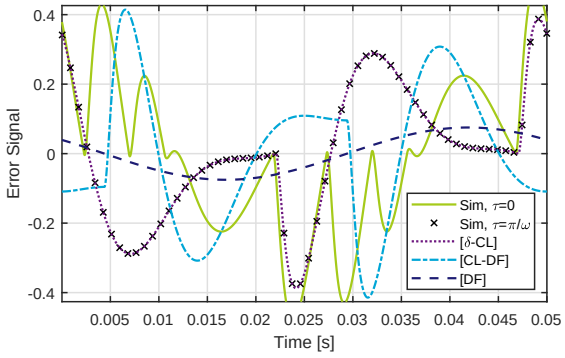

Fig. 14. Error time responses for (39) controlled using a CI and a linear controller C_{CI} with a 20 Hz unit magnitude reference. Simulated responses are given with either no ($\tau = 0$) or full ($\tau = \pi / \omega$) time regularization, in addition to modelled responses using the three analytical RC descriptions.

must be caused by Assumption 4. The CL-DF erroneously predicts its reset time. This prediction is consistent with its $\vec{q}_{DF,1} = 0$ assumed reset time (see Table III), but deviates considerably from the simulated signal.

B. Effects of Assumption 4

The effects of Assumption 4 can be isolated by applying full time regularization. This assumes $\Phi \ll 180°$. Φ is expected to be small if the combined effects of all prior resets have dampened out at a reset instant. It follows that:

- More errors are expected at high frequencies, since there is less time between resets, thus less time for reset-induced impulses to dampen out.
- Higher errors are expected for a lower PM_{BLS}, as a lower PM generally increases settling times.

Fig. 15 gives the worst-case performance metrics when full time regularization is used, as a function of PM_{BLS}. Assumption 4 is found to be violated at very low values of PM_{BLS}. δ-CL will thus give erroneous results there. For reasonable PM_{BLS}, Fig. 15 shows that prediction errors due to Assumption 4 shrink when PM_{BLS} increases. At most PM_{BLS} points δ-CL greatly outperforms the DF and CL-DF descriptions, both in ISE and L_∞ terms.

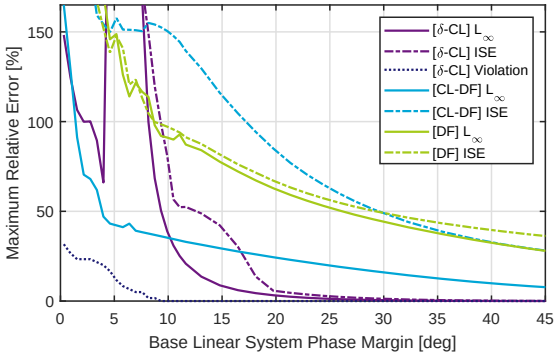

Fig. 15. Performance metrics plotted against PM_{BLS}, where the worst performing frequency between 10 and 100 Hz is given, per value of PM_{BLS}. The range of PM_{BLS} is obtained by sweeping β from 4.5 to 1.37, while otherwise using $\mathcal{R}_1^\star$ on (39). Full time regularization is used. The percentage of frequencies between 10 and 100 Hz violating Assumption 3 is given.

Fig. 16 provides ISE and Φ results for two controllers with different PM_{BLS} as function of frequency, using full time regularization. As such, all modelling errors are caused by Assumption 4, which means that the solutions should be exact if $\Phi = 0$. This holds, as can be seen in Fig. 16.

C. Effects of Assumption 5

This assumption extends the generality of δ-CL by permitting multi-sine references and disturbances. One of the worst cases for this assumption is if some other input has its peaks coinciding with the zero crossings of the base sinusoid, as this causes it to have a considerable effect on the reset times. Consider disturbance $\vec{d}$, introduced between $C(s)$ and $P(s)$, having a phase computed to meet this worst case scenario and magnitude parametrized by $\eta = |\vec{d}| \,/\, |\vec{r}_I|$. Fig. 17 gives sample predictions and simulations for various η.

The system without disturbance ($\eta = 0$) has a reset at (A), which is the one modelled by δ-CL. Assumption 5 considers

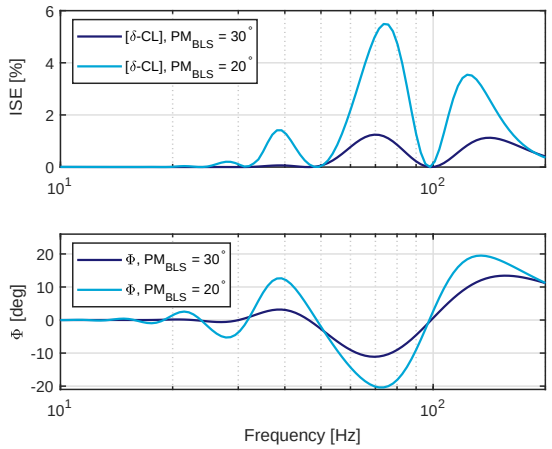

Fig. 16. ISE and Φ values, for $\mathcal{R}_1^\star$ and $\mathcal{R}_2^\star$ acting on (39), visualizing the relations between Φ, PM_{BLS} and ISE. Full time regularization is used.

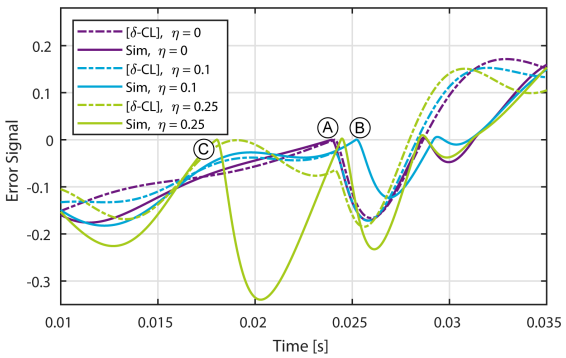

Fig. 17. Time domain simulations and δ-CL predictions for a 20 Hz reference and a 100 Hz disturbance with magnitudes η relative to the reference, using controller $\mathcal{R}_0^\star$ on (39). No time regularization is used. A half period response is shown. The disturbance phase is chosen such that its peaks coincide with zero-crossings of $\bar{q}(t)$ when there would not be a disturbance.

the corresponding reference to be the only one causing resets. Predictions with disturbance therefore also model their resets at (A). However, the reset for $\eta = 0.1$ occurs at (B), causing a slight error in predicted peak position. The case for $\eta = 0.25$ is far worse, as it generates an additional reset at (C), which is not captured at all yet inflicts the largest error peak.

The effects of Assumption 5 depend on numerous parameters, including plant model, controller and input type. Its validity should therefore be evaluated per individual system.

D. Method validity

The various error sources are found to be well-defined, as they can be clearly linked to Assumptions 1 or 4. In case both assumptions hold all modelling errors equal zero. As such the solution without assumptions, (27), is exact, which is as expected based on the mathematical derivation.

δ-CL is an approximation, relying on Assumptions 1 and 4. The former rarely holds in practice, yet does not necessarily inflict large errors, as additional resets are generally of lower magnitude than the modelled ones. Exceptions exist, as seen in Fig. 14 for $\tau = 0$. Increasing τ diminishes these errors.

Assumption 4 holds if PM_{BLS} is sufficiently large, in which case it inflicts small errors relative to Assumption 1. Based on Fig. 15, a $PM_{BLS} \gtrapprox 20°$ is advised for using δ-CL. These limits are system dependent.

IX. Simulation Results

The performance of δ-CL is further examined and compared to that of CL-DF and DF using various CgLp tunings, provided by Table IV. Optimal time regularization is used. Table V tabulates the peak and log-space average ISE and L_∞ metrics.

From Table V it can be concluded that, in terms of ISE, δ-CL consistently outperforms CL-DF and DF. In terms of L_∞, differences between δ-CL and CL-DF are less pronounced, with either method yielding similar results, though both performing significantly better than DF. As expected, prediction errors increase when PM_{BLS} decreases. From

TABLE IV

CgLp and PID controller details with ϕ_{RC} indicating the phase lead provided through reset at bandwidth as computed using DF analysis. For all controllers $\omega_i = 10$ Hz, $\omega_c = 100$ Hz and $\omega_f = 500$ Hz. Gain k_p is adjusted to achieve bandwidth ω_c.

	PM_{BLS}	ϕ_{RC}	γ	ω_r [Hz]	α	β
$\mathcal{R}_0$	20°	40°	0	34.41	1.24	2.17
$\mathcal{R}_1$	30°	30°	-0.2	83.46	1.18	2.87
$\mathcal{R}_2$	30°	30°	0	62.88	1.15	2.78
$\mathcal{R}_3$	30°	30°	0.2	37.55	1.12	2.68
$\mathcal{R}_4$	40°	20°	0	98.38	1.07	3.59
$\mathcal{R}_5$	40°	30°	0	62.88	1.15	3.79
$\mathcal{R}_6$	50°	30°	0	62.88	1.15	5.79
$\mathcal{R}_7$	50°	40°	0	34.41	1.24	5.81

comparing mean and median values for optimal and full time regularization it is concluded that the main error source for δ-CL must be unmodelled resets, as prediction errors reduce significantly if full time regularization is applied. The same does not hold for CL-DF nor DF, which retain similar ISE and L_∞ values when removing additional resets.

A. Examining results for $\mathcal{R}_2$

Results for $\mathcal{R}_2$ are analysed in greater detail. This controller is selected because it roughly represents the median of all controllers in terms of performance. Fig. 18 gives the Bode plot for this setup, showing that the PM_{BLS} is 30° and that reset adds $\phi_{RC} = 30°$, as predicted through DF analysis.

Fig. 19 shows the performance metrics for all three prediction methods. In terms of ISE, δ-CL outperforms CL-DF and DF. More subtle differences between δ-CL and CL-DF are found for the L_∞ metric, with either method improving upon the other in some frequency range.

A time domain response is used for further analysis, given by Fig. 20 for a $\omega = 20$ Hz reference. At this frequency Fig. 19 indicates that, when considering L_∞, CL-DF outperforms δ-CL. The time domain responses show that δ-CL captures the effects of reset instant (A) accurately. Reset (B), considerably smaller in magnitude, is not modelled, causing the found ISE and L_∞ errors. Considering CL-DF, Fig. 20 shows that it models the response to (A) with some offset. While this causes ISE errors, this erroneous placement works to its advantage

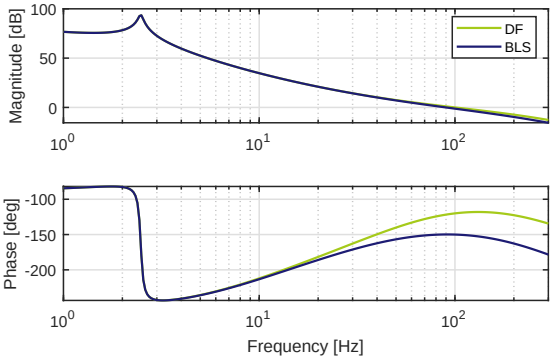

Fig. 18. Bode Plot for plant (39) with controller $\mathcal{R}_2$. The responses of the BLS and nonlinear RC modelled through DF analysis are shown.

TABLE V
ANALYTIC RCS DESCRIPTION METHOD PERFORMANCE USING PLANT (39) WITH THE CONTROLLERS IN TABLE IV. OPTIMAL TIME REGULARIZATION IS USED. THE RELATIVE PEAK AND LOG-SPACE AVERAGE ISE AND L_∞ RESULTS ARE GIVEN, EVALUATED BETWEEN 1 HZ AND BANDWIDTH. MEAN AND MEDIAN VALUES ARE GIVEN FOR BOTH OPTIMAL AND FULL TIME REGULARIZATION.

	$\max_\omega$ ISE			$\max_\omega L_\infty$			avg_ω ISE			$\text{avg}_\omega L_\infty$		
	δ-CL	CL-DF	DF	δ-CL	CL-DF	DF	δ-CL	CL-DF	DF	δ-CL	CL-DF	DF
Results for optimal time regularization:												
$\mathcal{R}_0$	69.0 %	94.0 %	114 %	33.1 %	19.0 %	94.1 %	12.5 %	16.1 %	23.6 %	5.30 %	4.35 %	22.6 %
$\mathcal{R}_1$	1.33 %	7.82 %	12.9 %	8.71 %	15.2 %	29.1 %	0.113 %	1.37 %	3.03 %	0.719 %	1.90 %	6.61 %
$\mathcal{R}_2$	2.63 %	11.0 %	16.8 %	7.22 %	10.7 %	31.1 %	0.383 %	1.93 %	4.13 %	1.20 %	1.78 %	7.62 %
$\mathcal{R}_3$	11.1 %	25.5 %	31.4 %	15.7 %	9.83 %	40.9 %	2.56 %	4.72 %	8.03 %	2.91 %	1.53 %	10.6 %
$\mathcal{R}_4$	0.00720 %	1.21 %	3.26 %	0.262 %	4.07 %	14.0 %	0.00120 %	0.215 %	0.791 %	0.0412 %	0.551 %	2.87 %
$\mathcal{R}_5$	1.63 %	7.77 %	12.6 %	5.94 %	5.55 %	22.6 %	0.287 %	1.59 %	3.34 %	0.963 %	1.13 %	6.02 %
$\mathcal{R}_6$	1.17 %	6.45 %	10.0 %	4.89 %	4.25 %	17.0 %	0.238 %	1.46 %	2.83 %	0.814 %	0.610 %	4.96 %
$\mathcal{R}_7$	12.9 %	38.0 %	40.0 %	13.7 %	5.62 %	30.2 %	3.26 %	10.5 %	12.3 %	3.32 %	1.37 %	10.2 %
mean:	12.5 %	24.0 %	30.1 %	11.2 %	9.28 %	34.9 %	2.38 %	4.74 %	7.26 %	1.91 %	1.65 %	8.94 %
median:	2.13 %	9.43 %	14.9 %	7.96 %	7.72 %	29.7%	0.335 %	1.76 %	3.73 %	1.08 %	1.45 %	7.12 %
Results for full time regularization:												
mean:	2.65 %	48.7 %	42.0 %	2.62 %	20.4 %	47.8 %	0.181 %	7.28 %	8.63 %	0.220 %	3.12 %	10.6 %
median:	0.0358 %	13.6 %	17.0 %	0.620 %	14.6 %	36.8%	0.00195 %	2.23 %	3.84 %	0.0438 %	2.34 %	7.30%

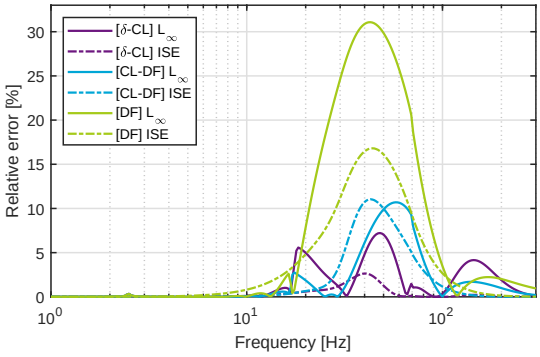

Fig. 19. L_∞ and ISE performance indicators for all three prediction methods over a range of frequencies, using plant (39) with controller $\mathcal{R}_2$. Optimal time regularization ($\tau = 2\pi / (10\,\omega_c)$) is used.

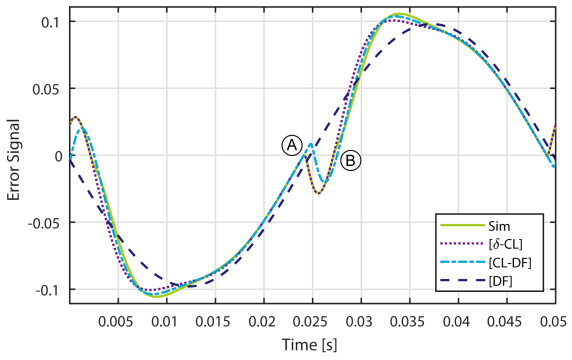

Fig. 20. Simulated and predicted error time responses for plant (39) with controller $\mathcal{R}_2$, using a 20 Hz sinusoidal $\vec{r}_I(t)$ with unit magnitude. The reset instants for a half period, (A) and (B), are indicated.

here, as the incorrect positioning of (A) compensates for not modelling (B) in evaluating the peak error, L_∞. As such, L_∞ performance of CL-DF is, in this case, better than that of δ-CL.

The erroneous impulse position prediction of CL-DF does not generally works to its advantage. Fig. 14 gives an example where large ISE errors are inflicted by the CL-DF reset placement assumption. Evaluating (18) shows that the error signal equals the BLS with added impulse responses. Thus, zero crossings occur near those of the BLS, provided that the impulse responses are sufficiently convergent. This supports that the reset placement assumption used by δ-CL is often more accurate than that of CL-DF.

X. CONCLUSION

Reset control can overcome fundamental limitations of linear control, whilst permitting design using the industry-preferred loop shaping methodology. Even though accurate tuning through loop shaping requires a thorough understanding of closed-loop behaviour, no frequency-domain methods found in literature describe the principles of how open-loop reset control design translates to closed-loop behaviour.

A rarely mentioned approach, which models open-loop reset control as a linear system with state-dependent impulse train inputs, is taken and generalized. It is shown that any generic closed-loop reset system behaves as the base-linear system with added impulse responses. This describes, to the authors' knowledge, for the first time the underlying principles that link open-loop reset control design to its closed-loop performance, using frequency-domain terms as required for loop shaping. This insight may be used to improve reset control design.

An analytical solution is obtained by inserting some well-defined assumptions. This description is critically examined using simulations and compared to existing methods. The novel description consistently provides a considerably more accurate time-domain prediction than the best performing analytical method found in literature, whilst having a similar performance in terms of predicted peak errors. It is shown how the various assumptions contribute to the prediction error, giving a good understanding of method limitations. High accuracy is attained if the base-linear system has sufficient phase margin and if unmodelled resets have a comparatively low magnitude, conditions met by various practical implementations.

Concluding, it is found that the presented description provides additional insight and improves predictions for reset control analysis, which can be used to improve reset element design. Further research should be conducted on how these results can be applied to practical reset control tuning.

REFERENCES

[1] T. Samad, S. Mastellone, P. Goupil, A. van Delft, A. Serbezov, and K. Brooks, "IFAC industry committee update, initiative to increase industrial participation in the control community," *IFAC Newsletter*, no. 2, 2019.

[2] H. W. Bode, *Network Analysis and Feedback Amplifier Design*. Princeton, New Jersy: D. Van Nostrand Company, Inc, 12th ed., 1945.

[3] J. C. Clegg, "A nonlinear integrator for servomechanisms," *Transactions of the American Institute of Electrical Engineers, Part II: Applications and Industry*, vol. 77, no. 1, pp. 41–42, 1958.

[4] A. Gelb and W. E. Vander Velde, *Multiple-input Describing Functions and Nonlinear System Design*. McGraw-Hill Book Company, 1st ed., 1968.

[5] I. Horowitz and P. Rosenbaum, "Non-linear design for cost of feedback reduction in systems with large parameter uncertainty," *International Journal of Control*, vol. 21, no. 6, pp. 977–1001, 1975.

[6] O. Beker, C. V. Hollot, Y. Chait, and H. Han, "Fundamental properties of reset control systems," *IFAC Proceedings Volumes (IFAC-PapersOnline)*, vol. 15, no. 1, pp. 187–192, 2004.

[7] Y. Guo, Y. Wang, and L. Xie, "Frequency-domain properties of reset systems with application in hard-disk-drive systems," *IEEE Transactions on Control Systems Technology*, vol. 17, no. 6, pp. 1446–1453, 2009.

[8] L. Hazeleger, M. Heertjes, and H. Nijmeijer, "Second-order reset elements for stage control design," *Proceedings of the American Control Conference*, vol. 2016-July, pp. 2643–2648, 2016.

[9] N. Saikumar, H. Hosseinnia, and M. Engineering, "Generalized Fractional Order Reset Element (GFrORE)," Tech. Rep. 1, Delft University of Technology, 2017.

[10] N. Karbasizadeh, A. A. Dastjerdi, N. Saikumar, D. Valério, and S. H. Hosseinnia, "Benefiting from Linear Behaviour of a Nonlinear Reset-based Element at Certain Frequencies," tech. rep., Delft University of Technology, 2020.

[11] N. Saikumar, R. K. Sinha, and S. Hassan HosseinNia, "Resetting disturbance observers with application in compensation of bounded nonlinearities like hysteresis in piezo-actuators," *Control Engineering Practice*, vol. 82, no. March 2018, pp. 36–49, 2019.

[12] A. Vidal and A. Baños, "QFT-based design of PI+CI reset compensators: Application in process control," *2008 Mediterranean Conference on Control and Automation - Conference Proceedings, MED'08*, pp. 806–811, 2008.

[13] A. Vidal and A. Baños, "Reset compensation for temperature control: Experimental application on heat exchangers," *Chemical Engineering Journal*, vol. 159, no. 1-3, pp. 170–181, 2010.

[14] D. Nešić, L. Zaccarian, and A. R. Teel, "Stability properties of reset systems," in *IFAC Proceedings Volumes (IFAC-PapersOnline)*, vol. 38, pp. 67–72, 2005.

[15] F. Fichera, P. Christophe, S. Tarbouriech, and L. Zaccarian, "Using Luenberger observers and dwell-time logic for feedback hybrid loops in continuous-time control systems," *International Journal of Robust and Nonlinear Control*, vol. 18, no. October 2014, pp. 557–569, 2008.

[16] V. Ghaffari, P. Karimaghaee, and A. Khayatian, "Reset law design based on robust model predictive strategy for uncertain systems," *Journal of Process Control*, vol. 24, no. 1, pp. 261–268, 2014.

[17] Y. Guo, Y. Wang, L. Xie, H. Li, and W. Gui, "Optimal reset law design of reset control systems with application to HDD systems," *Proceedings of the IEEE Conference on Decision and Control*, pp. 5287–5292, 2009.

[18] C. Prieur, S. Tarbouriech, and L. Zaccarian, "Lyapunov-based hybrid loops for stability and performance of continuous-time control systems," *Automatica*, vol. 49, no. 2, pp. 577–584, 2013.

[19] L. Li, F. Wu, and X. Wang, "A reset controller design method for MIMO linear systems," *Chinese Control Conference, CCC*, no. 2, pp. 2132–2136, 2013.

[20] K. R. Krishnan and I. M. Horowitz, "Synthesis of a non-linear feedback system with significant plant-ignorance for prescribed system tolerances," *International Journal of Control*, vol. 19, no. 4, pp. 689–706, 1974.

[21] Y. Zheng, Y. Chait, C. V. Hollot, M. Steinbuch, and M. Norg, "Experimental demonstration of reset control design," *Control Engineering Practice*, vol. 8, no. 2, pp. 113–120, 2000.

[22] O. Beker, C. V. Hollot, and Y. Chait, "Plant With Integrator: An Example of Reset Control Overcoming Limitations of Linear Feedback," *IEEE Transactions on Automatic Control*, vol. 46, no. 11, pp. 1797–1799, 2001.

[23] O. Beker, *Analysis of Reset Control Systems*. PhD thesis, University of Massachusetts, 2001.

[24] A. Feuer, G. C. Goodwin, and M. Salgado, "Potential benefits of hybrid control for linear time invariant plants," *Proceedings of the American Control Conference*, vol. 5, pp. 2790–2794, 1997.

[25] E. Akyüz, N. Saikumar, and S. H. Hosseinnia, "Reset Control for Vibration Isolation," tech. rep., Delft University of Technology, 2019.

[26] A. Banos and A. Barreiro, *Reset Control*. London: Springer, 1 ed., 2006.

[27] A. Palanikumar, N. Saikumar, and S. H. Hosseinnia, "No More Differentiator in PID: Development of Nonlinear Lead for Precision Mechatronics," *2018 European Control Conference, ECC 2018*, pp. 991–996, 2018.

[28] L. Chen, N. Saikumar, S. Baldi, and S. H. Hosseinnia, "Beyond the Waterbed Effect: Development of Fractional Order CRONE Control with Non-Linear Reset," *Proceedings of the American Control Conference*, vol. 2018-June, pp. 545–552, 2018.

[29] N. Saikumar, R. K. Sinha, and S. Hassan Hosseinnia, "'Constant in Gain Lead in Phase' Element-Application in Precision Motion Control," *IEEE/ASME Transactions on Mechatronics*, vol. 24, no. 3, pp. 1176–1185, 2019.

[30] N. Saikumar, D. Val, and S. H. Hosseinnia, "Complex order control for improved loop-shaping in precision positioning," *IEEE Conference on Decision and Control*, 2019.

[31] K. Heinen, "Frequency analysis of reset systems containing a Clegg integrator," 2018.

[32] N. Saikumar, K. Heinen, and S. H. Hosseinnia, "Loop-shaping for reset control systems: a higher-order sinusoidal-input describing functions approach." 2020.

[33] A. A. Dastjerdi, A. Astolfi, N. Saikumar, N. Karbasizadeh, D. Valerio, and S. H. HosseinNia, "Closed-loop frequency analyses of reset systems," tech. rep., Delft University of Technology, 2020.

[34] C. V. Hollot, O. Beker, Y. Chait, and Q. Chen, *On Establishing Classic Performance Measures for Reset Control Systems*. New York: Springer - Verlag, 2001.

[35] Y. Chait and C. V. Hollot, "On Horowitz's contributions to reset control," *International Journal of Robust and Nonlinear Control*, vol. 12, no. 4, pp. 335–355, 2002.

[36] W. M. Haddad, V. Chellaboina, and N. A. Kablar, "Active Control of Combustion Instabilities via Hybrid Resetting Controllers," in *Proceedings of the American Control Conference*, no. June, (Chicago), pp. 2378–2382, 2000.

[37] L. Zaccarian, D. Nešić, and A. R. Teel, "First order reset elements and the Clegg integrator revisited," *Proceedings of the American Control Conference*, vol. 1, pp. 563–568, 2005.

[38] M. F. Heertjes, K. G. Gruntjens, S. J. van Loon, N. van de Wouw, and W. P. Heemels, "Experimental Evaluation of Reset Control for Improved Stage Performance," *IFAC-PapersOnLine*, vol. 49, no. 13, pp. 93–98, 2016.

[39] Y. Guo, L. Xie, and Y. Wang, *Analysis and design of reset control systems*. London: The Institution of Engineering and Technology, 1 ed., 2016.

[40] P. W. J. M. Nuij, O. H. Bosgra, and M. Steinbuch, "Higher-order sinusoidal input describing functions for the analysis of non-linear systems with harmonic responses," *Mechanical Systems and Signal Processing*, vol. 20, no. 8, pp. 1883–1904, 2006.

[41] D. Paesa, C. Franco, S. Llorente, G. Lopez-Nicolas, and C. Sagues, "Reset observers applied to MIMO systems," *Journal of Process Control*, vol. 21, no. 4, pp. 613–619, 2011.

[42] G. Zhao and C. Hua, "Discrete-Time MIMO Reset Controller and Its Application to Networked Control Systems," *IEEE Transactions on Systems, Man, and Cybernetics: Systems*, vol. 48, no. 12, pp. 2485–2495, 2018.

[43] B. Kieft, N. Saikumar, and S. H. Hosseinnia, "Time regularization as a solution to mitigate quantization induced performance degradation," tech. rep., Delft University of Technology, 2020.

Chapter 7

Discussion

The paper presented in Chapter 6 provides three main results. First, a Reset Control System (RCS) description is derived linking open- with closed-loop, based on the novel impulse approach. Second, this is transformed into an exact frequency-domain RCS description for RCSs with periodic outputs. Third, an analytical solution is presented and analysed. This chapter further discusses each of these results, summarizing and expanding upon that what is written in the paper.

7-1 Impulsive description of Reset Control Systems

Section IV of the paper expresses, to the author's knowledge for the first time, RCS behaviour in terms of open-loop Reset Control (RC) design. The obtained solution holds for any generic RCS, as long as the solution is unique and exists. SISO and MIMO RCSs can be described alike. It is proven that any RCS solution equals the Base Linear System (BLS) summed by linear impulse responses. RCS design therefore comprises of tuning these impulse responses and the BLS in such way that some desired performance is obtained.

The BLS is linear, standard to loop shaping. The impulse responses follow from the transfer function between the reset states and the desired output, e.g. the error signal, in closed-loop. These responses are weighted by the RC states at the corresponding reset instants and by $I - A_\rho$. Matrix A_ρ therefore determines the reset weight.

Various characteristics of RCSs can be explained using the impulsive method:

1. Literature mentions that RCSs can have lower sensitivity peaks than the corresponding BLSs [86]. This implies that, at frequencies around the sensitivity peak, errors induced by the RCS must be lower than those of the BLS. The novel impulse analysis proves that the RCS error response equals the BLS with added impulse responses. It follows that, if the RCS errors are lower than those of the BLS, reset-induced impulses must partially cancel the BLS error signal.

2. Often, RCSs are found to have less overshoot in a step response than their BLS counterparts [23, 30, 85]. The obtained description provides a new way of explaining this advantage. It proves that, in this case, reset-induced impulse responses counteract overshoot peaks.

3. Describing Function (DF) analysis shows that RC either provides phase lead or reduces phase lag. This can be explained in time-domain terms. Impulse responses force the open-loop system to behave such that the best sinusoidal fit, as computed by DF analysis, is shifted with respect to the linear system. See, for instance, Figure 3-2.

   The expected effects of the added phase can also be found in RCS responses. More phase increases the phase margin, which, for linear systems, reduces error signals and decreases overshoot. Impulse responses may partially cancel the BLS error at some frequencies, or reduce overshoot. As such, reset may provide effects very similar to the case of having more phase margin. It follows that, with reset, requirements on phase margin may be loosened while maintaining the same performance.

   Diminished requirements on phase margin for RCS may, through the Bode gain-phase relationship, be traded for improved specifications elsewhere. Therefore, RC can improve system performance.

4. The impulsive description of RCSs explains the role of open-loop RC design in closed-loop. The RC shapes both the BLS and the reset-induced closed-loop impulse response. Practical design of RCSs should therefore consider both responses. For example, designers could look into how the impulse responses can be designed relative to the BLS, in order to achieve some desired mitigation of the BLS using impulse responses at particular frequencies.

Desired performance is achieved by designing the BLS and impulse responses such that some intended reset-induced advantage is obtained. Usually, the impulse responses are used to cancel the BLS error or overshoot, boosting performance when compared to that of the BLS. Although this work provides these underlying principles, it does not yet show how these insights can be used in practical design.

7-2 Exact frequency-domain solution

A novel, exact closed-loop frequency-domain solution is derived in the paper, Section V, for stable SISO RCSs with zero-crossing resets in the paper. Solution periodicity of the RCS is required to obtain a frequency-domain description through a Fourier series, using HOSIDF analysis. This description limits itself to stable SISO systems, as needed for the periodicity theorem used. The obtained solution is exact, but still requires solving for all reset times and states.

An analytical approach to solve for these reset times and states was pursued during this thesis, using certain assumptions. Numerical or different analytical approaches are imaginable. The numerical approach would likely yield results similar to CL-FR, as the setup requirements for either method are identical. Other analytical solutions may provide new advantages, for example by using different assumptions. The description provided can in any case serve as a starting point for future derivations, which may further improve modelling accuracy.

7-3 Analytical solution

The exact frequency-domain solution provided by the paper in Section V requires knowledge of both reset times and states. These are approximated in Section VI, using several well-defined assumptions, yielding a solution more accurate in time-domain terms than the various descriptions found in literature. The effects of these assumptions are discussed, referring to the assumption numbers as stated in the paper, Section VI.

1. The first assumption simplifies the problem by modelling two resets per input period only. This is known to not hold [30], and thus causes modelling errors. The consequences for partially resetting systems without time regularization are worse than for full resetting systems with time regularization. The other available analytical methods in literature, DF and CL-DF, also utilize this assumption.

   The effects of this assumption may be limited in practice, as ignored resets are generally smaller in magnitude than the main, modelled reset. Nevertheless, it is found that this assumption is responsible for the vast majority of the modelling errors. This follows from the paper, Table V, which shows that results with multiple resets per period (optimal time regularization) for the developed δ-CL method are significantly worse than in the case where two resets per period are enforced (full time regularization).

2. The second assumption was never found to be violated during this thesis.

3. The third assumption is found to be violated if the phase margin of the BLS is very low. However, this assumption is known to always hold for real systems. Any violation therefore implies that other assumptions cause this one to not hold.

4. The fourth assumption yields comparatively small modelling errors. This is inferred from the results with full time regularization, as given in the paper, Table V, in which case modelling errors are solely caused by this assumption. The prediction errors with full time regularization are considerably lower than those with optimal time regularization. It follows that prediction errors inflicted by this assumption are relatively small.

   Inflicted errors decrease further if the BLS phase margin increases. This work found that, for the system under consideration, phase margins above 20° imposed no significant errors. The exact number depends on which particular setup is used.

5. The fifth assumption extends results for multi-sine references or disturbances, and must be evaluated for each individual case.

It is shown that there are no modelling errors if all assumptions hold. This implies that the underlying mathematical derivation is correct, validating the impulse modelling approach.

Chapter 8

Conclusion

Reset Controllers (RCs) can be used in combination with linear controllers to overcome fundamental limitations inherent to linear control, whilst permitting the industry-preferred loop shaping methodology. Although a thorough understanding of closed-loop behaviour in frequency-domain terms is imperative for accurate design using loop shaping, no analytical frequency-domain methods fundamentally linking open-loop RC design to its closed-loop behaviour are found in literature.

A rarely used approach for modelling RCs is taken and expanded, modelling RC as a linear system with state-dependent timed impulse train inputs. This open-loop formulation is used to show that all generic Reset Control System (RCS)s behave as their Base Linear System (BLS) with added impulse responses. This describes the underlying principles that link open-loop RC design to closed-loop performance, filling the identified research gap. The result is transformed into frequency-domain terms, as required for loop shaping.

An analytical solution is obtained by inserting some well-defined assumptions. This solution is critically examined using simulations and compared to existing methods. It is concluded that the novel description consistently provides a considerably more accurate time-domain prediction than the best performing analytical method found in literature, whilst having a similar performance in terms of predicted peak errors.

It is shown how the various assumptions contribute to the prediction error by decoupling them using time regularization, giving a good understanding of method limitations. High accuracy is attained if the BLS has sufficient phase margin and if unmodelled resets have a comparatively low magnitude, conditions met by various practical implementations.

To conclude, it is found that the presented description provides additional insight, by showing how open-loop RC design affects closed-loop performance. The fundamental understanding of closed-loop RC behaving as the sum of the BLS and linear impulse responses enhances insight into RC design. Analytical predictions for RC analysis are improved, which can be used to better design RCs for industry.

Chapter 9

Recommendations

This thesis merely provides the first step into analysis based on the impulsive description method. Several steps are possible to expand upon the ideas presented here. First, research can be conducted on extending the generality of the presented method. It is also imaginable that the precision of the newly developed δ-CL description can be further improved at the cost of increasing mathematical complexity. Finally, new ways of incorporating harmonics in design are needed to utilize the enhanced modelling precision. These three aspects are further elaborated upon:

1. Research should be conducted on extending the δ-CL method for MIMO systems. A major roadblock is the periodicity condition required for frequency-domain analysis, which is shown for SISO cases only [36]. A MIMO extension of this periodicity theorem would allow the remainder of the derivation to be extended to MIMO.

   The entire method derivation, besides this periodicity theorem, quite naturally extends to a MIMO case as given by Eq. (2-1). That description permits having multiple reset matrices and laws, which is often needed for MIMO systems. The outline of this extension would be as follows:

   Consider the SISO result, which shows that the Reset Control System (RCS) output equals the Base Linear System (BLS) with added impulse responses. Intuitively, an extension to multiple k, thus to MIMO will equal the BLS with, summed over all k, added impulse responses corresponding to the k-th reset law and matrix. A frequency-domain description of this extension requires a MIMO periodicity theorem. Research is needed on how to effectively design these MIMO Reset Control (RC)s, as related literature is very limited.

2. The proposed method could be made significantly more accurate by modelling more than two resets per period. This follows from the results, which show that, as long as the phase margin of the BLS is sufficiently high, the vast majority of prediction errors are due to unmodelled resets. As such, if more resets per period are modelled, significant prediction accuracy improvements will be achieved.

3. Research is needed that investigates how harmonics can be incorporated in loop shaping design for closed-loop performance. To this date, a comprehensive method of utilizing harmonics in RC synthesis does not exist. Several works have attempted to incorporate this, but these works mostly yielded lookup-table like results for open-loop systems. Extending such research to the novel, more accurate, closed-loop description could yield useful design principles for industry.

Appendix A

MATLAB Code

This appendix provides all essential MATLAB codes necessary for obtaining the results presented in this thesis. The subsequent appendix provides corresponding Simulink files.

A-1 Main File

The code below is the 'main' file driving the analysis. This code calls upon all other functions presented in this appendix. Multiple Reset Control (RC) tunings can be evaluated during one run.

```
% Ruben Buitenhuis, 24/06/2020, TU Delft
clearvars; close all;
s = tf('s');

%% ------------------------------------------------------------------------
% INPUT SECTION
% ------------------------------------------------------------------------

% Frequencies to consider in analysis
Wmin = 1;       %[Hz]. Lowest frequency to simulate for
Wmax = 300;     %[Hz]. Highest frequency to simulate for
Wnum = 100;     % Number of frequency points evaluated for

% Combining set parameters, do not alter.
W = logspace(log10(Wmin*2*pi),log10(Wmax*2*pi),Wnum);

% Define lists of controller parameters:
% - Reset parameter gamma
% - Reset corner frequency Wr
% - Reset adjustment parameter Alpha
% - PID parameter beta
% See corresponding paper for exact defnitions of these. Define
% parameters as vectors, simulations will be carried out over each entry
```

```
% set. Each of the vectors must be of equal length
dsgn.Gamma = [0,-0.2,0,0.2,0,0,0,0];
dsgn.Wr = [34.41,83.46,62.88,37.55,98.38,62.88,62.88,34.41].*2*pi;
dsgn.Alpha = [1.24,1.18,1.15,1.12,1.07,1.15,1.15,1.24];
dsgn.beta = [2.17,2.87,2.78,2.68,3.59,3.79,5.79,5.81];
% Some more parameters:
% - harmMax: number of harmonics considered in analysis
% - wc: bandwidth [rad/s]
% - wf: cutoff frequency for low-pass filter [rad/s]
% - wi: zero position of tamed integrator zero
% These vectors must have equal length to those given before.
dsgn.harmMax = 1000*ones(size(dsgn.Gamma));
dsgn.wc = 100*2*pi*ones(size(dsgn.Gamma));
dsgn.wf = 5.*dsgn.wc;
dsgn.wi = dsgn.wc./10;
% Time regularization parameter. Options:
% - 0: no time regularization.
% - 1: full time regularization: enforcing two resets per period.
% - 2: optimal time regularization: see [Kieft, Bas. Not yet published].
% Select time regularization type, see paper for definitions
dsgn.timeReg = 1*ones(size(dsgn.Gamma));

% Reference settings
smlk.maginput = 1;                  % [-] input amplitude
smlk.pinput = 0;                    % [rad] input phase shift

% Plant transfer function
P = 3.038e04/(s*s + 0.7413*s + 243.3);

%% ------------------------------------------------------------------------
% SIMULATIONS
% ------------------------------------------------------------------------
% The implementation shown here is tailored to CgLp. However, any other
% reset element can be introduced by changing the R.{A,B,C,D} matrices.
% This loop is ran for each entry in the list of controller parameters
for loop = 1:length(dsgn.Gamma)
    % CgLp Design Parameters
    R.resetType = "CgLp";
    R.wr = dsgn.Wr(loop);
    R.wra = R.wr/dsgn.Alpha(loop);
    R.gamma = dsgn.Gamma(loop);
    % State-space of reset element
    %
    % Matrices for FORE CgLp are inserted here, but can be changed into
    % any other (SISO) reset element.
    R.A = [-R.wra,0;dsgn.wf(loop),-dsgn.wf(loop)];
    R.B = [R.wra;0];
    R.C = [dsgn.wf(loop)/R.wr,1-dsgn.wf(loop)/R.wr];
    R.D = 0;
    R.Arho = [R.gamma,0;0,1];
    R.tf = ss(R.A,R.B,R.C,R.D);

    % Controller prior to reset element, set to unity gain.
```

```
77      K.tf = tf(1);
78      % Controller appending reset element. PID is used here.
79      C = minreal((s+dsgn.wi(loop))/s*...
80          (s+dsgn.wc(loop)/dsgn.beta(loop))...
81          /(s+dsgn.wc(loop)*dsgn.beta(loop)));
82      % Combine plant and second controller
83      G.tf = C*P;
84
85      % Correct gain to attain desired bandwidth
86      Rval = hosidfcalc(R.tf,R.Arho,1,dsgn.wc(loop));
87      Lwc = evalfr(G.tf*Rval*K.tf,1j*dsgn.wc(loop));
88      gainMat = abs(Lwc)\1;
89      K.tf = K.tf*gainMat;
90
91      %% ------------------------------------------------------------------
92      % ANALYSIS
93      % ------------------------------------------------------------------
94      % Obtain DF and BLS data
95      [sidf.L,sidf.S,sidf.E,sidf.n,bls.L,bls.S,bls.E,bls.n,...
96          data.sidf.pm,data.bls.pm] = getDF_BLS(G.tf,R.tf,R.Arho,K.tf,W,...
97          dsgn.wc(loop),smlk.maginput,smlk.pinput);
98      bodePlot(sidf.L,bls.L,W);    % Plot Bode
99      % Run simulations
100     [simd.t,simd.e,simd.Smax] = getSimResults(smlk,W,dsgn.timeReg(loop));
101     % HOSIDF calculation
102     [d_cl.S,d_cl.n,d_cl.Phi,d_cl.E,flags] = getDeltaCL(G.tf,R.tf,...
103         R.Arho,K.tf,W,dsgn.harmMax(loop),smlk.maginput,smlk.pinput);
104     [cldf.S,cldf.n,cldf.E] = getCLDF(G.tf,R.tf,R.Arho,K.tf,W,...
105         dsgn.harmMax(loop),smlk.maginput,smlk.pinput);
106     % Provide warning if flags are set, indicating bad performance
107     if sum(flags) > 0; warning('Check Flags'); end
108
109     % Transform obtained frequency-domain descriptions into time domain
110     % signals, using the sampling times of the simulation to enable a
111     % fair comparison.
112     [d_cl.t,d_cl.e,d_cl.Smax] = error2Time(...
113         d_cl.E,d_cl.n,W,simd.t,smlk.maginput,smlk.pinput);
114     [cldf.t,cldf.e,cldf.Smax] = error2Time(...
115         cldf.E,cldf.n,W,simd.t,smlk.maginput,smlk.pinput);
116     [sidf.t,sidf.e,sidf.Smax] = error2Time(...
117         sidf.E,sidf.n,W,simd.t,smlk.maginput,smlk.pinput);
118     [bls.t,bls.e,bls.Smax] = error2Time(...
119         bls.E,bls.n,W,simd.t,smlk.maginput,smlk.pinput);
120
121     %% ------------------------------------------------------------------
122     % DATA ACQUISITION
123     % ------------------------------------------------------------------
124     % [Note] The section below uses script 'performanceMetrics' to
125     % obtain Linf and ISE error values for all frequencies, and stores
126     % these in output structure 'data'. Adapt based on which data is
127     % requested. For example, 'Smax' and 'S' data are useful for drawing
128     % sensitivity plots.
129     [data.d_cl(loop).Linf,data.d_cl(loop).ISE] = ...
```

```
130         performanceMetrics(d_cl,simd,W);
131     [data.cldf(loop).Linf,data.cldf(loop).ISE] = ...
132         performanceMetrics(cldf,simd,W);
133     [data.sidf(loop).Linf,data.sidf(loop).ISE] = ...
134         performanceMetrics(sidf,simd,W);
135     [data.bls(loop).Linf,data.bls(loop).ISE] = ...
136         performanceMetrics(bls,simd,W);
137     data.W(loop,:) = W;
138 end
```

A-2 Impulse method calculation

The code given here is used to compute δ-CL. Computations of $\exp^{At}$ - type terms, with matrix A and time t, are performed using an impulse response. These responses are considerably easier to compute than the exact solution, gaining computational efficiency at the cost of some precision.

```
1  function [S_nw,n,Phi,E_nw,flag] = getDeltaCL(G,R,Arho,K,W,nMax,varargin)
2  % function S_nw = getDeltaCL(G,R,Arho,K,W,nMax)
3  % function [S_nw,n,Phi,E_nw,flag] = getDeltaCL(G,R,Arho,K,W,nMax)
4  % function [S_nw,n,Phi,E_nw,flag] = getDeltaCL(G,R,Arho,K,W,nMax,mag,phi)
5  %
6  % This method computes the delta-CL description method of Reset Control,
7  % which originates from an impulsive formulation.
8  %
9  % ------------------------------------------------------------------------
10 % INPUTS
11 % ------------------------------------------------------------------------
12 % G:        Linear system placed after the reset element.
13 % R:        Reset element.
14 % Arho:     Reset matrices corresponding to reset element.
15 % K:        Linear system placed before the reset element.
16 % W:        List of all frequencies to be evaluated [rad/s].
17 % nMax:     Highest harmonic to be considered in analysis.
18 % mag:      List of input magnitudes
19 % phi:      List of reference phases
20 %
21 % ------------------------------------------------------------------------
22 % OUTPUTS
23 % ------------------------------------------------------------------------
24 % S_nw:         Cell matrix with the following dimensions:
25 %               - First dimension: frequencies
26 %               - Second dimension: harmonics
27 %               Each entry is a sensitivity matrix. To acquire the error,
28 %               sum the sinusoids described by the sensitivity. Take care
29 %               to multiply each sensitivity by the reference r according
30 %               to *|r|exp(1j*n*angle(r)). This corrects for having
31 %               multiple frequencies in one signal. The total predicted
32 %               error signal is obtained by summing over all inputs.
33 % n:            Vector with all harmonics
34 % Phi:          Matrix with phase caused by reset. It is assumed that
```

```
35 %                asin(Phi) = Phi for all frequencies, and that
36 %                exp(1j*(pi/2+Phi)) = 1j - Phi, which holds for Phi << 1.
37 %                This output can be used for error checking.
38 % E_nw:          Cell matrix with error signal, defined as with S_nw.
39 % flags:         Vector with one entry per frequency point. Has values:
40 %                     1: Assumption 2 violated
41 %                     2: Assumption 3 violated
42 %                     3: Assumptions 2 and 3 violated
43 %
44 % ------------------------------------------------------------------------
45 % BLOCK DIAGRAM
46 % ------------------------------------------------------------------------
47 %
48 % y <-.-[G]<-[R]<-[K]<-o+<-r
49 %     |_________________^-
50 %
51 % Ruben Buitenhuis, TU Delft. Last modification 24/06/2020
52
53 % Initialize constants
54 s = tf('s');                          % Laplace Operator
55 sz_W    = length(W);                  % Number of frequencies
56 sz_n    = ceil(nMax/2);               % Number of harmonics
57 sz_Wn   = sz_n*sz_W;                  % Number of harmonic frequencies
58 W       = reshape(W,sz_W,1);          % Frequencies to compute
59 n       = reshape(1:2:nMax,1,sz_n);   % All harmonics to consider, only odd
60 Wn      = reshape(n.*W,sz_Wn,1);      % All harmonic frequencies
61 [AR,BR,CR,~] = ssdata(R);            % Reset element state-space
62 I       = eye(1);                     % Identity matrix
63 IR      = eye(size(AR));              % Identity matrix within R
64
65 % If provided, compute reference as phasor:
66 if length(varargin) >= 2
67     Ref = varargin{1}.*exp(1j*varargin{2});
68     Ref = reshape(Ref,numel(Ref),1);
69 else
70     % Default value
71     Ref = ones(length(G),1);
72 end
73
74 % Warning to cover numerical expm(A) approximation used
75 if max(W)/min(W) > 1000
76     warning(['Large range of frequencies requested in W. '...
77         ,'Numerical errors possible at high frequencies']);
78 end
79
80 % Various transfer functions based on the BLS
81 Sbls  = (I+G*R*K)\I;                  % BLS sensitivity (no reset)
82 SblsG = Sbls*G;                       % BLS sensitivity * G
83 KSbls = K*Sbls;                       % K * BLS sensitivity
84 % Compute per frequency point the responses of these TFs
85 S1_nw = reshape(freqresp(Sbls,Wn),sz_Wn,1);
86 S1G_nw = reshape(freqresp(SblsG,Wn),sz_Wn,1);
87 KS1_1w = reshape(freqresp(KSbls,W),sz_W,1);
```

```
88
89  % Define various impulse TFs used in deriving the result. Notice that the
90  % term (Arho-I) is removed - instead, B = IR is used. The removed term is
91  % added later. This approach ensures that less impulse evaluations are
92  % needed, as these are computationally intensive.
93  H = (IR-(s*IR-AR)\BR*KSbls*G*CR)/(s*IR-AR);
94  Qdelta = KSbls*G*(CR*inv(s*IR-AR));
95  ARdelta = ss(AR,IR,IR,zeros(size(IR)));
96  % Store state-space matrices
97  [AQ,~,CQ,~] = ssdata(Qdelta);
98
99  % Analytically expm(A_H,A_R or A_Q, all*pi/omega) should be computed.
100 % However, this is computationally intensive. Instead, impulse responses
101 % of these elements are used to approximate the real value. An impulse
102 % models C(set to IR)*expm(A*t)*B(again, set to IR). Using t = pi/omega,
103 % interpolation is used to find the actual values at all values of omega.
104 [temp.yH,temp.tH] = impulse(H,pi/min(W)+eps);
105 [temp.yA,temp.tA] = impulse(ARdelta,pi/min(W)+eps);
106 [temp.yQ,temp.tQ] = impulse(Qdelta,pi/min(W)+eps);
107 % For ARdelta, only one set of evaluations is needed:
108 expmAR = ...
109     permute(interp1(temp.tA,temp.yA,pi./W,'linear','extrap'),[2,3,1]);
110
111 % Convergence test. Results are accurate if and only if the results above
112 % converge before t = pi/min(W).
113 eta = 0.8;      % Compare the final eta% response to the first(1-eta)%
114 test.sumyH1 = sum(abs(temp.yH(1:floor(eta*length(temp.tH)),:,:)),'all');
115 test.sumyH2 = sum(abs(temp.yH(ceil(eta*length(temp.tH)):end,:,:)),'all');
116 test.sumyA1 = sum(abs(temp.yA(1:floor(eta*length(temp.tA)),:,:)),'all');
117 test.sumyA2 = sum(abs(temp.yA(ceil(eta*length(temp.tA)):end,:,:)),'all');
118 test.sumyQ1 = sum(abs(temp.yQ(1:floor(eta*length(temp.tQ)),:,:)),'all');
119 test.sumyQ2 = sum(abs(temp.yQ(ceil(eta*length(temp.tQ)):end,:,:)),'all');
120 % Give warnings for numerical errors
121 test.threshold = 0.01;  % Somewhat arbitrary threshold value
122 if test.sumyH1 < test.sumyH2*test.threshold
123     warning(['Impulse response H not sufficiently convergent. '...
124         ,'Expect numerical errors. Solve by adding a frequency point '...
125         ,'in W lower than the current lowest value']);
126 end
127 if test.sumyA1 < test.sumyA2*test.threshold
128     warning(['Impulse response A_R not sufficiently convergent. '...
129         ,'Expect numerical errors. Solve by adding a frequency point '...
130         ,'in W lower than the current lowest value']);
131 end
132 if test.sumyQ1 < test.sumyQ2*test.threshold
133     warning(['Impulse response Q not sufficiently convergent. '...
134         ,'Expect numerical errors. Solve by adding a frequency point '...
135         ,'in W lower than the current lowest value']);
136 end
137
138 % For the other responses, an 'infinite' sum over all prior resets is
139 % needed. Here, we assume that the impulse settling time is low in
140 % comparison to the lowest frequency evaluated.
```

```
141 expmQi = zeros(1,length(temp.yQ(1,1,:)),sz_W);
142 expmH = zeros(length(temp.yH(1,:,1)),length(temp.yH(1,1,:)),sz_W);
143 % For all frequencies
144 for wloop = 1:sz_W
145     % Use the data known, as these are checked for convergence. Use all
146     % data known for computing prior reset instances.
147     nReset = floor(W(wloop)/min(W));
148     % Compute the harmonic values for all resets in this frequency
149     valsQi = permute(interp1(temp.tQ,temp.yQ,pi/W(wloop)*(1:nReset)',...
150         'linear'),[2,3,1]);
151     valsH = permute(interp1(temp.tH,temp.yH,pi/W(wloop)*(1:nReset)',...
152         'linear'),[2,3,1]);
153     % Sum result over all prior resets, utilizing periodicity.
154     for rloop = 1:nReset
155         % Periodicity: sign flip for every additional point
156         expmQi(:,:,wloop) = expmQi(:,:,wloop)+(-1)^(rloop+1)...
157             *valsQi(:,:,rloop);
158         expmH(:,:,wloop) = expmH(:,:,wloop)+(-1)^(rloop+1)...
159             *valsH(:,:,rloop);
160     end
161 end
162
163 % Impulse HOSIDF computation. This code is heavily based on the HOSIDF
164 % calculation by Kars Heinen..
165
166 % Initialize output matrix:
167 Rn_1w = zeros(sz_Wn,1);
168 Phi = zeros(sz_W,1);
169
170 % Flags, indicating if Assumption 2 or 3 are violated
171 flag = zeros(size(W));
172 % Compute for all required frequencies
173 for wloop = 1:numel(W)
174     % Due to setup of n all entries in n are odd, which is required. Even
175     % harmonics are not provided by the output.
176     % Extract frequency
177     wr = W(wloop);
178     % Add reset matrix to impulse responses
179     val1 = -expmQi(:,:,wloop)*(Arho-IR);
180     val2 = -expmH(:,:,wloop)*(Arho-IR);
181     % Compute x at a descending zero crossing reset
182     x_trdown = (IR/(IR-val2...
183         +(wr^2*IR+AR^2)\(AR*BR*val1)))...
184         *((wr^2*IR+AR^2)\(wr*BR)...
185         *abs(KS1_1w(wloop)*Ref));
186     % Val3 is an intermediate result to simplify computing Bstar
187     val3 = (IR+expmAR(:,:,wloop)*Arho)\expmAR(:,:,wloop)*(Arho-IR);
188     % Compute Bstar
189     Bstar = ((IR-val3)*((wr^2*IR+AR^2)\(wr*IR)))\x_trdown;
190     % Compute Impulse HOSIDF
191     Lambda = wr^2*IR + AR^2;
192     Delta = IR + expmAR(:,:,wloop);
193     DeltaR = IR + Arho*expmAR(:,:,wloop);
```

```
194     GammaR = DeltaR\Arho*Delta/Lambda;
195     ThetaD = (-2*wr^2/pi)*Delta*(GammaR-IR/Lambda);
196     for nloop = 1:sz_n
197         % Define matrices not dependent on Arho
198         index = (nloop-1)*sz_W+wloop; % Index where to look for n,w entry
199         % Compute the HOSIDF entry for R at given n, wr
200         Rn_1w(index) = Rn_1w(index)...
201             +CR/(1i*wr*n(nloop)*IR-AR)*1i*ThetaD*Bstar;
202         % Phase and assumption checks. These only need to be performed
203         % for the first harmonic.
204         if nloop == 1
205             % Compute Phi, which is assumed to be small
206             PhiTemp = -asin((expmQi(:,:,wloop)...
207                 *(Arho-IR)*x_trdown)./abs(KS1_1w(wloop)*Ref));
208             % Extract real part, in case a complex value emerged. A
209             % complex value indicates that assumption 2 is violated,
210             % which is flagged as such in that case.
211             Phi(wloop) = real(PhiTemp);
212             if imag(PhiTemp) ~= 0       % Assumption 2 violated
213                 flag(wloop) = 1;
214             end
215             % Verify if assumption 3 is violated, and set flag if so.
216             if (CQ*AQ*(CQ\expmQi(:,:,wloop)*(Arho-IR))) ...
217                     >= abs(KS1_1w(wloop)*Ref)*W(wloop)
218                 flag(wloop) = flag(wloop)+2;
219             end
220         end
221     end
222 end
223
224 % Initiate outputs
225 S_nw = cell(sz_W,sz_n);
226 E_nw = cell(sz_W,sz_n);
227
228 % Compute the output, per frequency point, per harmonic:
229 for wloop = 1:sz_W
230     % First harmonic, different equation than the other harmonics:
231     E_nw{wloop,1} = S1_nw(wloop)*Ref...
232         -S1G_nw(wloop)*Rn_1w(wloop)...
233         *(I.*exp(1j...
234         *(angle(KS1_1w(wloop)*Ref)+diag(Phi(wloop)))));
235     % Use Pseudoinverse for sensitivity, this boosts accuracy if
236     % reference is provided.
237     S_nw{wloop,1} = E_nw{wloop,1}*pinv(abs(Ref).*exp(1j*angle(Ref)));
238     for nloop = 2:sz_n      % Compute for all higher harmonics
239         index = (nloop-1)*sz_W+wloop; % Index where to look for n,w entry
240         E_nw{wloop,nloop} = -S1G_nw(index)*Rn_1w(index)...
241             *(I.*exp(1j*n(nloop)...
242             *(angle(KS1_1w(wloop)*Ref)+diag(Phi(wloop)))));
243         % Utilize pseudoinverse sensitivity definition
244         S_nw{wloop,nloop} = E_nw{wloop,nloop}*pinv(abs(Ref)...
245             .*exp(1j*n(nloop)*angle(Ref)));
246     end
```

```
247 end
248 end
```

A-3 CL-DF calculation

```
1  function [S_nw,n,E_nw] = getCLDF(G,R,Arho,K,W,nMax,varargin)
2  % function S_nw = getCLDF(G,R,Arho,K,W,nMax)
3  % function [S_nw,n,E_nw] = getCLDF(G,R,Arho,K,W,nMax)
4  % function [S_nw,n,E_nw] = getCLDF(G,R,Arho,K,W,nMax,mag,phi)
5  %
6  % This function computes the closed-loop HOSIDF formulation based on the
7  % work by Saikumar, Niranjan - not yet published. This code permits a
8  % MIMO system with 1 reset matrix.
9  %
10 % ------------------------------------------------------------------------
11 % INPUTS
12 % ------------------------------------------------------------------------
13 % G:         Linear system placed after the reset element.
14 % R:         Reset element.
15 % Arho:      Reset matrices corresponding to reset element.
16 % K:         Linear system placed before the reset element.
17 % W:         List of all frequencies to be evaluated [rad/s].
18 % nMax:      Highest harmonic to be considered in analysis.
19 % mag:       List of input magnitudes
20 % phi:       List of reference phases
21 %
22 % ------------------------------------------------------------------------
23 % OUTPUTS
24 % ------------------------------------------------------------------------
25 % S_nw:          Cell matrix with the following dimensions:
26 %                - First dimension: frequencies
27 %                - Second dimension: harmonics
28 %                Each entry is a sensitivity matrix. To acquire the error,
29 %                sum the sinusoids described by the sensitivity. Take care
30 %                to multiply each sensitivity by the reference r according
31 %                to *|r|exp(1j*n*angle(r)). This corrects for having
32 %                multiple frequencies in one signal. The total predicted
33 %                error signal is obtained by summing over all inputs.
34 % n:             Vector with all harmonics
35 % E_nw:          Cell matrix with error signal, defined as with S_nw.
36 %
37 % ------------------------------------------------------------------------
38 % BLOCK DIAGRAM
39 % ------------------------------------------------------------------------
40 %
41 % y <-.-[G]<-[R]<-[K]<-o+<-r
42 %     |________________^-
43 %
44 % Ruben Buitenhuis, TU Delft. Last modification 24/06/2020
45
```

```
% Initialize constants
sz_W = length(W);                                % Number of frequencies
W = reshape(W,sz_W,1);                           % Frequencies to compute
n = 1:2:nMax; n = reshape(n,1,length(n));        % All harmonics to consider
sz_n = length(n);                                % Number of harmonics
Wn = reshape(n.*W,sz_n*sz_W,1);                  % All harmonic frequencies
szWn = length(Wn);                               % Number of harmonic freqs
[szPlnt,~] = size(G);                            % Plant size (assumed square)
I = eye(szPlnt);                                 % Identity matrix

% If provided, compute reference as phasor:
if length(varargin) >= 2
    Ref = varargin{1}.*exp(1j*varargin{2});
    Ref = reshape(Ref,numel(Ref),1);
else
    % Default value
    Ref = ones(length(G),1);
end

% Initiate calculation matrices
L_1w = zeros(szPlnt,szPlnt,sz_W);
K_nw = zeros(szPlnt,szPlnt,szWn);
R_n_1w = zeros(szPlnt,szPlnt,szWn);
R_L_nw = zeros(szPlnt,szPlnt,szWn);

% Initiate outputs
S_nw = cell(sz_W,sz_n);
E_nw = cell(sz_W,sz_n);

% Calculate necessary matrices
G_nw = reshape(freqresp(G,Wn),szPlnt,szPlnt,szWn);
% Diagonal parts, use a cell structure
for dloop = 1:szPlnt
    K_nw(dloop,dloop,:) = reshape(freqresp(K,Wn),1,1,szWn);
    R_n_1w(dloop,dloop,:) = reshape(hosidfcalc(R,Arho,n,W),1,1,szWn);
    R_L_nw(dloop,dloop,:) = reshape(freqresp(R,Wn),1,1,szWn);
end

% Compute the sensitivity matrices
for wloop = 1:sz_W
    L_1w(:,:,wloop) = G_nw(:,:,wloop)*R_n_1w(:,:,wloop)*K_nw(:,:,wloop);
    S_nw{wloop,1} = (I+L_1w(:,:,wloop))\I;
    E_nw{wloop,1} = S_nw{wloop,1}*diag(abs(Ref(1:szPlnt)))*...
        diag(exp(1j*1*angle(Ref(1:szPlnt))));
    % Harmonics
    for nloop = 2:sz_n
        index = (nloop-1)*sz_W+wloop;
        S_nw{wloop,nloop} = -(I+G_nw(:,:,index)*R_L_nw(:,:,index)*...
            K_nw(:,:,index))\G_nw(:,:,index)*R_n_1w(:,:,index)*...
            (abs(K_nw(:,:,index)).*exp(1j*n(nloop)*...
            angle(K_nw(:,:,index))))*(abs(S_nw{wloop,1}).*...
            exp(1j*n(nloop)*angle(S_nw{wloop,1})))*...
            diag(exp(1j*(n(nloop)-1)*angle(Ref(1:szPlnt))));
```

```
99          E_nw{wloop,nloop} = S_nw{wloop,nloop}*...
100             diag(abs(Ref(1:szPlnt)))*diag(exp(1j*angle(Ref(1:szPlnt))));
101     end
102 end
103 end
```

A-4 HOSIDF calculation

```
1  function [G] = hosidfcalc(sysRC, Arho, orders, freqs)
2  % G = hosidfcalc(SYSRC, ARHO, ORDERS, FREQS)
3  % Calculates the higher order sinusoidal input describing function for
4  % the asked orders n and frequencies freqs, either in open-loop or in
5  % closed-loop.
6  %
7  % SYS:    Reset controller in state-space
8  % ARHO:   Reset matrix
9  % ORDERS: Describing Function orders to calculate HOSIDF for
10 % FREQS:  Frequencies to calculate HOSIDF for
11 %
12 % OUTPUTS
13 % G:      Matrix with HOSIDF entries. Data over freqs is given along
14 %         the first dimension, data over orders along the second
15 %         dimension.
16 %
17 % First iteration by Kars Heinen. Adapted by Ruben Buitenhuis. 31/10/2019
18
19 % Controller data, output setup, removing even harmonics
20 AR = sysRC.a; BR = sysRC.b; CR = sysRC.c; DR = sysRC.d;
21 G = NaN(numel(freqs),numel(orders));
22
23 % Open Loop HOSIDF.
24 % For all orders, for all frequencies
25 for k = 1:numel(orders)
26     n = orders(k);
27     if mod(n,2) == 0
28         G(:,k) = 0;
29     else
30         for i = 1:numel(freqs)
31             w = freqs(i);
32             Lambda = w^2*eye(size(AR)) + AR^2;
33             Delta = eye(size(AR)) + expm(pi/w*AR);
34             DeltaR = eye(size(AR)) + Arho*expm(pi/w*AR);
35             GammaR = DeltaR\Arho*Delta/Lambda;
36             ThetaD = (-2*w^2/pi)*Delta*(GammaR-eye(size(Lambda))/Lambda);
37             if (n==1)
38                 G(i,k) = CR/(1i*w*eye(size(AR)) - AR)*...
39                     (eye(size(AR)) + 1i*ThetaD)*BR+DR;
40             else
41                 G(i,k) = CR/(1i*w*n*eye(size(AR)) - AR)*1i*ThetaD*BR;
42             end
43         end
44     end
```

```
45 end
46 end
```

A-5 DF and BLS calculation

```
1  function [Lrc,Src,Erc,nrc,Lbls,Sbls,Ebls,nbls,PMrc,PMbls] = getDF_BLS(G,R
       ,Arho,K,W,wc,varargin)
2  % function [Lrc,Src,Erc,nrc,Lbls,Sbls,Ebls,nbls,PMrc,PMbls] =
3  %                                   getDF_BLS(G,R,Arho,K,W,wc)
4  % function [Lrc,Src,Erc,nrc,Lbls,Sbls,Ebls,nbls,PMrc,PMbls] =
5  %                                   getDF_BLS(G,R,Arho,K,W,wc,mag,phi)
6  %
7  % This function computes the DF analysis and Base Linear System for a
8  % system described by G, K and R according to the block diagram below.
9  %
10 % ------------------------------------------------------------------------
11 % INPUTS
12 % ------------------------------------------------------------------------
13 % G:        Linear system placed after the reset element.
14 % R:        Reset element.
15 % Arho:     Reset matrices corresponding to reset element.
16 % K:        Linear system placed before the reset element.
17 % W:        List of all frequencies to be evaluated [rad/s].
18 % wc:       Crossover frequency
19 % mag:      Input magnitude
20 % phi:      Reference phase
21 %
22 % ------------------------------------------------------------------------
23 % OUTPUTS
24 % ------------------------------------------------------------------------
25 % Lrc:      Reset control loop gain values for frequencies W.
26 % Lbls:     Base-linear-system loop gain values for frequencies W.
27 % Src:      Reset control sensitivity values for frequencies W.
28 % Sbls:     Base-linear-system error values for frequencies W.
29 % Erc:      Reset control error values for frequencies W.
30 % Ebls:     Base-linear-system sensitivity values for frequencies W.
31 % nrc:      Reset control harmonics used.
32 % nbls:     Base-linear-system harmonics.
33 % PMrc:     Phase margin of the nonlinear system, as predicted by DF.
34 % PMbls:    Phase margin of the base-linear system.
35 %
36 % ------------------------------------------------------------------------
37 % BLOCK DIAGRAM
38 % ------------------------------------------------------------------------
39 %
40 % y <-.-[G]<-[R]<-[K]<-o+<-r
41 %     |_________________^-
42 %
43 % Ruben Buitenhuis, TU Delft. Last modification 24/06/2020
44
45 % Evaluate the various system component responses
46 Gval = reshape(freqresp(G,W),length(W),1);
```

```
47 Kval = reshape(freqresp(K,W),length(W),1);
48 Rval = hosidfcalc(R,Arho,1,W);
49 Rbls = reshape(freqresp(R,W),length(W),1);
50
51 % If provided, compute reference as phasor:
52 if length(varargin) >= 2
53     Ref = varargin{1}.*exp(1j*varargin{2});
54 else
55     % Default value
56     Ref = ones(length(G),1);
57 end
58
59 % Compute nonlinear and linear loop gain
60 Lrc = Gval.*Kval.*Rval;
61 Lbls = Gval.*Kval.*Rbls;
62 % Compute sensitivities and errors
63 Src = num2cell(1./(1+Lrc));
64 Sbls = num2cell(1./(1+Lbls));
65 Erc = num2cell(1./(1+Lrc)*Ref);
66 Ebls = num2cell(1./(1+Lbls)*Ref);
67 % Harmonics
68 nrc = 1;
69 nbls = 1;
70 % Compute linear and reset control phase margins
71 PMrc = mod(180+interp1(W,phase(Lrc),wc,'linear','extrap'),360);
72 PMbls = mod(180+interp1(W,phase(Lbls),wc,'linear','extrap'),360);
73 end
```

A-6 Simulation driver

```
1  function [t,e,Smax] = getSimResults(smlk,W,timeReg)
2  % function [t,e,Smax] = getSimResults(smlk,W,timeReg)
3  % This function drives the Simulink Reset Control model and extracts
4  % relevant results.
5  %
6  % ------------------------------------------------------------------------
7  % INPUTS
8  % ------------------------------------------------------------------------
9  % smlk:     Structure with input magnitude .maginput and input phase
10 %               .pinput describing the reference.
11 % W:        [rad/s] list of frequencies to simulate over.
12 % timereg:  Time regularization. Options:
13 %               0: no time regularization
14 %               1: full time regularization (2 resets per period)
15 %               2: optimal time regularization (see Kieft, 2020).
16 %
17 % ------------------------------------------------------------------------
18 % OUTPUTS
19 % ------------------------------------------------------------------------
20 % t:        Cell array with in each cell a time series corresponding to
21 %               the simulation for corresponding frequency in W.
22 % e:        Cell array with in each cell the error time series
```

```
%               corresponding to the same entry in t.
% Smax:     Cell array with in each cell the pseudo sensitivity,
%               corresponding to W.
%
% Ruben Buitenhuis, TU Delft, 03/02/2020

% Initiate output vectors
t = cell(length(W),1);
e = cell(length(W),1);
Smax = cell(length(W),1,1);

% Simulation settings
nperiod = 8;          % Number of full oscillations to simulate for
smlk.pertrans = 1;  % Magnitude transient duration, aiding settling

disp('Starting simulations');
% Simulate for each frequency
for wloop = 1:length(W)
    % Compute some more simulation settings
    smlk.winput = W(wloop);
    smlk.Tend = 2*nperiod*pi/W(wloop);
    % Implement time regularization
    if timeReg == 0 % No time regularization
        smlk.treg = pi/W(wloop)*0;
    elseif timeReg == 1
        % Full time regularization --> 0.8*half period is used to allow
        % transients to happen. This usually enforces 2 resets / period.
        smlk.treg = pi/W(wloop)*0.8;
    else            % Optimal, as per [Kieft, Bas. (2020)].
        smlk.treg = 1/(10*100);
    end
    %-----------------------------------------------------------------
    % Simulate
    %-----------------------------------------------------------------
    % Assign smlk structure in base workspace, as Simulink uses that
    smlkold = evalin('base', 'smlk');
    assignin('base','smlk',smlk);

    % Simulate using Simulink
    simout = sim('resetControlSim','SimulationMode','accel',...
        'AbsTol','1e-6');
    data.t = simout.tout;
    data.r = simout.signals(:,1);
    data.e = simout.signals(:,2);
    data.u = simout.signals(:,3);
    data.y = simout.signals(:,4);
    data.rcount = simout.signals(:,5);

    % Restore original smlk in base workspace
    assignin('base','smlk',smlkold);

    %-----------------------------------------------------------------
    % Data processing
```

```
76      %-------------------------------------------------------------------
77      eSim = reshape(data.e,length(data.e),1);
78      tSim = reshape(data.t,length(data.t),1);
79      w = W(wloop);
80      % Extract last period from dataset
81      loct = find(tSim>(2*(nperiod-1))*pi/w,1);
82      t{wloop,1} = (tSim(loct:end)-2*(nperiod-1)*pi/w)';
83      e{wloop,1} = eSim(loct:end,:)';
84      % Psuedo uncertainty: compute sine wave coinciding with error peak
85      [eMax,loc] = max(abs(eSim),[],2);
86      % Compute used phase
87      if eSim(loc) >= 0
88          phi = -2*pi*loc/length(eSim)+pi/2;
89      else
90          phi = -2*pi*loc/length(eSim)+3*pi/2;
91      end
92      % Pseudo uncertainty
93      Smax{wloop,1} = (eMax./smlk.maginput).*exp(1j*(phi-smlk.pinput));
94  end
95  disp('Finished simulations');
96  end
```

A-7 Time Domain conversion

```
1   function [tlist,e,Smax] = error2Time(E_nw,n,W,tlist,varargin)
2   % function [tlist,e,Smax] = error2Time(E_nw,n,W,tlist)
3   % function [tlist,e,Smax] = error2Time(E_nw,n,W,tlist,mag,phi)
4   %
5   % -------------------------------------------------------------------------
6   % INPUTS
7   % -------------------------------------------------------------------------
8   % E_nw:     Cell matrix (frequencies,harmonics) with on each entry the
9   %           error response of corresponding frequency and harmonic in
10  %           phasor notation.
11  % n:        List of all harmonics used by E_nw.
12  % W:        List of all frequencies used by E_nw.
13  % tlist:    Cell matrix with cells along the first dimension, cells
14  %           corresponding to frequencies in W, each providing a time
15  %           vector to compute results for.
16  % mag:      List of input magnitudes
17  % phi:      List of reference phases
18  %
19  % -------------------------------------------------------------------------
20  % OUTPUTS
21  % -------------------------------------------------------------------------
22  % tlist:    Identical to input tlist, for convenience
23  % e:        Cell matrix with one cell per frequency in W, giving the time
24  %           error responses for all time points in corresponding tlist.
25  % Smax:     Cell matrix giving pseudo sensitivity as phasor, per
26  %           frequency in W
27  %
28  % Ruben Buitenhuis, TU Delft. Last modification 24/06/2020
```

```
29
30 % If provided, extract magnitude and phase
31 if length(varargin) >= 2
32     mag = varargin{1};
33     phi = varargin{2};
34 else
35     % Default value
36     mag = 1;
37     phi = 0;
38 end
39
40 sz_W = length(W);
41 e = cell(sz_W,1,1);
42 Smax = cell(sz_W,1,1);
43
44 for wloop = 1:sz_W
45     % Extract frequency
46     wr = W(wloop);
47     % Extract time vector corresponding to frequency wr. This is done
48     % to ensure time points between simulation and prediction correspond,
49     % enabling a fair comparison.
50     t = tlist{wloop,1,1};
51     % Compute first harmonic
52     e{wloop,1} = abs(E_nw{wloop,1}).*sin(wr*t...
53         +angle(E_nw{wloop,1}));
54     % Add the harmonic responses to the first one:
55     if length(n) > 1
56         for nloop = 2:length(n)
57             e{wloop,1} = e{wloop,1}...
58                 +abs(E_nw{wloop,nloop}).*sin(n(nloop)*wr*t...
59                 +angle(E_nw{wloop,nloop}));
60         end
61     end
62     % Computing Pseudo Sensitivity, which takes the maximum error in one
63     % time period and models a sinusoid over top, with phase such that
64     % the sinusoid peak coincides with the error peak.
65     [eMax,loc] = max(abs(e{wloop,1,1}));
66     % Parameter psi captures the phase shift of the peak error. Compute
67     % this phase for either positive or negative peak:
68     if e{wloop,1,1}(loc) >= 0
69         psi = -2*pi*loc/length(e{wloop,1,1})+pi/2;
70     else
71         psi = -2*pi*loc/length(e{wloop,1,1})+3*pi/2;
72     end
73     Smax{wloop,1,1} = (eMax./mag).*exp(1j*(psi-phi));
74 end
```

A-8 Performance evaluation

```
1 function [Linf,ISE] = performanceMetrics(predData,simData,W)
2 % function [Linf,ISE] = performanceMetrics(predData,simData,W)
3 % This function computes the performance metrics for simulated data
```

```
% stored in predData when compared to simulated data stored in simData.
% Relative metrics Linf and ISE are provided for all entries in W.
%
% ------------------------------------------------------------------------
% INPUTS
% ------------------------------------------------------------------------
% predData: Structure with entries t and e, each an array of cells with
%               one cell per corresponding frequency in W. E.g., cell
%               predData.t{10} gives the time samples for the 10th
%               frequency in W. Cell predData.e{10} then has the
%               corresponding predicted error samples.
% simData:  Strucute akin to predData, but with simulated error data.
% W:        Vector with all frequencies used.
%
% ------------------------------------------------------------------------
% OUTPUTS
% ------------------------------------------------------------------------
% Linf:     Vector with Linf data per frequency point in W.
% ISE:      Vector with ISE data per frequency point in W.
%
% Ruben Buitenhuis, TU Delft. Last modification 13/06/2020

% Initiate matrices with absolute metrics
dLinf = zeros(1,length(W));
dLinfref = zeros(1,length(W));
ISE = zeros(1,length(W));
ISEref = zeros(1,length(W));

% Compute absolute ISE and dLinf measures per frequency
for wloop = 1:length(W)
    % Compute ISE using numerical integration
    ISE(1,wloop) = trapz(predData.t{wloop,1},...
        (predData.e{wloop,1}(1,:)-simData.e{wloop,1}(1,:)).^2);
    % Linf: peak value
    dLinf(1,wloop) = abs(vecnorm(predData.e{wloop,1}(1,:),'Inf',2)...
        -vecnorm(simData.e{wloop,1}(1,:),'Inf',2));
    % Compure reference, total error of prediction.
    ISEref(1,wloop) = trapz(predData.t{wloop,1},...
        (predData.e{wloop,1}(1,:)).^2);
    dLinfref(1,wloop) = vecnorm(predData.e{wloop,1}(1,:),'Inf',2);
end

% Compure relative metrics, give as result
Linf(1,:) = (dLinf(1,:)./dLinfref(1,:))*100;
ISE(1,:) = ISE(1,:)./ISEref(1,:)*100;
```

A-9 Figure colours

This script provides the RGB values for the various plots - providing grey-scale colours as well as the colour palette standard to Delft University of Technology.

```
function [Colors] = getReportColors()
% function [Colors] = getReportColors();
% returns the RGB codes of gray-compatible colors in structure Colors.
%
% Grayscale colors are provided, along with similarly shaded TU Delft
% colors and alternative colors.

Colors.c0 = [0,0,0];                    % Black
Colors.c0col = [0.1137 0.1098 0.4510];  % Night
Colors.c1 = [2.7,2.7,2.7]./10;          % Dark Gray
Colors.c1col = [0.4275 0.0902 0.4980];  % Purple
Colors.c1alt = [0.8863 0.1020 0.1020];  % Red
Colors.c2 = [4.7,4.7,4.7]./10;          % Gray
Colors.c2col = [0,166,214]./255;        % Cyan
Colors.c2alt = [0.4196 0.5255 0.5373];  % Metal
Colors.c3 = [6.6,6.6,6.6]./10;          % Light Gray
Colors.c3col = [0.6471 0.7922 0.1020];  % Green
Colors.c3alt = [1 0.7686 0];            % Yellow
Colors.w = [1,1,1];                     % White
```

A-10 Bode plot

This code, though tailored to a Bode Plot, is used as a template for all figures provided in this thesis. Colours, linewidths, font-sizes and other figure settings are standardized.

```
function [] = bodePlot(Lsidf,Lbls,W)
% function [] = bodePlot(sidf,bls,W) plots the Bode plot for the reset
% control system given by sidf and the base-linear sytem Lbls. These
% vectors must have entries corresponding to frequency points W [rad/s].
%
% Ruben Buitenhuis, 24/06/2020

colors = getReportColors();
fig3 = figure(11052020);
pos = get(fig3,'position');
set(fig3,'position',pos.*[1 1 1 0.8]);

% Magnitude plot
subplot(2,1,1)
semilogx(W./2/pi,20*log10(abs(Lsidf)),'linestyle','-','linewidth',...
    1.5,'color',colors.c3); hold on; grid on;
semilogx(W./2/pi,20*log10(abs(Lbls)),'linestyle','-','linewidth',...
    1.5,'color',colors.c0);
ylabel('Magnitude [dB]')
xlim([min(W),max(W)]./2/pi);
legend('DF','BLS','location','ne');
set(gca,'FontSize',10.5,'linewidth',1)
% Phase plot
subplot(2,1,2)
semilogx(W./2/pi,rad2deg(phase(Lsidf)),'linestyle','-','linewidth',...
    1.5,'color',colors.c3); hold on; grid on;
```

```
27 semilogx(W./2/pi,rad2deg(phase(Lbls)),'linestyle','-','linewidth',...
28     1.5,'color',colors.c0);
29 ylabel('Phase [deg]');
30 xlabel('Frequency [Hz]');
31 xlim([min(W),max(W)]./2/pi);
32 set(gca,'FontSize',10.5,'linewidth',1)
33
34 % The following line requires the align_Ylabels function created by:
35 % Author: Giuliano Bernardi
36 % KU Leuven, Department of Electrical Engineering (ESAT/SCD)
37 %
38 % This function is available through the MATHWORKS website.
39 %
40 % Visual impact only - comment out if package is not available.
41 align_Ylabels(fig3);
```

Appendix B

Simulink setup

The Simulink system used throughout this thesis is presented in this appendix. Two scripts are provided, a reference generator with initial transient and a zero crossing detector, both of which are referred to by the Simulink system given in Figure B-1.

B-1 Reference generator

```
function r = fcn(t,perTrans,mag,omega,phase)

% Compute reference signal, sinusoid only
tTrans = 2*pi/max(omega)*perTrans;  % Time at which transient ends.
% Sinusoid with linearly increasing magnitude starting from 0 during
% transient. This decreases settling times.
r = min(1,t/tTrans).*mag.*sin(omega.*t+phase);
```

B-2 Zero-crossing detector

```
function [ocross,xr,rcount,tprev] = fcn(e,eprev,Arho,x,t,treg,rcount,
    tprev)
% Simulink script

% Detect a zero crossing (given that a reset is permitted, using time
% regularization), and update parameters:
ocross = 0;
xr = x;
if eprev*e <= 0 && t-tprev >= treg(1)
    ocross = 1;              % Flag that a 0-crossing occurs
    xr = Arho*x;             % Update states
    rcount = rcount + 1;     % Count this as reset
    tprev = t;              % Update last reset time
end
```

B-3 Simulink block diagram

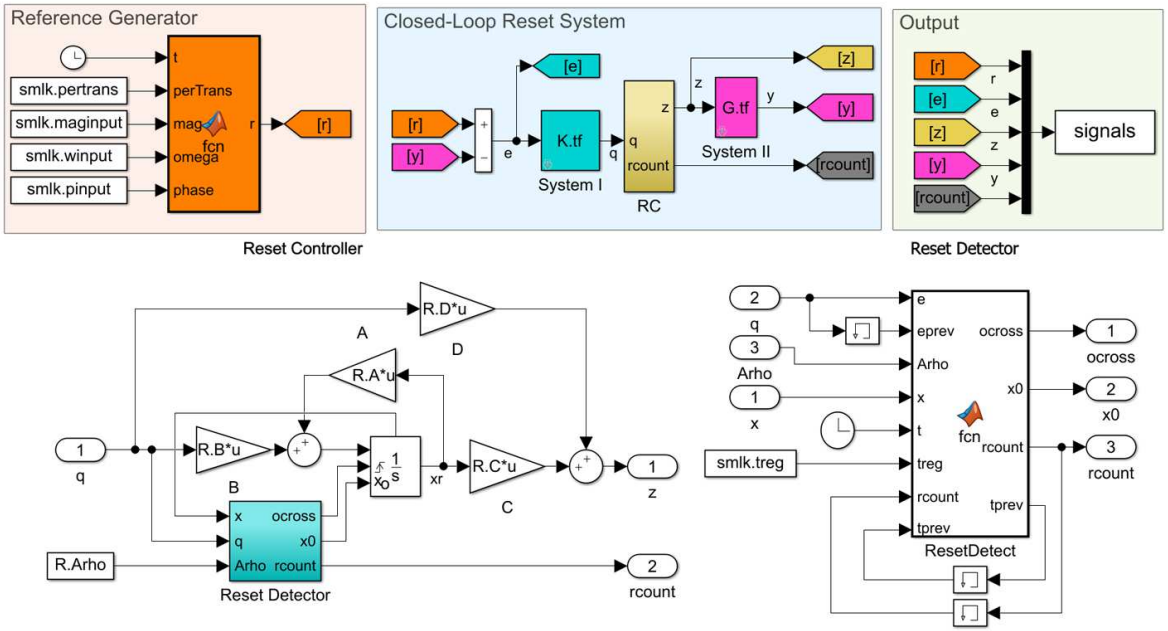

Figure B-1: Simulink setup which is used to gather the results in this thesis. The overall system (top), reset controller (bottom-right) and reset detector (bottom-right) are given. The reference generator function is given by Section B-1, the zero crossing detector by Section B-2

.

Bibliography

[1] T. Samad, S. Mastellone, P. Goupil, A. van Delft, A. Serbezov, and K. Brooks, "IFAC industry committee update, initiative to increase industrial participation in the control community," *IFAC Newsletter*, no. 2, 2019.

[2] J. G. Ziegler and N. B. Nichols, "Optimum settings for automatic controllers," *Trans. ASME*, vol. 64, pp. 759–768, 1942.

[3] R. M. Schmidt, G. Schitter, and J. van Eijk, *The design of high performance mechatronics.* Delft University Press, 2011.

[4] K. J. Åström and B. Wittenmark, *Computer-Controlled Systems.* Mineola, NY: Dover Publications, 3rd ed., 2011.

[5] H. W. Bode, *Network Analysis and Feedback Amplifier Design.* Princeton, New Jersy: D. Van Nostrand Company, Inc, 12th ed., 1945.

[6] S. Skogestad and I. Postlethwaite, *Multivariable Feedback Control: Analysis and Design.* John Wiley & Son, 2nd ed., 2005.

[7] W. C. Foster, D. Lgieseking, and W. K. Waymeyer, "A nonlinear filter for independent gain and phase (with applications)," *Journal of Fluids Engineering, Transactions of the ASME*, vol. 88, no. 2, pp. 457–462, 1966.

[8] B. Hunnekens, N. Van De Wouw, M. Heertjes, and H. Nijmeijer, "Synthesis of variable gain integral controllers for linear motion systems," *IEEE Transactions on Control Systems Technology*, vol. 23, no. 1, pp. 139–149, 2015.

[9] M. F. Heertjes, K. G. Gruntjens, S. J. Van Loon, N. Kontaras, and W. P. Heemels, "Design of a variable gain integrator with reset," *Proceedings of the American Control Conference*, vol. 2015-July, pp. 2155–2160, 2015.

[10] C. Edwards and S. K. Spurgeon, *Sliding Mode Control: Theory and Applications.* Boca Raton, FL: Taylor & Francis Group, 1998.

[11] H. K. Khalil, *Nonlinear systems*. Prentice hall, 3rd ed., 2002.

[12] J. B. Lewis, "The use of nonlinear feedback to improve the transient response of a servomechanism," *Transactions of the American Institute of Electrical Engineers, Part II: Applications and Industry*, vol. 71, no. 6, pp. 449–453, 1953.

[13] A. Van Der Maas, N. Van De Wouw, and W. P. Heemels, "Filtered Split-Path Nonlinear Integrator (F-SPANI) for improved transient performance," *Proceedings of the American Control Conference*, pp. 3500–3505, 2017.

[14] D. A. Deenen, M. F. Heertjes, W. P. Heemels, and H. Nijmeijer, "Hybrid integrator design for enhanced tracking in motion control," *Proceedings of the American Control Conference*, pp. 2863–2868, 2017.

[15] M. Heertjes and Y. Knops, "Low-pass filter with hybrid integrator-gain switching for increased bandwidth," in *ENOC*, 2017.

[16] S. J. Van Den Eijnden, Y. Knops, and M. F. Heertjes, "A Hybrid Integrator-Gain Based Low-Pass Filter for Nonlinear Motion Control," *2018 IEEE Conference on Control Technology and Applications, CCTA 2018*, pp. 1108–1113, 2018.

[17] M. F. Heertjes, S. V. D. Eijnden, and B. Sharif, "Hybrid Integrator-Gain System for Active Vibration Isolation with Improved Transient Response," *Joint 8th IFAC Symposium on Mechatronic Systems and 11th IFAC Symposium on Nonlinear Control Systems*, 2019.

[18] K. Heinen, "Frequency analysis of reset systems containing a Clegg integrator," 2018.

[19] J. C. Clegg, "A nonlinear integrator for servomechanisms," *Transactions of the American Institute of Electrical Engineers, Part II: Applications and Industry*, vol. 77, no. 1, pp. 41–42, 1958.

[20] A. Gelb and W. E. Vander Velde, *Multiple-input Describing Functions and Nonlinear System Design*. McGraw-Hill Book Company, 1st ed., 1968.

[21] Y. Zheng, Y. Chait, C. V. Hollot, M. Steinbuch, and M. Norg, "Experimental demonstration of reset control design," *Control Engineering Practice*, vol. 8, no. 2, pp. 113–120, 2000.

[22] O. Beker, C. V. Hollot, and Y. Chait, "Plant With Integrator: An Example of Reset Control Overcoming Limitations of Linear Feedback," *IEEE Transactions on Automatic Control*, vol. 46, no. 11, pp. 1797–1799, 2001.

[23] K. R. Krishnan and I. M. Horowitz, "Synthesis of a non-linear feedback system with significant plant-ignorance for prescribed system tolerances," *International Journal of Control*, vol. 19, no. 4, pp. 689–706, 1974.

[24] A. Feuer, G. C. Goodwin, and M. Salgado, "Potential benefits of hybrid control for linear time invariant plants," *Proceedings of the American Control Conference*, vol. 5, pp. 2790–2794, 1997.

[25] A. Vidal and A. Baños, "Reset compensation for temperature control: Experimental application on heat exchangers," *Chemical Engineering Journal*, vol. 159, no. 1-3, pp. 170–181, 2010.

[26] J. E. Bobrow, F. Jabbari, and Kiem Thai, "An active truss element and control law for vibration suppression," *Smart Materials and Structures*, vol. 4, no. 4, pp. 264–269, 1995.

[27] V. Ghaffari, P. Karimaghaee, and A. Khayatian, "Reset law design based on robust model predictive strategy for uncertain systems," *Journal of Process Control*, vol. 24, no. 1, pp. 261–268, 2014.

[28] E. Akyüz, N. Saikumar, and S. H. Hosseinnia, "Reset Control for Vibration Isolation," tech. rep., Delft University of Technology, 2019.

[29] N. Saikumar, D. Val, and S. H. Hosseinnia, "Complex order control for improved loop-shaping in precision positioning," *IEEE Conference on Decision and Control*, 2019.

[30] A. Banos and A. Barreiro, *Reset Control*. London: Springer, 1 ed., 2006.

[31] Y. Guo, Y. Wang, L. Xie, H. Li, and W. Gui, "Optimal reset law design of reset control systems with application to HDD systems," *Proceedings of the IEEE Conference on Decision and Control*, pp. 5287–5292, 2009.

[32] A. Palanikumar, N. Saikumar, and S. H. Hosseinnia, "No More Differentiator in PID: Development of Nonlinear Lead for Precision Mechatronics," *2018 European Control Conference, ECC 2018*, pp. 991–996, 2018.

[33] L. Chen, N. Saikumar, S. Baldi, and S. H. Hosseinnia, "Beyond the Waterbed Effect: Development of Fractional Order CRONE Control with Non-Linear Reset," *Proceedings of the American Control Conference*, vol. 2018-June, pp. 545–552, 2018.

[34] N. Saikumar, R. K. Sinha, and S. Hassan Hosseinnia, "'Constant in Gain Lead in Phase' Element-Application in Precision Motion Control," *IEEE/ASME Transactions on Mechatronics*, vol. 24, no. 3, pp. 1176–1185, 2019.

[35] N. Saikumar, K. Heinen, and S. H. Hosseinnia, "Loop-shaping for reset control systems: a higher-order sinusoidal-input describing functions approach." 2020.

[36] A. A. Dastjerdi, A. Astolfi, N. Saikumar, N. Karbasizadeh, D. Valerio, and S. H. HosseinNia, "Closed-loop frequency analyses of reset systems," tech. rep., Delft University of Technology, 2020.

[37] Y. Chait and C. V. Hollot, "On Horowitz's contributions to reset control," *International Journal of Robust and Nonlinear Control*, vol. 12, no. 4, pp. 335–355, 2002.

[38] C. V. Hollot, O. Beker, Y. Chait, and Q. Chen, *On Establishing Classic Performance Measures for Reset Control Systems*. New York: Springer - Verlag, 2001.

[39] W. M. Haddad, V. Chellaboina, and N. A. Kablar, "Active Control of Combustion Instabilities via Hybrid Resetting Controllers," in *Proceedings of the American Control Conference*, no. June, (Chicago), pp. 2378–2382, 2000.

[40] D. Nešić, L. Zaccarian, and A. R. Teel, "Stability properties of reset systems," in *IFAC Proceedings Volumes (IFAC-PapersOnline)*, vol. 38, pp. 67–72, 2005.

[41] L. Zaccarian, D. Nešić, and A. R. Teel, "First order reset elements and the Clegg integrator revisited," *Proceedings of the American Control Conference*, vol. 1, pp. 563–568, 2005.

[42] D. Paesa, C. Franco, S. Llorente, G. Lopez-Nicolas, and C. Sagues, "Reset observers applied to MIMO systems," *Journal of Process Control*, vol. 21, no. 4, pp. 613–619, 2011.

[43] C. Prieur, S. Tarbouriech, and L. Zaccarian, "Lyapunov-based hybrid loops for stability and performance of continuous-time control systems," *Automatica*, vol. 49, no. 2, pp. 577–584, 2013.

[44] L. Li, F. Wu, and X. Wang, "A reset controller design method for MIMO linear systems," *Chinese Control Conference, CCC*, no. 2, pp. 2132–2136, 2013.

[45] C. Yuan and F. Wu, "Hybrid control for switched linear systemswith average dwell time," *IEEE Transactions on Automatic Control*, vol. 60, no. 1, pp. 240–245, 2015.

[46] G. Zhao and C. Hua, "Discrete-Time MIMO Reset Controller and Its Application to Networked Control Systems," *IEEE Transactions on Systems, Man, and Cybernetics: Systems*, vol. 48, no. 12, pp. 2485–2495, 2018.

[47] Y. Guo, L. Xie, and Y. Wang, *Analysis and design of reset control systems*. London: The Institution of Engineering and Technology, 1 ed., 2016.

[48] Q. Chen, C. V. Hollot, and Y. Chait, "Stability and asymptotic performance analysis of a class of reset control systems," *Proceedings of the IEEE Conference on Decision and Control*, vol. 1, pp. 251–256, 2000.

[49] M. F. Heertjes, K. G. Gruntjens, S. J. van Loon, N. van de Wouw, and W. P. Heemels, "Experimental Evaluation of Reset Control for Improved Stage Performance," *IFAC-PapersOnLine*, vol. 49, no. 13, pp. 93–98, 2016.

[50] I. Horowitz and P. Rosenbaum, "Non-linear design for cost of feedback reduction in systems with large parameter uncertainty," *International Journal of Control*, vol. 21, no. 6, pp. 977–1001, 1975.

[51] O. Beker, C. V. Hollot, Y. Chait, and H. Han, "Fundamental properties of reset control systems," *IFAC Proceedings Volumes (IFAC-PapersOnline)*, vol. 15, no. 1, pp. 187–192, 2004.

[52] A. Vidal and A. Baños, "QFT-based design of PI+CI reset compensators: Application in process control," *2008 Mediterranean Conference on Control and Automation - Conference Proceedings, MED'08*, pp. 806–811, 2008.

[53] W. H. T. M. Aangenent, G. Witvoet, W. P. M. H. Heemels, M. J. G. van de Molengraft, and M. Steinbuch, "Performance analysis of reset control systems," *International Journal of Robust and Nonlinear Control*, vol. 18, no. October 2014, pp. 557–569, 2008.

[54] D. Nešić, A. R. Teel, and L. Zaccarian, "Stability and performance of SISO control systems with first-order reset elements," *IEEE Transactions on Automatic Control*, vol. 56, no. 11, pp. 2567–2582, 2011.

[55] F. Fichera, P. Christophe, S. Tarbouriech, and L. Zaccarian, "Using Luenberger observers and dwell-time logic for feedback hybrid loops in continuous-time control systems," *International Journal of Robust and Nonlinear Control*, vol. 18, no. October 2014, pp. 557–569, 2008.

[56] S. J. A. M. V. D. Eijnden, M. F. Heertjes, and H. Nijmeijer, "Robust stability and nonlinear loop-shaping design for hybrid integrator-gain-based control systems," *Proceedings of 2019 American Control Conference (ACC)*, pp. 3063–3068, 2019.

[57] M. Ivens, "Robust Reset Control using Adaptive / Iterative Learning Control," tech. rep., Delft University of Technology, 2018.

[58] J. Zheng, Y. Guo, M. Fu, Y. Wang, and L. Xie, "Improved reset control design for a PZT positioning stage," *Proceedings of the IEEE International Conference on Control Applications*, no. October, pp. 1272–1277, 2007.

[59] A. Baños, J. Carrasco, and A. Barreiro, "Reset Times-Dependent Stability of Reset Control Systems," *Automatic Control, IEEE Transactions on*, vol. 34, no. 4, pp. 460–462, 2010.

[60] H. Hu, Y. Zheng, Y. Chait, and C. V. Hollot, "On the zero-input stability of control systems with Clegg integrators," *Proceedings of the American Control Conference*, vol. 1, no. June, pp. 408–410, 1997.

[61] R. Yue, S. A. Billings, and Z.-Q. Lang, "An Investigation into the Characteristics of Nonlinear Frequency Response Functions , Part 1 : Understanding the Higher Dimensional Frequency Spaces," tech. rep., University of Sheffield, 2004.

[62] Á. Vidal and A. Baños, "Reset compensation applied on industrial heat exchangers," *ETFA 2009 - 2009 IEEE Conference on Emerging Technologies and Factory Automation*, 2009.

[63] D. Rijlaarsdam, *Frequency Domain Based Performance Optimization of Systems with Static Nonlinearities*. PhD thesis, Eindhoven University of Technology, 2012.

[64] D. Rijlaarsdam, P. Nuij, J. Schoukens, and M. Steinbuch, "A comparative overview of frequency domain methods for nonlinear systems," *Mechatronics*, vol. 42, pp. 11–24, 2017.

[65] Y. Guo, Y. Wang, and L. Xie, "Frequency-domain properties of reset systems with application in hard-disk-drive systems," *IEEE Transactions on Control Systems Technology*, vol. 17, no. 6, pp. 1446–1453, 2009.

[66] M. Enqvist and L. Ljung, "Linear approximations of nonlinear FIR systems for separable input processes," *Automatica*, vol. 41, no. 3, pp. 459–473, 2005.

[67] J. Schoukens, R. Pintelon, G. Vandersteen, and Y. Rolain, "Design of excitation signals for nonparametric measurements on MIMO-systems in the presence of nonlinear distortions," *2010 IEEE International Instrumentation and Measurement Technology Conference, I2MTC 2010 - Proceedings*, pp. 1–5, 2010.

[68] J. Schoukens, R. Pintelon, T. Dobrowiecki, and Y. Rolain, "Identification of Linear Systems with Nonlinear Distortions," *IFAC Proceedings Volumes (IFAC-PapersOnline)*, vol. 36, no. 16, pp. 1723–1734, 2003.

[69] D. A. George, "Continuous nonlinear systems," tech. rep., Massachusetts Institute of Technology, 1959.

[70] D. J. Antunes, J. P. Hespanha, and C. J. Silvestre, "Volterra integral approach to impulsive renewal systems: Application to networked control," *IEEE Transactions on Automatic Control*, vol. 57, no. 3, pp. 607–619, 2012.

[71] M. Vidyasagar, *Nonlinear systems analysis (2nd Ed)*. Englewood Cliffs, New Jersey: Prentice hall, 1993.

[72] J. C. Peyton Jones and S. A. Billings, "Describing functions, volterra series, and the analysis of non-linear systems in the frequency domain," *International Journal of Control*, vol. 53, no. 4, pp. 871–887, 1991.

[73] P. W. J. M. Nuij, O. H. Bosgra, and M. Steinbuch, "Higher-order sinusoidal input describing functions for the analysis of non-linear systems with harmonic responses," *Mechanical Systems and Signal Processing*, vol. 20, no. 8, pp. 1883–1904, 2006.

[74] P. W. J. M. Nuij, O. H. Bosgra, and M. Steinbuch, "Higher-order sinusoidal input describing functions for the analysis of non-linear systems with harmonic responses," *Mechanical Systems and Signal Processing*, vol. 20, no. 8, pp. 1883–1904, 2006.

[75] D. Rijlaarsdam, P. Nuij, J. Schoukens, and M. Steinbuch, "Spectral analysis of block structured nonlinear systems and higher order sinusoidal input describing functions," *Automatica*, vol. 47, no. 12, pp. 2684–2688, 2011.

[76] P. W. J. M. Nuij, O. H. Bosgra, and M. Steinbuch, "Higher-order sinusoidal input describing functions for the analysis of non-linear systems with harmonic responses," *Mechanical Systems and Signal Processing*, vol. 20, no. 8, pp. 1883–1904, 2006.

[77] X. Hou, "Tuning of the Constant in gain Lead in phase Element for Mass-like Systems," 2019.

[78] Y. Salman, "Tuning a Novel Reset Element through Describing Function and HOSIDF Analysis," 2018.

[79] M. S. Bahnamiri, N. Karbasizadeh, A. A. Dastjerdi, N. Saikumar, and S. H. HosseinNia, "Tuning of CgLp based reset controllers: Application in precision positioning systems," Tech. Rep. 2009, Delft University of Technology, 2020.

[80] L. Hazeleger, M. Heertjes, and H. Nijmeijer, "Second-order reset elements for stage control design," *Proceedings of the American Control Conference*, vol. 2016-July, pp. 2643–2648, 2016.

[81] A. Baños, S. Dormido, and A. Barreiro, "Limit cycles analysis of reset control systems with reset band," *Nonlinear Analysis: Hybrid Systems*, vol. 5, no. 2, pp. 163–173, 2011.

[82] A. Banos and A. Vidal, "Definition and tuning of a PI+CI reset controller," *2007 European Control Conference, ECC 2007*, pp. 4792–4798, 2007.

[83] A. Vidal, A. Baños, J. C. Moreno, and M. Berenguel, "PI+CI compensation with variable reset: Application on solar collector fields," *IECON Proceedings (Industrial Electronics Conference)*, pp. 321–326, 2008.

[84] A. Baños and A. Vidal, "Design of reset control systems: The PI CI compensator," *Journal of Dynamic Systems, Measurement and Control, Transactions of the ASME*, vol. 134, no. 5, pp. 1–11, 2012.

[85] A. Baños and A. Vidal, "Design of PI+CI reset compensators for second order plants," *IEEE International Symposium on Industrial Electronics*, pp. 118–123, 2007.

[86] N. Saikumar, R. K. Sinha, and S. Hassan HosseinNia, "Resetting disturbance observers with application in compensation of bounded nonlinearities like hysteresis in piezo-actuators," *Control Engineering Practice*, vol. 82, no. March 2018, pp. 36–49, 2019.

[87] N. Karbasizadeh, A. A. Dastjerdi, N. Saikumar, D. Valério, and S. H. Hosseinnia, "Benefiting from Linear Behaviour of a Nonlinear Reset-based Element at Certain Frequencies," tech. rep., Delft University of Technology, 2020.

Glossary

List of Acronyms

3mE	Mechanical, Maritime and Materials Engineering
BLA	Best Linear Approximator
BLS	Base Linear System
CgLp	Constant in gain, Lead in phase
CI	Clegg Integrator
CL-DF	Closed-loop Describing Function
CL-FR	Closed-loop Frequency Response
DCSC	Delft Center for Systems and Control
DF	Describing Function
FORE	First Order Reset Element
GCI	Generalized CI
GFORE	Generalized FORE
GFRF	Generalized Frequency Response Function
GSORE	Generalized SORE
HOSIDF	Higher Order Sinusoidal Input Describing Function
HTE	High Tech Engineering
LTI	Linear Time Invariant
MIMO	Multi Input Multi Output
NFRF	Nonlinear Frequency Response Function
PI	Proportional Integral
PID	Proportional Integral Derivative
RC	Reset Control
RCS	Reset Control System
SIDF	Sinusoidal Input Describing Function

SISO	Single Input Single Output
SORE	Second Order Reset Element
SOSRE	Second Order Single Reset Element
TU Delft	Delft University of Technology

List of Symbols

α	Parameter linking ω_r to $\omega_{r\alpha}$
$\bar{k}$	Number of reset laws
β	Damping parameter
$\not{R}$	Reset element description
$\not{I}$	RCS description
δ	Reset band size
γ	Reset parameter
ω	Frequency
ω_0	Particular frequency point
ω_f	Low-pass filter cut-off frequency
ω_r	Reset element cut-off frequency without taking nonlinearity into account
$\omega_{r\alpha}$	Reset element cut-off frequency taking nonlinearity into account
τ_I	PID integrator time constant
$\vec{e}$	Error signal
$\vec{q}$	RC input
$\vec{q}_0$	Magnitude of sinusoidal $\vec{q}$
$\vec{r}_I$	Reference signal
$\vec{x}$	RC states
$\vec{x}^+$	Post-reset RC states
$\vec{x}_{cl}$	RCS states
$\vec{y}$	Output signal
$\vec{z}$	RC output
A_G	Process state-space matrix of G
A_K	Process state-space matrix of K
A_R	RC Process state-space matrix
$A_{\rho,k}$	Reset matrices
$A_{\rho cl,k}$	Closed-loop reset matrix
A_{cl}	RCS process state-space matrix
B_G	Input state-space matrix of G
B_K	Input state-space matrix of K
B_R	RC input state-space matrix
B_{cl}	RCS input state-space matrix

C_G	Output state-space matrix of G
C_K	Output state-space matrix of K
C_R	RC output state-space matrix
C_{cl}	Closed-loop reset controller output state-space matrix
D_G	Feed-through state-space matrix of G
D_K	Feed-through state-space matrix of K
D_R	RC feed-through state-space matrix
D_{cl}	RCS feed-through state-space matrix
G	Linear system appending the RC
h	Variable reset band size
K	Linear system prepending the RC
k	Reset law index
k_p	PID gain
L_{BLS}	BLS loop gain
m_q	Dimension of RC output
m_y	Number of reference, error and output signal channels
m_z	Dimension of RC input
N	Slope of gain, in dB per decade
n	Harmonic number
n_{cl}	Number of RCS states
n_{ol}	Number of RC states
p_r	Reset percentage
Q	Frequency-domain RC output
R	Frequency-domain reset element
R_L	Base-linear RC
$R_{DF,n}$	The n-th order HOSIDF of system R
s	Laplace variable
S_{BLS}	BLS sensitivity
$S_{CLDF,n}$	The n-th order sensitivity approximation using CL-DF
t	Time
t_p	Time of the last occurred reset
t_R	Set of all reset instants
T_{BLS}	BLS complementary sensitivity
$t_{R,k}$	Set of all reset instants belonging to reset law k
$t_{r,k}$	Time at a reset instant belonging to reset law k
Z	Frequency-domain RC input